University of Kentucky
UKnowledge

Theses and Dissertations--Electrical and Computer Engineering | Electrical and Computer Engineering

2019

ADVANCED FAULT AREA IDENTIFICATION AND FAULT LOCATION FOR TRANSMISSION AND DISTRIBUTION SYSTEMS

Wen Fan
University of Kentucky, wen.fan@uky.edu
Digital Object Identifier: https://doi.org/10.13023/etd.2019.396

Right click to open a feedback form in a new tab to let us know how this document benefits you.

Recommended Citation

Fan, Wen, "ADVANCED FAULT AREA IDENTIFICATION AND FAULT LOCATION FOR TRANSMISSION AND DISTRIBUTION SYSTEMS" (2019). *Theses and Dissertations--Electrical and Computer Engineering*. 144.
https://uknowledge.uky.edu/ece_etds/144

This Doctoral Dissertation is brought to you for free and open access by the Electrical and Computer Engineering at UKnowledge. It has been accepted for inclusion in Theses and Dissertations--Electrical and Computer Engineering by an authorized administrator of UKnowledge. For more information, please contact UKnowledge@lsv.uky.edu.

STUDENT AGREEMENT:

I represent that my thesis or dissertation and abstract are my original work. Proper attribution has been given to all outside sources. I understand that I am solely responsible for obtaining any needed copyright permissions. I have obtained needed written permission statement(s) from the owner(s) of each third-party copyrighted matter to be included in my work, allowing electronic distribution (if such use is not permitted by the fair use doctrine) which will be submitted to UKnowledge as Additional File.

I hereby grant to The University of Kentucky and its agents the irrevocable, non-exclusive, and royalty-free license to archive and make accessible my work in whole or in part in all forms of media, now or hereafter known. I agree that the document mentioned above may be made available immediately for worldwide access unless an embargo applies.

I retain all other ownership rights to the copyright of my work. I also retain the right to use in future works (such as articles or books) all or part of my work. I understand that I am free to register the copyright to my work.

REVIEW, APPROVAL AND ACCEPTANCE

The document mentioned above has been reviewed and accepted by the student's advisor, on behalf of the advisory committee, and by the Director of Graduate Studies (DGS), on behalf of the program; we verify that this is the final, approved version of the student's thesis including all changes required by the advisory committee. The undersigned agree to abide by the statements above.

Wen Fan, Student

Dr. Yuan Liao, Major Professor

Dr. Aaron Cramer, Director of Graduate Studies

ADVANCED FAULT AREA IDENTIFICATION AND FAULT LOCATION FOR TRANSMISSION AND DISTRIBUTION SYSTEMS

DISSERTATION

A dissertation submitted in partial fulfillment of the requirements for the degree of Doctor of Philosophy in the College of Engineering at the University of Kentucky

By

Wen Fan

Lexington, Kentucky

Director: Dr. Yuan Liao, Professor of Electrical and Computer Engineering

Lexington, Kentucky

2019

Copyright © Wen Fan 2019

ABSTRACT OF DISSERTATION

ADVANCED FAULT AREA IDENTIFICATION AND FAULT LOCATION FOR TRANSMISSION AND DISTRIBUTION SYSTEMS

Fault location reveals the exact information needed for utility crews to timely and promptly perform maintenance and system restoration. Therefore, accurate fault location is a key function in reducing outage time and enhancing power system reliability.

Modern power systems are witnessing a trend of integrating more distributed generations (DG) into the grid. DG power outputs may be intermittent and can no longer be treated as constants in fault location method development. DG modeling is also difficult for fault location purpose. Moreover, most existing fault location methods are not applicable to simultaneous faults. To solve the challenges, this dissertation proposes three impedance-based fault location algorithms to pinpoint simultaneous faults for power transmission systems and distribution systems with high penetration of DGs.

The proposed fault location algorithms utilize the voltage and/or current phasors that are captured by phasor measurement units. Bus impedance matrix technique is harnessed to establish the relationship between the measurements and unknown simultaneous fault locations. The distinct features of the proposed algorithms are that no fault types and fault resistances are needed to determine the fault locations. In particular,

Type I and Type III algorithms do not need the information of source impedances and prefault measurements to locate the faults. Moreover, the effects of shunt capacitance are fully considered to improve fault location accuracy. The proposed algorithms for distribution systems are validated by evaluation studies using Matlab and Simulink SimPowerSystems on a 21 bus distribution system and the modified IEEE 34 node test system. Type II fault location algorithm for transmission systems is applicable to untransposed lines and is validated by simulation studies using EMTP on a 27 bus transmission system.

Fault area identification method is proposed to reduce the number of line segments to be examined for fault location. In addition, an optimal fault location method that can identify possible bad measurement is proposed for enhanced fault location estimate. Evaluation studies show that the optimal fault location method is accurate and effective.

The proposed algorithms can be integrated into the existing energy management system for enhanced fault management capability for power systems.

KEYWORDS: Fault location, simultaneous faults, fault area identification, power systems, distributed generations, phasor measurement units.

Wen Fan

October 9, 2019

ADVANCED FAULT AREA IDENTIFICATION AND FAULT LOCATION FOR TRANSMISSION AND DISTRIBUTION SYSTEMS

By

Wen Fan

Dr. Yuan Liao

_____

Director of Dissertation

Dr. Aaron Cramer

_____

Director of Graduate Studies

October 9, 2019

_____

Date

ACKNOWLEDGEMENTS

I would like to express my sincerest thanks of gratitude to my Doctoral Advisory Committee professors Dr. Yuan Liao, Dr. Joseph Sottile, Dr. Yuming Zhang, Dr. Himanshu Thepliyal and Dr. Zongming Fei for their valuable guidance and support.

Table of Contents

List of Tables

List of Figures

Chapter 1 Introduction

In this chapter, Section 1.1 gives an overview of fault location, Section 1.2 conducts a literature review of the existing fault location methods, and Section 1.3 describes the motivations and objectives of this dissertation, followed by the dissertation outline in Section 1.4.

1.1 Background

Electric power systems serve to deliver power from generations to the end customers. Faults that occur on power lines will interrupt the power delivery service and result in power outages. Unintentional power outages cause inconvenience to customers and lower customer satisfaction. Moreover, any unexpected loss of power can put the public at risk.

To restore power for the customers interrupted, it is essential to locate and repair the faulted components first. Although sometimes the system reconfiguration may restore power for partial customers interrupted, full restoration of power will count on the repair of faulted components [1].

Fault location reveals the exact information needed for utilities to dispatch maintenance crews to repair faulted components and restore power delivery service. Therefore, accurate fault location plays a pivotal role in speedy maintenance and fast system restoration [1][2]. Furthermore, accurate fault location improves system reliability. Utilities have reported significant improvements in reliability indices [3], including system average interruption duration index (SAIDI), system average interruption frequency index (SAIFI), customer average interruption duration index (CAIDI), and momentary average interruption frequency index (MAIFI). Last but not least, accurate fault location reduces outage time and thus improves customer satisfaction.

Faults can be caused by various reasons. Most of the reasons are lightning, vegetation, animal, and excavation. When trees are planted without regard to their surroundings or are not properly maintained, they may grow into the powerlines and disrupt the power delivery service [4]. Severe weather such as ice storm may cause tree branches falling upon power lines, and lightning can cause insulation breakdown. Animal contact to power lines, transformers, or protection equipment may also lead to faults.

Faults can be classified into two categories: open circuit faults and short circuit faults. The latter is further classified into asymmetrical faults and symmetrical faults. Asymmetrical faults include single-line-to-ground (LG) faults, line-to-line (LL) faults, and line-to-line-to-ground (LLG) faults. Symmetrical faults include three-phase (LLL) faults and three-phase-to-ground (LLLG) faults. This research focuses on short circuit faults.

Depending on the faulty phase(s), asymmetrical faults are given different names. LG faults include phase-A-to-ground (AG) faults, phase-B-to-ground (BG) faults, and phase-C-to-ground (CG) faults. LL faults include phase-A-to-phase B (AB) faults, phase-B-to-phase-C (BC) faults, and phase-A-to-phase-C (AC) faults. LLG faults include phase-A-to-phase-B-to-ground (ABG) faults, phase-B-to-phase-C-to-ground (BCG) faults, and phase-A-to-phase-C-to-ground (ACG) faults.

Other than the aforementioned single faults, simultaneous faults can occur in the power systems. Simultaneous faults are the situations where two or more faults occur in the power systems at the same time but at different locations. A simultaneous fault can have multiple, different types of short circuit faults or the same type of short circuit faults.

Recently, there is an increasing deployment of distribution generations (DG), especially inverter-based generations (IBG), in power distribution systems. Fault location is challenging for these cases because the source impedance of IBG is hard to obtain due to the complexity and uncertainty of IBG modeling, and the short circuit current contribution from IBG may not be monitored. In addition, DG power outputs may be intermittent and can no longer be treated as constants in fault location method development.

1.2 Literature Review

Various fault location methods have been proposed in the past. Most of the existing methods are impedance-based. The impedance-based methods estimate the distance to fault as a function of total line impedance using voltage and current measurements from single or multiple ends [5]. Generally, those methods can be classified into three classes based on the number and location of the recorded data used: single-end methods [1][6][7], double-end methods [8]-[10], and wide-area measurement-based methods [11]-[13].

The single-end fault location methods utilize data from only one terminal of the line to locate the fault. Takagi and Yamakoshi [6] estimate the fault location by utilizing one-terminal voltage and current data to calculate the reactance of a faulty line. Results of the method are influenced by fault resistance, load flow, and mutual impedance. Pereira *et al.* [7] also find fault location using one-terminal data. However, the method does not require postfault current measurements. Moreover, prefault current measurements are not required if saturation does not occur. Krishnathevar and Ngu [1] identify the fault location by developing a current distribution factor to compute the fault current. The

method works for all types of fault expect unbalanced three-phase fault. The authors also attempt to solve the multiple estimation problems based on the computed fault current.

The double-end fault location methods utilize data from both ends of the line to pinpoint the fault. The data used can be synchronized or unsynchronized. Lee *et al.* [8] calculate the fault location using synchronized measurements obtained by phasor measurement units (PMU). In addition, the authors exploit the calculated arc voltage amplitude to decide whether the fault is permanent or transient. The decision is helpful for recloser purpose. Liao and Elangovan [9] present a double-end fault location method based on unsynchronized voltage and current measurements without the need of using line parameters. The method is able to estimate the location of asymmetric faults. Kang *et al.* [10] find fault location on series-compensated double-circuit transmission lines. Boundary conditions under different fault types are used to extract the fault location. The authors consider the mutual coupling between parallel transmission lines and effects of shunt capacitance.

The wide-area measurement-based methods take advantage of the sparsity of measurement devices deployed in the electric power grid. The purpose of such methods is to locate the fault using a limited number of measurement devices. The measurement devices can be deployed at the faulty line terminals or buses far away from the faulty line. Dobakhshari and Ranjbar [11] present a wide-area focused method based on positive-sequence voltage measurements. The fault location is formulated and solved by a linear weighted least squares method. The authors also attempt to identify the measurement error to improve fault location estimation accuracy. Jiao and Liao [12] locate the fault on untransposed transmission lines using wide-area voltage measurements. The method

considers the inherent unbalance of untransposed transmission lines. The fault location method is also applicable to transposed transmission lines. In addition, the authors utilize optimal estimation theory to make the most of the available measurements to improve estimation accuracy. Feng and Abur [13] formulate the fault location problem as a sparse estimation problem, which can be solved by L_1 norm regularization optimization. The authors point out that a significant large system can be decomposed into multiple areas by decomposing the sparse estimation problem into several subproblems. In this way, the efficiency of the method will be conserved.

Feng and Abur [13] also present an optimal meter placement scheme while solving the sparse estimation problem. Shahraeini *et al.* [14] discuss meters placement and their required communication infrastructure. Xiu and Liao [15] present fault location observability analysis and propose an optimal meter placement method to uniquely identify fault location across a network.

With more DGs being integrated into the grid recently, fault location techniques considering DGs have been researched [16]-[24]. In [16], the author uses synchronized voltage and current measurements at the interconnection of DG to locate the fault. A voltage-matching method is proposed to extract the fault location in [18]. The sequence network technique is used to estimate the fault location in [19], where the load uncertainty is considered. Reference [21] presents a fault location method based on both phase and sequence network. The authors of [22] describe a DG high-frequency impedance model to estimate the fault location by measuring the system high-frequency line reactance. A method based on unsynchronized smart meter data to pinpoint the fault

is presented in [24], where the bus impedance matrix is constructed using only the series impedance of feeders.

Although various fault location approaches exist, simultaneous faults are rarely addressed in the literature. Majidi *et al.* [25] present a novel method for simultaneous faults based on voltage sag values. This method demands a large number of voltage measurements, and the fault is limited to network nodes.

Besides impedance-based fault location methods, some authors adopt traveling-wave-based methods. Traveling-wave focused methods generally make use of wavelet transform technique to capture time arrival difference and then locate the fault [26]. Spoor and Zhu [27] utilize single-end unsynchronized traveling wave data and continuous wavelet transform technique to pinpoint the fault. Lopes *et al.* [28] estimate fault location based on synchronized double-end traveling wave data, with considering data transmission latency. Korkali *et al*. [29] adopt discrete wavelet transform technique to capture the time of arrival of traveling waves. The authors provide a wide-area measurement-based solution for large-scale systems, where the fault location problem is further converted to an optimization problem based on the shortest propagation times of traveling waves.

Since traveling-wave-based methods require very high sampling rate measurements and lots of signal processing, the methods have not been widely adopted. In addition, the huge cost for utilities to deploy meters on a large scale to capture arrival times of traveling waves is one barrier for implementing traveling-wave-based methods in real power systems.

There are also several authors that propose intelligence-based fault location methods. The authors of [30] and [31] utilize artificial neural network (ANN) technique to locate the fault in radial and multi-ring distribution network, respectively. Reference [32] finds the fault location using voltage measurements based on fuzzy logic technique. The machine learning approach is adopted in [33] that uses measurements from smart meters across the power grid.

Furthermore, various efforts have been spent to identify the faulted line sections. In [34], a pattern search technique is adopted to identify the faulted line section. In [35], a multiple-hypothesis method is developed to determine the faulted line section based on the available evidence from the activated protective devices. The authors of [36] identify the faulted section by analyzing the transient fault signals. A graph theory based method is described in [37] to identify faulted feeder sections in a distribution system.

1.3 Research Motivations and Objectives

Based on the literature review, there is a need for developing new fault location algorithms that can accurately locate simultaneous faults on transmission and distribution systems with increasing deployment of DGs. The new algorithms need to consider untransposed lines, shunt capacitances, and unbalanced distribution systems. There may be only sparse measurements captured from different locations in the system, which may not be from the terminals of the faulted lines. There may also be bad measurements due to various reasons. DG modeling for fault location is also a challenge.

This dissertation aims to develop novel, general algorithms to locate faults for power systems to deal with the aforementioned challenges. Specifically, the research has the following objectives:

(1) Develop a fault area identification method to identify the faulted sections.

(2) Develop accurate fault location algorithms that can pinpoint simultaneous faults in transmission systems and distribution systems integrated with DGs. The developed algorithms shall have the following features:

   a. ability to utilize sparse voltage and/or current measurements to locate simultaneous faults;
   b. ability to locate simultaneous faults without the information of fault types, fault resistances, source impedances, and prefault measurements;
   c. ability to locate simultaneous faults for unbalanced distribution systems integrated with multiple DGs;
   d. ability to locate simultaneous faults on either transposed or untransposed transmission lines;
   e. ability to fully consider the shunt capacitances of power lines.

(3) Develop an optimal fault location estimation method that is able to detect and identify bad measurements. The method shall provide the best fault location estimates based on available data.

1.4 Dissertation Outline

This dissertation proposes new impedance-based fault location algorithms to pinpoint simultaneous faults for power transmission systems and distribution systems with high penetration of DGs. Chapter 2 presents the proposed fault area identification method. The method reduces the number of line segments that need to be examined for fault location purpose. Case studies for distribution and transmission systems are reported at the end of Chapter 2. In Chapter 3, three fault location algorithms are proposed for distribution

systems with high penetration of DGs. The proposed algorithms are validated by evaluation studies using Matlab and Simulink SimPowerSystems on a 21 bus distribution system and the modified IEEE 34 node test system. Chapter 4 proposes an optimal fault location method for distribution systems with DGs. The method can identify possible bad measurements and enhance fault location estimate. Extensive case studies show that the proposed optimal fault location method is accurate and effective. In Chapter 5, a fault location algorithm is proposed to pinpoint simulations faults in transmission systems that have double circuit lines. The lines can be transposed or untransposed. Evaluation studies on a 27 bus transmission system are reported. Finally, Chapter 6 draws the conclusions of the proposed fault area identification methods, fault location algorithms, and optimal fault location methods.

Chapter 2 Fault Area Identification for Power Systems

In this chapter, the proposed fault area identification method [39][40] for power transmission and distribution systems with DGs is presented in Section 2.2. Extensive simulation studies have been carried out to evaluate the proposed method in Section 2.3. Subsections 2.3.1 and 2.3.2 evaluate the proposed method on a 21 bus distribution system with DGs and the modified IEEE 34 Node Test System, and Subsection 2.3.3 evaluates the proposed method on a 27 bus transmission system. A summary is provided in Section 2.4.

2.1 Introduction

In the past, fault location algorithms are usually successively applied to each line section until all possible sections are attempted. In this chapter, a fault area identification method is proposed to pinpoint the faulted area of the power network and reduce the number of line segments that need to be examined for fault location. As a result, the computational burden of fault location analysis is reduced. The method is based on synchronized current phasor measurements at the fundamental frequency. It can be applied to transmission systems and distribution systems with DGs. It is applicable to a single fault as well as simultaneous faults.

2.2 Proposed Fault Area Identification Method

The method is based on graph theory through which a connection matrix is developed to represent the power network [37][39][40]. Either a distribution network or a transmission network could be divided into several protection areas based on the topology of the network. A fault area identification vector (FAIV) is developed to identify the faulted

protection area(s) when a fault event occurs. FAIV is determined by connection matrix $\boldsymbol{N}$ and current vector $\boldsymbol{I}$ as

$$\boldsymbol{FAIV} = |\boldsymbol{NI}| \tag{2.1}$$

where,

$|.|$ denotes the magnitude of a vector or matrix;

$\boldsymbol{N}$ represents the relationship between protection areas and currents that flow through the area boundaries;

$\boldsymbol{I}$ consists of all currents that flow through the area boundaries.

The connection matrix is obtained in the following steps:

(1) Assume a network is divided into k protection areas, and there are l currents flow through the area boundaries. Initialize a k by l zero matrix;

(2) If the lth current flows out of the kth protection area, update N_{kl} to -1;

(3) If the lth current flows into the kth protection area, update N_{kl} to 1;

(4) Repeat steps (2) and (3) until $\boldsymbol{N}$ is updated for all protection areas and currents.

Although it is natural to choose current directions as of substation to end-users, the current directions could be arbitrarily selected. This is because the formation of connection matrix $\boldsymbol{N}$ depends on current directions in steps (2) and (3). Since the selection of current directions is arbitrary, the developed method is naturally applicable to bidirectional power flow distribution systems in presence of DGs.

In practice, FAIV could be calculated for each phase, separately. For example, FAIV for phase A is determined as

$$\boldsymbol{FAIV}_A = |\boldsymbol{NI}_A| \tag{2.2}$$

where $\boldsymbol{I}_A$ is the current vector for phase A.

If the value of the kth element of $\boldsymbol{FAIV}_A$ during the fault is significantly greater than the value preceding the fault, then the kth protection area is determined as a faulted area with a fault involving phase A. To quantify the criterion, let $|\Delta \boldsymbol{FAIV}_A|$ be the absolute difference between pre- and during- fault values of $\boldsymbol{FAIV}_A$. When $|\Delta \boldsymbol{FAIV}_A|$ exceeds a pre-specified threshold value, a fault is considered to occur in the system.

Similarly, the approach is also applicable to phase B and C. This approach has the advantage that FAIV is associated with the corresponding phases. That is, it is capable of identifying the faulted area(s) and faulted phase(s) at the same time.

It is evident that the resolution fault area identification depends on the number of meters placed in the network. The more meters available, the more accurate the fault area identification will be. Ideally, if there will be meters placed at each end of every line section, then the protection areas can be partitioned arbitrarily. In practical applications, protection area partition will have to consider the location and availability of meters.

2.3 Evaluation Studies

This section presents the simulation results for the proposed fault area identification method. The method is tested on a 21 bus distribution system with DGs, the modified IEEE 34 Node Test System with DGs [41], and a 27 bus transmission system. In addition, the method is tested for single and simultaneous fault cases.

2.3.1 Identifying Faulted Area for a 21 Bus Distribution System with DGs

A self-made 21 bus distribution system is used for the evaluation study of the proposed fault area identification method. In Figure 2.1, the substation is located as bus 1, and three DGs are located at bus 10, 14, and 20, respectively. Note that DG1 is a single-phase

source, and some of the distribution lines are single and two phases. Therefore, the proposed fault area identification method will be tested on an unbalanced distribution system with DGs.

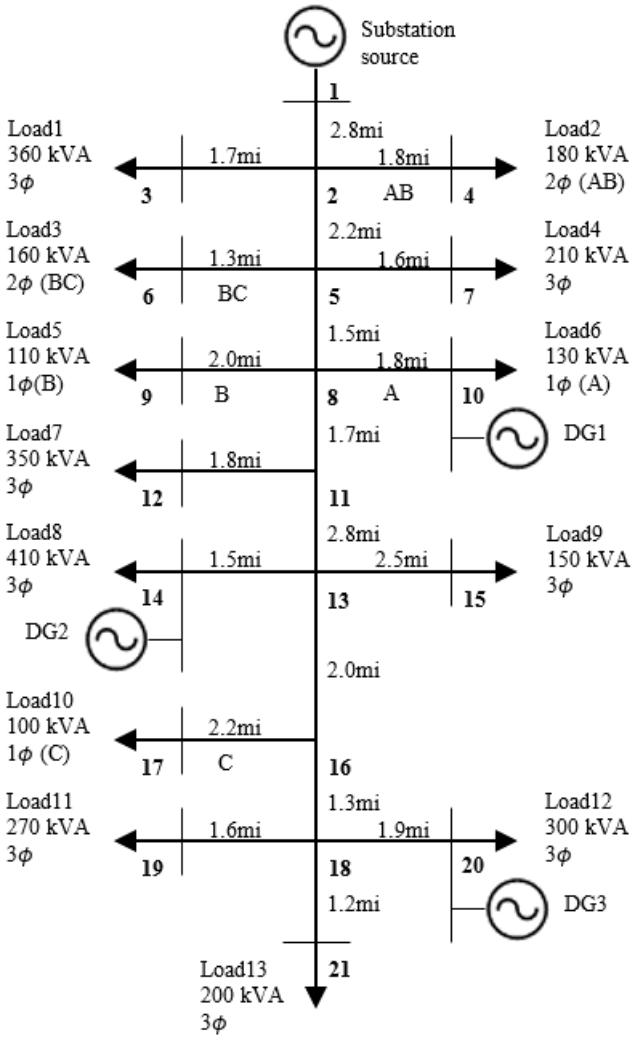

Figure 2.1 A 21 bus distribution system with DGs used for fault area identification analysis

The distribution network is divided into 4 protection areas, as seen in Figure 2.2. Note that the parameters of the system are not shown due to the limitation of space. In the figure, Area 1, Area 2, Area 3, and Area 4 represent protection areas 1, 2, 3, and 4,

respectively. We can then establish the connection matrix $\boldsymbol{N}$ and the current vector $\boldsymbol{I}$ based on Figure 2.2.

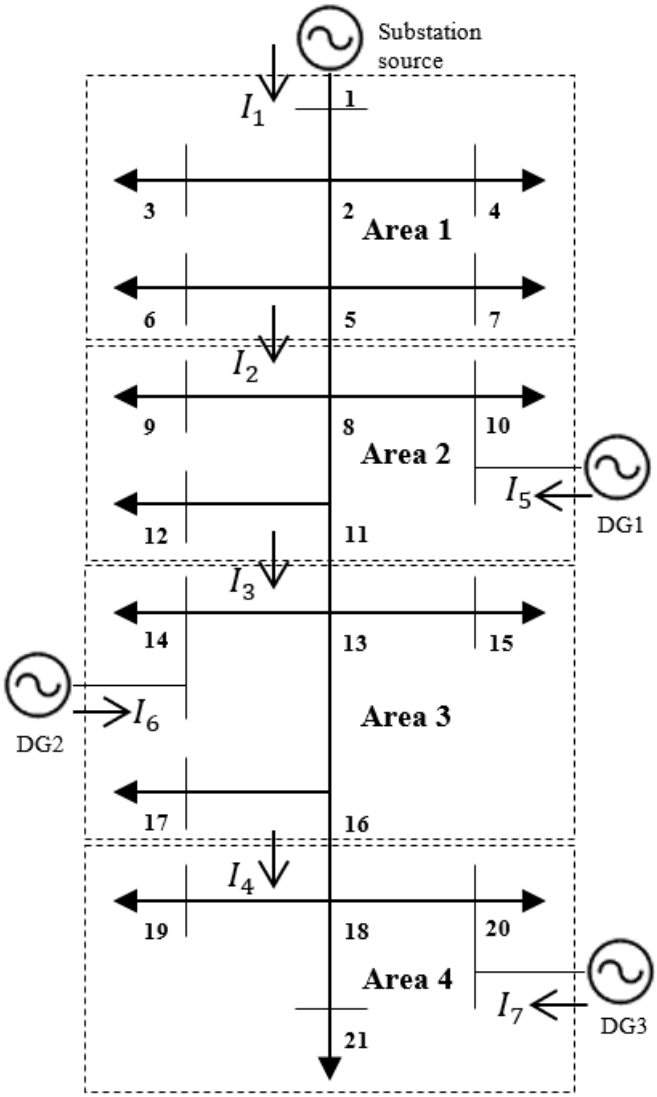

Figure 2.2 A 21 bus distribution system being divided into 4 protection areas for fault area identification analysis

The connection matrix $\boldsymbol{N}$ is:

$$\boldsymbol{N} = \begin{bmatrix} 1 & -1 & 0 & 0 & 0 & 0 & 0 \\ 0 & 1 & -1 & 0 & 1 & 0 & 0 \\ 0 & 0 & 1 & -1 & 0 & 1 & 0 \\ 0 & 0 & 0 & 1 & 0 & 0 & 1 \end{bmatrix} \tag{2.3}$$

The current vector $\boldsymbol{I}$ is:

$$\boldsymbol{I} = [I_1\ I_2\ I_3\ I_4\ I_5\ I_6\ I_7]^T \tag{2.4}$$

where superscript T denotes the transpose of a vector. Note that the units of the current phasors are ampers for this case study.

Substituting (2.3) and (2.4) into (2.2) will yield the FAIV. The FAIV preceding the fault is shown in Table 2.1. In the table, column 1 lists the area numbers. The FAIV of phase A, B, and C are listed in columns 2-4, respectively.

Table 2.1 FAIV of the 21 bus distribution system with DGs preceding the fault

Area Number	$\lvert\boldsymbol{FAIV}_A\rvert$	$\lvert\boldsymbol{FAIV}_B\rvert$	$\lvert\boldsymbol{FAIV}_C\rvert$
1	39.018	49.258	37.673
2	32.172	29.104	14.931
3	23.970	23.826	36.711
4	33.433	33.272	33.251

Note that the connection matrix $\boldsymbol{N}$ and current vector $\boldsymbol{I}$ illustrated here are also used to obtain FAIV during the fault. However, the values of $\boldsymbol{I}$ need to be replaced based on currents during the fault instead of preceding the fault. In addition, for this 21 bus distribution system, the pre-specified threshold value of $|\Delta\boldsymbol{FAIV}|$ is 100.

2.3.1.1 Single Fault Case

For the single fault study, an AG fault is imposed in protection area 1 on the line between bus 2 and 5. The absolute differences of FAIV preceding the fault and during the AG fault are listed in Table 2.2. Phase with abnormal value is listed in column 5.

It is observed that $|\Delta \boldsymbol{FAIV}_A|$ of area 1 is significantly larger than the pre-specified threshold value 100. This observation indicates that a fault is in area 1. Moreover, phase A is the only abnormal phase, and thus, the fault is determined as an AG fault.

Table 2.2 $|\Delta \boldsymbol{FAIV}|$ of the 21 bus distribution system with DGs between preceding the fault and during an AG fault

Area Number	$\|\Delta \boldsymbol{FAIV}_A\|$	$\|\Delta \boldsymbol{FAIV}_B\|$	$\|\Delta \boldsymbol{FAIV}_C\|$	Abnormal Phase
1	903.871	3.698	2.641	Phase A
2	11.460	1.802	0.728	-
3	6.831	0.388	0.580	-
4	8.805	0.277	0.287	-

It is evidenced that the proposed fault area identification method is able to correctly identify the faulted area and the faulted phase for single fault events.

2.3.1.2 Simultaneous Faults Case

For simultaneous faults, two faults are imposed in the study. One fault is a CG fault, which is imposed in area 2 on the line between bus 8 and 11. The other fault is a three-phase fault, imposed in area 4 on the line between bus 18 and 20. The absolute difference value of FAIV preceding the fault and during the simultaneous fault is presented in Table 2.3.

Based on the results listed in Table 2.3, it can be determined that there is a CG fault in area 2 and a fault involving all phases in area 4. This result is accurate.

Table 2.3 $|\Delta \boldsymbol{FAIV}|$ of the 21 bus distribution system with DGs between preceding the fault and during a simultaneous fault

Area Number	$\|\Delta \boldsymbol{FAIV}_A\|$	$\|\Delta \boldsymbol{FAIV}_B\|$	$\|\Delta \boldsymbol{FAIV}_C\|$	Abnormal Phase
1	9.447	11.705	21.490	-
2	12.950	10.110	761.473	Phase C
3	12.083	13.502	34.361	-
4	842.564	962.161	722.380	Phase A, B, and C

This example demonstrated that the proposed fault area identification method not only correctly identifies the faulted areas, but also identifies faulted phases for simultaneous faults.

2.3.2 Identifying Faulted Area for the Modified IEEE 34 Bus Distribution System with DGs

This subsection presents the evaluation studies based on simulation results. The proposed fault area identification method is applied to the modified IEEE 34 Node Test System shown in Figure 2.3. It is important to note that the test system is an unbalanced distribution system.

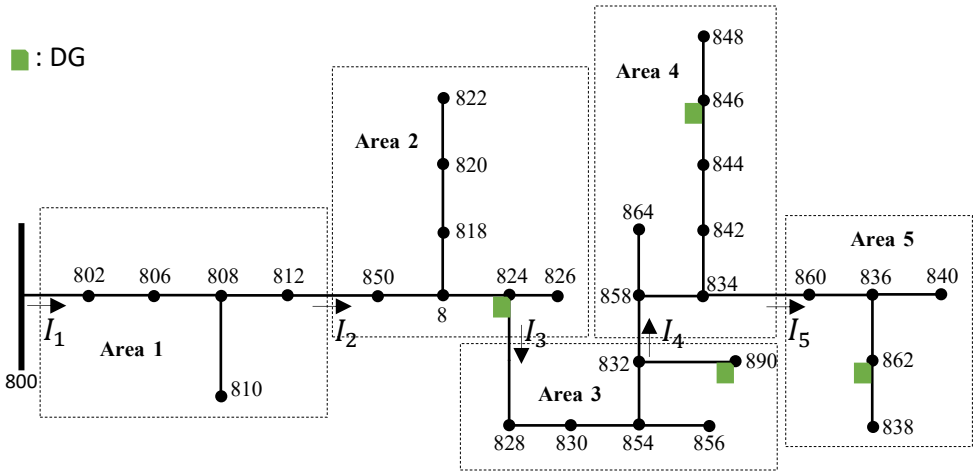

Figure 2.3 The modified IEEE 34 Bus Test System being divided into 5 protection areas for fault area identification analysis

As seen in Figure 2.3, there are four DGs in the test system. The DGs are at buses 824, 846, 862, and 890. The DGs are modeled as solar farms in the average model using Simscape Power Systems Toolbox in Simulink [42]. Each DG has the ability to provide 200 kW power at the normal operating conditions. Since the total load of the test system is 1769 KW [41], the DG penetration is around 45 percent. That is, the modified test system is an unbalanced distribution system with high penetration of DGs.

The test system is divide into five protection areas, as seen in Figure 2.3. The connection matrix $\boldsymbol{N}$ is:

$$\boldsymbol{N} = \begin{bmatrix} 1 & -1 & 0 & 0 & 0 \\ 0 & 1 & -1 & 0 & 0 \\ 0 & 0 & 1 & -1 & 0 \\ 0 & 0 & 0 & 1 & -1 \\ 0 & 0 & 0 & 0 & 1 \end{bmatrix} \tag{2.5}$$

The current vector $\boldsymbol{I}$ is:

$$\boldsymbol{I} = [I_1\ I_2\ I_3\ I_4\ I_5]^T \tag{2.6}$$

Again, superscript T denotes the transpose of a vector. Note that the current phasors are in ampers.

The fault area identification vector $\boldsymbol{FAIV}$ is obtained by substituting (2.5) and (2.6) into (2.2). The results of $\boldsymbol{FAIV}$ preceding the fault are shown in Table 2.4. The first column of the table lists the numbers for protection areas. The remain part of the columns list the FAIV values for phase A, B, and C, respectively.

In Table 2.4, it is observed that all values of FAIV are quite small. This is because the network is in normal operation without any fault. In addition, the values of FAIV for each phase of a certain protection area is not equal. This observation is expected because the test system is not a balanced system, as mentioned previously.

Table 2.4 FAIV of the modified IEEE 34 bus distribution system with DGs preceding the fault

Area number	$\lvert\boldsymbol{FAIV}_A\rvert$	$\lvert\boldsymbol{FAIV}_B\rvert$	$\lvert\boldsymbol{FAIV}_C\rvert$
1	0.4507	4.5718	2.6307
2	17.0125	0.3733	0.3708
3	5.3298	3.2478	3.0341
4	11.0265	11.7100	11.3418
5	11.3639	16.5882	18.5307

Note that the connection matrix $\boldsymbol{N}$ and current vector $\boldsymbol{I}$ illustrated here are also used to obtain FAIV during the fault. However, the values of $\boldsymbol{I}$ need to be replaced based

on currents during the fault instead of preceding the fault. In addition, for the modified IEEE 34 bus distribution system, the pre-specified threshold value of $|\Delta \boldsymbol{FAIV}|$ is 100.

2.3.2.1 Single Fault Case

Consider a BCG fault that occurs on the line segment between bus 828 and 830. The absolute differences of FAIV preceding the fault and during the fault are summarized in Table 2.5. For each protection area in the first column, the second to fourth columns list the values of $|\Delta \boldsymbol{FZIV}|$ for phase A, B, and C, respectively.

From Table 2.5, it is clear that that $|\Delta \boldsymbol{FZIV}_B|$ and $|\Delta \boldsymbol{FZIV}_C|$ for protection area 3 exceeds the pre-specified threshold value 100. Thus, it is determined that there is a fault involving phase B and C in the protection area 3. The indication is expected because the line between bus 828 and 830 is in protection area 3.

Table 2.5 $|\Delta \boldsymbol{FAIV}|$ of the modified IEEE 34 bus distribution system with DGs between preceding the fault and during a BC fault

Area number	$\|\Delta \boldsymbol{FZIV}_A\|$	$\|\Delta \boldsymbol{FZIV}_B\|$	$\|\Delta \boldsymbol{FZIV}_C\|$	Abnormal Phase
1	0.0016	0.5764	0.2641	-
2	1.2623	0.2163	0.1945	-
3	18.9083	496.0368	430.1065	Phase B and C
4	13.1086	9.8152	20.8072	-
5	16.3792	24.0290	42.959	-

2.3.2.2 Simultaneous Faults Case

Impose an AG fault on a single lateral line that between bus 806 and 808. In the same time, impose an LLLG fault on the line between bus 828 and 830. The absolute difference of FAIV preceding and during the fault is shown in Table 2.6.

It is found that $|\Delta \boldsymbol{FZIV}_A|$ for protection area 1 and $|\Delta \boldsymbol{FZIV}_A|$, $|\Delta \boldsymbol{FZIV}_B|$, and $|\Delta \boldsymbol{FZIV}_C|$ for protection area 3 exceeds the pre-specified threshold value 100. This observation indicates that there is an AG fault in protection area 1, and another fault involving phase A, B, and C in area 3.

Since the line between bus 806 and 808 is in protection area 1, and the line between bus 828 and 830 is in protection area 3, the decision is accurate.

Table 2.6 $|\Delta \boldsymbol{FAIV}|$ of the modified IEEE 34 bus distribution system with DGs between preceding the fault and during a simultaneous fault

Area number	$\|\Delta \boldsymbol{FZIV}_A\|$	$\|\Delta \boldsymbol{FZIV}_B\|$	$\|\Delta \boldsymbol{FZIV}_C\|$	Abnormal Phase
1	421.3153	0.7453	0.3931	Phase A
2	14.5554	0.2640	0.2858	-
3	460.8100	544.0321	539.5311	Phase A, B, and C
4	12.3621	8.6128	1.4382	-
5	34.8307	22.6271	8.7457	-

2.3.3 Identifying Faulted Area for a 27 Bus Transmission Systems

This subsection presents the results for the proposed fault area identification method for a 27 bus transmission system shown in Figure 2.4. In the figure, the lengths of transmission lines are shown in parentheses. In particular, the line between bus 9 and bus 10 is a long

double-circuit transmission line. The transmission system is modeled in EMTP [46] to obtain the measurements at each bus for fault scenarios with different fault locations, types, and resistances. The measurements obtained then are utilized to test the developed method that is implemented in Matlab [42].

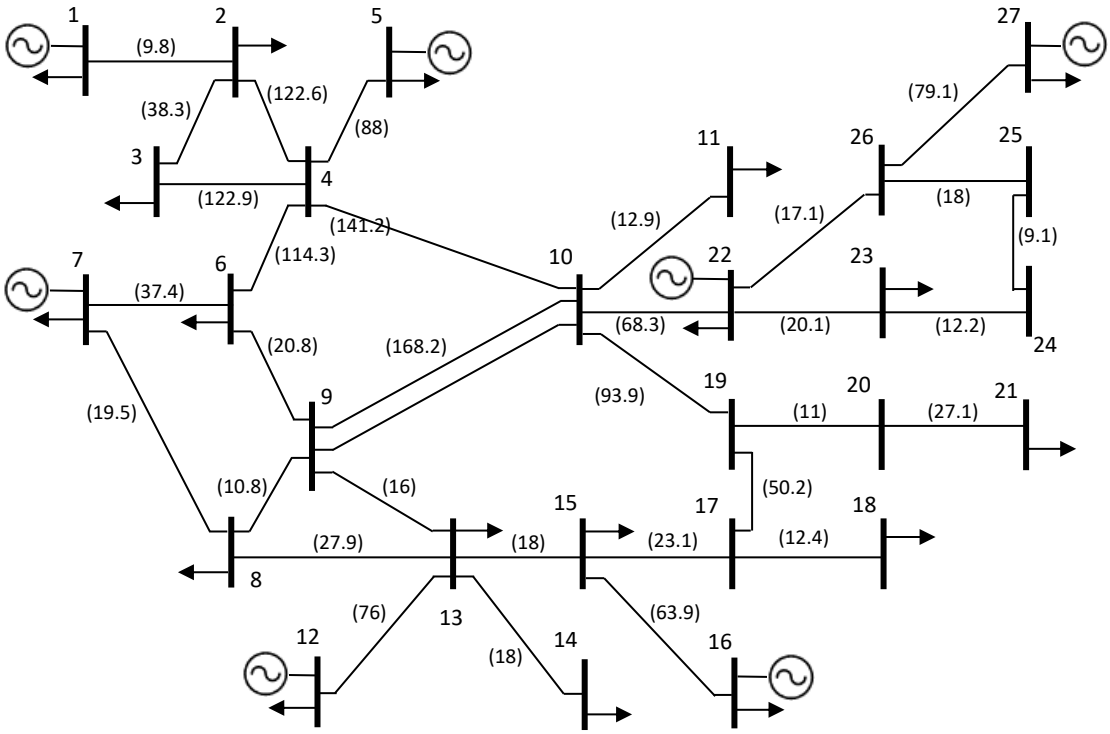

Figure 2.4 A 27 bus transmission system used for fault area identification analysis

The studied transmission system is partitioned into five protection areas as shown in Figure 2.5. Due to the space limitation, the bus numbers, line lengths, and the direction of currents are not labeled in Figure 2.5. To clarify the current directions, the rules used to select the direction of currents are explained as follows:

(1) It is natural to select the direction as current flows from a generator into a protection area.

(2) For line currents that flow from bus to bus, the current direction is selected as from a smaller bus number to a larger bus number.

In this case study, the above rules are obeyed expect that the current direction between bus 17 and 19.

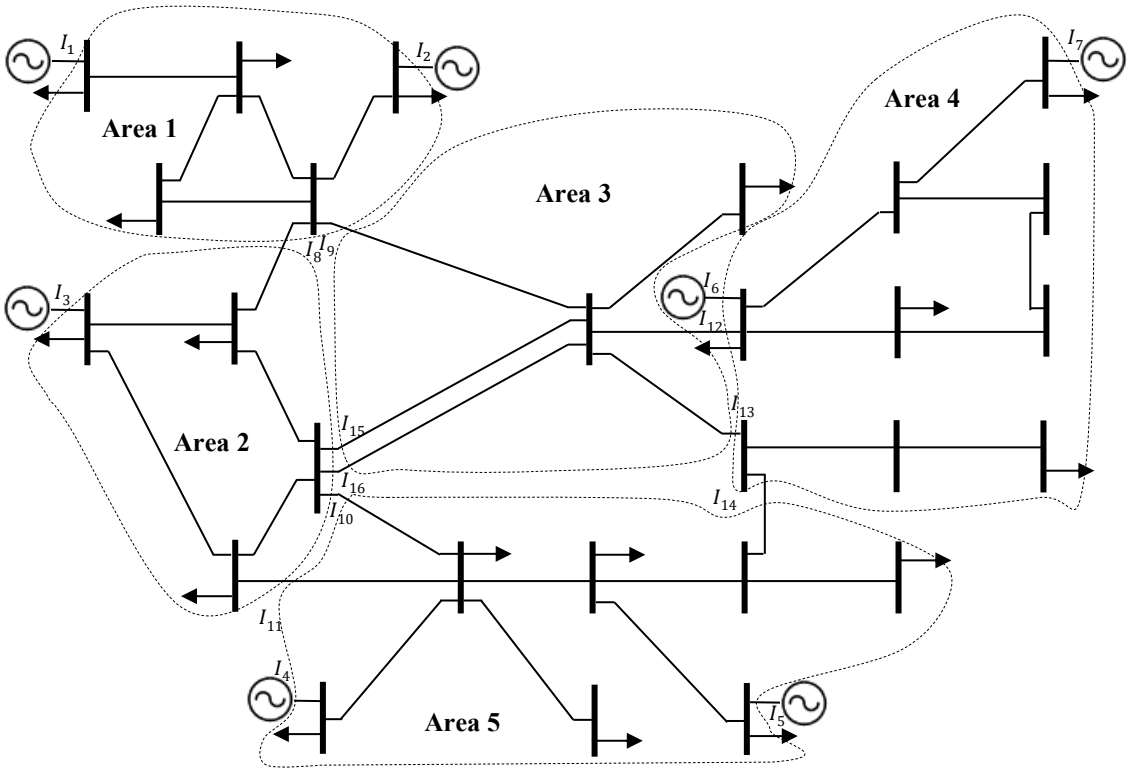

Figure 2.5 A 27 bus transmission system being divided into 5 protection areas for fault area identification analysis

The connection matrix ***N*** is:

$$\boldsymbol{N} = \begin{bmatrix} 1 & 0 & 0 & 0 & 0 \\ 1 & 0 & 0 & 0 & 0 \\ 0 & 1 & 0 & 0 & 0 \\ 0 & 0 & 0 & 0 & 1 \\ 0 & 0 & 0 & 0 & 1 \\ 0 & 0 & 0 & 1 & 0 \\ 0 & 0 & 0 & 1 & 0 \\ -1 & 1 & 0 & 0 & 0 \\ -1 & 0 & 1 & 0 & 0 \\ 0 & -1 & 0 & 0 & 1 \\ 0 & -1 & 0 & 0 & 1 \\ 0 & 0 & -1 & 1 & 0 \\ 0 & 0 & -1 & 1 & 0 \\ 0 & 0 & 0 & -1 & 1 \\ 0 & -1 & 1 & 0 & 0 \\ 0 & -1 & 1 & 0 & 0 \end{bmatrix}^T \tag{2.7}$$

It is important to note that there is a superscript T in (2.7), where T denotes transpose of a matrix.

The current vector $\boldsymbol{I}$ is given by

$$\boldsymbol{I} = [I_1 \quad I_2 \quad I_3 \quad \cdots \quad I_{16}]^T \tag{2.8}$$

and the current phasors are in per unit for this case study.

The FAIV is then obtained by substituting (2.7) and (2.8) into (2.2). The results of FAIV preceding the fault are summarized in Table 2.7. The first column of Table 2.7 lists the protection area numbers. The rest columns of Table 2.7 list the values of FAIV for phase A, B, and C, respectively.

From Table 2.7, it is observed that the values of FAIV for a certain protection area preceding the fault are identical. The observation is reasonable because the transmission system is a balanced system preceding the fault.

Table 2.7 FAIV of the 27 bus transmission system preceding the fault

Area Number	$\boldsymbol{FAIV_A}$	$\boldsymbol{FAIV_B}$	$\boldsymbol{FAIV_C}$
1	3.606	3.606	3.606
2	2.496	2.496	2.496
3	4.224	4.224	4.224
4	4.027	4.027	4.027
5	4.653	4.653	4.653

Note that the connection matrix $\boldsymbol{N}$ and current vector $\boldsymbol{I}$ illustrated in this subsection are also used to get the FAIV during the fault. However, the values of $\boldsymbol{I}$ need to be calculated based on currents during the fault instead of preceding the fault. In addition, the pre-specified threshold value is 5 per unit for this transmission system.

2.3.3.1 Single Fault Case

Consider a BC fault that occurs on the line between bus 6 and 9. The results of $|\boldsymbol{\Delta FAIV}|$ between preceding the fault and during the fault are summarized in Table 2.8. The first column of the table lists the protection area numbers. The second to fourth columns of the table list the values of $|\boldsymbol{\Delta FAIV}|$ for phase A, B, and C, respectively.

It is observed that $|\boldsymbol{\Delta FZIV_B}|$ and $|\boldsymbol{\Delta FZIV_C}|$ for protection area 2 is larger than the pre-specified threshold value 5. Hence, a fault involving phase B and phase C in the protection area 2 can be determined.

Table 2.8 $|\Delta \boldsymbol{FAIV}|$ of the 27 bus transmission system between preceding the fault and during a BC fault

Area Number	$\|\Delta \boldsymbol{FAIV}_A\|$	$\|\Delta \boldsymbol{FAIV}_B\|$	$\|\Delta \boldsymbol{FAIV}_C\|$	Abnormal Phase
1	0.018	0.518	0.766	-
2	0.957	38.420	35.004	Phase B and C
3	0.590	1.566	1.553	-
4	0.027	0.664	1.132	-
5	0.020	1.477	1.573	-

This example demonstrates that the proposed fault area identification method is able to identify the fault area and faulted phase for a single fault in transmission systems.

2.3.3.2 Simultaneous Faults Case

Impose a BC fault on the line between bus 6 and 9. In the meanwhile, impose a BG fault on the double-circuit line between bus 9 and 10. The results of $|\Delta \boldsymbol{FAIV}|$ between preceding the fault and during the fault are summarized in Table 2.9.

Table 2.9 shows that $|\Delta \boldsymbol{FAIV}_B|$ and $|\Delta \boldsymbol{FAIV}_C|$ for protection area 2 and $|\Delta \boldsymbol{FZIV}_C|$ for protection area 3 are larger than the pre-specified threshold value 5. Thus, a simultaneous fault can be determined to be existing in the transmission system. This is expected because the line between bus 6 and 9 is in protection area 2 and the line between bus 9 and 10 is in protection area 3.

Table 2.9 $|\Delta \boldsymbol{FAIV}|$ of the 27 bus transmission system between preceding the fault and during a simultaneous fault

Area Number	$\lvert\Delta \boldsymbol{FAIV}_A\rvert$	$\lvert\Delta \boldsymbol{FAIV}_B\rvert$	$\lvert\Delta \boldsymbol{FAIV}_C\rvert$	Abnormal Phase
1	0.056	0.711	0.699	-
2	0.984	38.149	33.503	Phase B and C
3	0.227	9.603	2.558	Phase B
4	0.131	1.280	0.974	-
5	0.209	1.709	1.521	-

It is evidenced that the proposed fault area identification method not only identifies the faulted areas but also identifies faulted phases for simultaneous faults in the transmission systems.

2.4 Summary

The fault area identification method is developed in this chapter. The method aims to pinpoint the faulted area and reduce the number of line segments needed to be examined for fault location. It is assumed the topology of the power network is known. The method uses synchronized current phasor measurements to identify the faulted protection area and faulted phases.

The developed method is evaluated for distribution systems and transmission systems. Evaluation studies show that the fault area identification method is applicable to distribution systems with DGs and transmission systems. Moreover, evaluation studies

validate the method is able to handle single fault cases as well as simultaneous faults events.

Chapter 3 Fault Location Algorithms for Simultaneous Faults in Distribution Systems with DGs

In this chapter, three fault location algorithms for locating simultaneous faults in a distribution system with DGs are proposed [40][43][44]. Certainly, the proposed algorithms are able to locate a single fault as well.

Without loss of generality, let us consider a simultaneous fault that occurs in a distribution system. Fictitious fault buses will be added during the fault. Then the bus impedance matrix with added fictitious fault buses can be established. Furthermore, the measured voltages at each bus during the fault are functions of the relevant driving point and transfer impedances. Moreover, the driving point and the transfer impedances are derived in terms of the fault locations. Therefore, the measured voltages during the fault can be derived in terms of the fault locations as well. Consequently, the fault locations can be solved using the available voltage measurements.

Three types of fault location algorithms are proposed. Type I and Type III algorithms do not require source impedances and require current measurements at all sources. Type II algorithm requires source impedances and requires only voltage measurements at selected locations.

In this chapter, Section 3.1 describes the foundation that used to develop the proposed new fault location algorithms, Section 3.2, 3.3, and 3.4 presents the proposed Type I, Type II, and Type III algorithms, respectively. Section 3.5 reports the evaluation studies, followed by the summary.

3.1 The Basis for the proposed fault location Algorithms

Without loss of generality, we assume that a three-phase fault occurs on a three-phase line segment of a distribution network. In addition, it is assumed that the network has one substation and one DG.

During the fault, the currents injected into the network include the source currents and the fault current. The source currents flow into the network from sources connected to buses, and the fault current flows out of the network at the fault point. Hence, the fault voltage at any bus can be expressed as

$$\boldsymbol{E}_L = \boldsymbol{Z}_{LK}\boldsymbol{I}_K - \boldsymbol{Z}_{LF}\boldsymbol{I}_F \tag{3.1}$$

The notations are explained as follows:

$\boldsymbol{E}_L$ is the voltage at bus L during the fault, and $\boldsymbol{E}_L = [E_{L^1}\ E_{L^2}\ E_{L^3}]^T$. In this chapter, the superscript T denotes the transpose of a vector or matrix, and the superscripts 1, 2, 3 denote phases A, B, and C.

$\boldsymbol{I}_K$ represents the source currents. The sources include the substation and DG. Thus, $\boldsymbol{I}_K = [I_{S^1}\ I_{S^2}\ I_{S^3}\ I_{DG^1}\ I_{DG^2}\ I_{DG^3}]^T$, or $\boldsymbol{I}_K = [I_S\ \ I_{DG}]^T$. The subscript S denotes the substation.

$\boldsymbol{I}_F$ is the fault current vector at the added fictitious fault bus F, and $\boldsymbol{I}_F = [I_{F^1}\ I_{F^2}\ I_{F^3}]^T$.

$\boldsymbol{Z}_{LK}$ is the transfer impedance between bus L and source buses. Hence, $\boldsymbol{Z}_{LK}$ is given by

$$\boldsymbol{Z}_{LK} = \begin{bmatrix} Z_{L^1S^1} & Z_{L^1S^2} & Z_{L^1S^3} & Z_{L^1DG^1} & Z_{L^1DG^2} & Z_{L^1DG^3} \\ Z_{L^2S^1} & Z_{L^2S^2} & Z_{L^2S^3} & Z_{L^2DG^1} & Z_{L^2DG^2} & Z_{L^2DG^3} \\ Z_{L^3S^1} & Z_{L^3S^2} & Z_{L^3S^3} & Z_{L^3DG^1} & Z_{L^3DG^2} & Z_{L^3DG^3} \end{bmatrix}$$

The matrix for $\boldsymbol{Z}_{LK}$ can be written more compactly as

$$\boldsymbol{Z}_{LK} = [\boldsymbol{Z}_{LS} \quad \boldsymbol{Z}_{LDG}]$$

In which $\boldsymbol{Z}_{LS}$ is the first three columns of $\boldsymbol{Z}_{LK}$, and $\boldsymbol{Z}_{LDG}$ is the last three columns of $\boldsymbol{Z}_{LK}$.

$\boldsymbol{Z}_{LF}$ is the transfer impedance between bus L and fault bus F. We may write $\boldsymbol{Z}_{LF}$ in matrix form as

$$\boldsymbol{Z}_{LF} = \begin{bmatrix} Z_{L^1F^1} & Z_{L^1F^2} & Z_{L^1F^3} \\ Z_{L^2F^1} & Z_{L^2F^2} & Z_{L^2F^3} \\ Z_{L^3F^1} & Z_{L^3F^2} & Z_{L^3F^3} \end{bmatrix}$$

The fault current vector $\boldsymbol{I}_F$ can be extracted from (3.1) using the Pseudo inverse technique

$$\boldsymbol{I}_F = (\boldsymbol{Z}_{LF}^T \boldsymbol{Z}_{LF})^{-1}[\boldsymbol{Z}_{LF}^T(\boldsymbol{Z}_{LK}\boldsymbol{I}_K - \boldsymbol{E}_L)] \tag{3.2}$$

Note that we do not take the inverse of $\boldsymbol{Z}_{LF}$ directly in (3.2). This is because $\boldsymbol{Z}_{LF}$ may not be a square matrix.

Since (3.1) is applicable to any bus in the network, the fault voltage $\boldsymbol{E}_F$ at the fault bus F is obtained by substituting F for L in (3.1). Then, we have,

$$\boldsymbol{E}_F = \boldsymbol{Z}_{FK}\boldsymbol{I}_K - \boldsymbol{Z}_{FF}\boldsymbol{I}_F \tag{3.3}$$

where $\boldsymbol{Z}_{FK}$ is the transfer impedance between bus F and source buses, and $\boldsymbol{Z}_{FF}$ is the driving point impedance at bus F. $\boldsymbol{Z}_{FK}$ and $\boldsymbol{Z}_{FF}$ can be written in a similar way to $\boldsymbol{Z}_{LK}$ and $\boldsymbol{Z}_{LF}$ by substituting F for L, respectively. It should be pointed out that $\boldsymbol{Z}_{FK}$, $\boldsymbol{Z}_{FF}$, and $\boldsymbol{Z}_{LF}$ are functions of the desired unknown fault location variable.

The complex power S consumed by the fault resistance is

$$S = \boldsymbol{E}_F \boldsymbol{I}_F^* \tag{3.4}$$

where the superscript * denotes complex conjugate of a vector.

The fault resistance is purely resistive, and it does not consume reactive power. Therefore,

$$\text{Imag}(S) = 0 \tag{3.5}$$

where Imag(.) returns the imaginary part of its argument.

Given the voltage measurement during the fault at bus L and currents at sources, equation (3.5) contains only one unknown variable: the fault location. The bus L can be a source bus or any other bus, and most likely be the source bus since the method requires source currents. The Newton-Raphson technique can be applied to (3.5) to solve the fault location. The derivation holds for any type of faults.

Alternatively, by assuming voltage measurements from two buses L_1 and L_2 are available, the voltages during the fault are given by

$$\boldsymbol{E}_{L_1} = \boldsymbol{Z}_{L_1K}\boldsymbol{I}_K - \boldsymbol{Z}_{L_1F}\boldsymbol{I}_F \tag{3.6}$$

$$\boldsymbol{E}_{L_2} = \boldsymbol{Z}_{L_2K}\boldsymbol{I}_K - \boldsymbol{Z}_{L_2F}\boldsymbol{I}_F \tag{3.7}$$

where, $\boldsymbol{E}_{L_1}$ and $\boldsymbol{E}_{L_2}$ are voltage measurements at buses L_1 and L_2 during the fault.

It follows from (3.6) and (3.7) that

$$\begin{aligned}\left[\boldsymbol{Z}_{L_1F}^T\boldsymbol{Z}_{L_1F}\right]^{-1}\left[\boldsymbol{Z}_{L_1F}^T\left(\boldsymbol{Z}_{L_1K}\boldsymbol{I}_K - \boldsymbol{E}_{L_1}\right)\right] = \\ \left[\boldsymbol{Z}_{L_2F}^T\boldsymbol{Z}_{L_2F}\right]^{-1}\left[\boldsymbol{Z}_{L_2F}^T\left(\boldsymbol{Z}_{L_2K}\boldsymbol{I}_K - \boldsymbol{E}_{L_2}\right)\right]\end{aligned} \tag{3.8}$$

The fault location is the only unknown variable contained in (3.8), which can be estimated based on the Newton-Raphson technique.

In general, when measurements from more than two buses are available, optimal estimation theory can be used to detect possible bad measurements and enhance fault location estimation accuracy. The optimal fault location estimation is presented in Chapter 4.

Since $\boldsymbol{I}_K$ and $\boldsymbol{Z}_{LK}$ can be modified according to the number of DGs, the fault location method can be applied to a distribution network with multiple DGs. Since $\boldsymbol{I}_F$ and $\boldsymbol{Z}_{LF}$ can be adjusted according to the number of fault nodes, the fault location method can be applied to any type of fault.

3.2 Proposed Type I Fault Location Algorithm

In recent years, the distribution systems have witnessed an increasing deployment of DG, especially IBG such as solar PV systems with smart inverters. The source impedance of IBG is hard to obtain due to the complexity and uncertainty of IBG modeling.

In this subsection, the proposed Type I fault location algorithm will be presented. The algorithm is capable of locating simultaneous faults as well as a single fault for distribution systems with DGs. It uses current measurements captured at the substation and DG sites, and voltage measurements captured at the selected locations. In practice, it is natural to use the voltage measurements at the local substation. The measurements used are phasor values at the fundamental frequency. It is important to note that source impedances are not needed, and the bus impedance matrix does not contain source impedance.

A scenario involving a simultaneous fault is illustrated in Figure 3.1. In the figure, two faults occur at location F_1 on line segment P_1Q_1 with fault location m_1, and at location F_2 on line segment P_2Q_2 with fault location m_2, respectively. Note that m_1 is not necessarily equal to m_2.

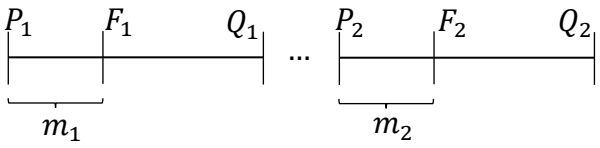

Figure 3.1 Illustration of a simultaneous fault in distribution systems

The current injections to the network include the line currents at the sources and the fault currents. During the fault, the fault currents are leaving the network. Based on superposition theory, the voltage at any bus L during the fault can be expressed as

$$\boldsymbol{E}_L = \boldsymbol{Z}_{LK}\boldsymbol{I}_K - \boldsymbol{Z}_{LF_1}\boldsymbol{I}_{F_1} - \boldsymbol{Z}_{LF_2}\boldsymbol{I}_{F_2} \tag{3.9}$$

where,

$\boldsymbol{E}_L$: the voltage at bus L during the fault;

$\boldsymbol{Z}_{LK}$: the transfer impedance between bus L and source bus K;

$\boldsymbol{I}_K$: line currents during the fault at source bus K. $\boldsymbol{I}_K = \left[I_{substation}, I_{DG_1}, I_{DG_2}, \dots\right]^T$;

$\boldsymbol{Z}_{LF_1}$, $\boldsymbol{Z}_{LF_2}$: the transfer impedance between bus L and fault buses F_1, F_2, respectively;

$\boldsymbol{I}_{F_1}$, $\boldsymbol{I}_{F_2}$: the fault currents at the fictitious fault buses F_1, F_2, respectively.

Assume that voltage measurements from two buses L_1 and L_2 are known. Substituting $\boldsymbol{E}_{L_1}$ and $\boldsymbol{E}_{L_2}$into (3.9) yields

$$\boldsymbol{E}_{L_1} = \boldsymbol{Z}_{L_1K}\boldsymbol{I}_K - \boldsymbol{Z}_{L_1F_1}\boldsymbol{I}_{F_1} - \boldsymbol{Z}_{L_1F_2}\boldsymbol{I}_{F_2} \tag{3.10}$$

$$\boldsymbol{E}_{L_2} = \boldsymbol{Z}_{L_2K}\boldsymbol{I}_K - \boldsymbol{Z}_{L_2F_1}\boldsymbol{I}_{F_1} - \boldsymbol{Z}_{L_2F_2}\boldsymbol{I}_{F_2} \tag{3.11}$$

where,

$\boldsymbol{E}_{L_1}$, $\boldsymbol{E}_{L_2}$: the voltage at bus L_1 and L_2 during the fault, respectively;

$\boldsymbol{Z}_{L_1F_1}$, $\boldsymbol{Z}_{L_1F_2}$: the transfer impedances between bus L_1 and fault buses F_1, F_2, respectively;

$\boldsymbol{Z}_{L_2F_1}$, $\boldsymbol{Z}_{L_2F_2}$: the transfer impedances between bus L_2 and fault buses F_1, F_2, respectively.

We can write (3.10) and (3.11) in matrix format as

$$\begin{bmatrix}\boldsymbol{E}_{L_1}\\ \boldsymbol{E}_{L_2}\end{bmatrix} = \begin{bmatrix}\boldsymbol{Z}_{L_1K}\\ \boldsymbol{Z}_{L_2K}\end{bmatrix}\boldsymbol{I}_K - \begin{bmatrix}\boldsymbol{Z}_{L_1F_1} & \boldsymbol{Z}_{L_1F_2}\\ \boldsymbol{Z}_{L_2F_1} & \boldsymbol{Z}_{L_2F_2}\end{bmatrix}\begin{bmatrix}\boldsymbol{I}_{F_1}\\ \boldsymbol{I}_{F_2}\end{bmatrix} \tag{3.12}$$

For brevity, we may simplify the coefficients of (3.12), which then becomes

$$\boldsymbol{E}_{L_1L_2} = \boldsymbol{Z}_{L_1L_2K}\boldsymbol{I}_K - \boldsymbol{Z}_{L_1L_2F_1F_2}\boldsymbol{I}_{F_1F_2} \tag{3.13}$$

From (3.13), the fault current vector is then derived as

$$\boldsymbol{I}_{F_1F_2} = \left(\boldsymbol{Z}^T_{L_1L_2F_1F_2}\boldsymbol{Z}_{L_1L_2F_1F_2}\right)^{-1}\boldsymbol{Z}^T_{L_1L_2F_1F_2}\left(\boldsymbol{Z}_{L_1L_2K}\boldsymbol{I}_K - \boldsymbol{E}_{L_1L_2}\right) \tag{3.14}$$

Note that $\boldsymbol{Z}_{L_1L_2F_1F_2}$ is not always a square matrix. This is why we do not take the inverse of $\boldsymbol{Z}_{L_1L_2F_1F_2}$ directly in (3.14).

Based on (3.13), the voltages at the fault locations F_1 and F_2 can be expressed as

$$\boldsymbol{E}_{F_1F_2} = \boldsymbol{Z}_{F_1F_2K}\boldsymbol{I}_K - \boldsymbol{Z}_{F_1F_2F_1F_2}\boldsymbol{I}_{F_1F_2} \tag{3.15}$$

The dimensions of the matrices depend on the available phases of involved circuits. For example, assuming both faults are three phases, $\boldsymbol{Z}_{F_1F_2F_1F_2}$ takes the following expanded form:

$$\boldsymbol{Z}_{F_1F_2F_1F_2} = \begin{bmatrix} \boldsymbol{Z}_{F_1^1F_1^1} & \boldsymbol{Z}_{F_1^1F_1^2} & \boldsymbol{Z}_{F_1^1F_1^3} & \boldsymbol{Z}_{F_1^1F_2^1} & \boldsymbol{Z}_{F_1^1F_2^2} & \boldsymbol{Z}_{F_1^1F_2^3} \\ \boldsymbol{Z}_{F_1^2F_1^1} & \boldsymbol{Z}_{F_1^2F_1^2} & \boldsymbol{Z}_{F_1^2F_1^3} & \boldsymbol{Z}_{F_1^2F_2^1} & \boldsymbol{Z}_{F_1^2F_2^2} & \boldsymbol{Z}_{F_1^2F_2^3} \\ \boldsymbol{Z}_{F_1^3F_1^1} & \boldsymbol{Z}_{F_1^3F_1^2} & \boldsymbol{Z}_{F_1^3F_1^3} & \boldsymbol{Z}_{F_1^3F_2^1} & \boldsymbol{Z}_{F_1^3F_2^2} & \boldsymbol{Z}_{F_1^3F_2^3} \\ \boldsymbol{Z}_{F_2^1F_1^1} & \boldsymbol{Z}_{F_2^1F_1^2} & \boldsymbol{Z}_{F_2^1F_1^3} & \boldsymbol{Z}_{F_2^1F_2^1} & \boldsymbol{Z}_{F_2^1F_2^2} & \boldsymbol{Z}_{F_2^1F_2^3} \\ \boldsymbol{Z}_{F_2^2F_1^1} & \boldsymbol{Z}_{F_2^2F_1^2} & \boldsymbol{Z}_{F_2^2F_1^3} & \boldsymbol{Z}_{F_2^2F_2^1} & \boldsymbol{Z}_{F_2^2F_2^2} & \boldsymbol{Z}_{F_2^2F_2^3} \\ \boldsymbol{Z}_{F_2^3F_1^1} & \boldsymbol{Z}_{F_2^3F_1^2} & \boldsymbol{Z}_{F_2^3F_1^3} & \boldsymbol{Z}_{F_2^3F_2^1} & \boldsymbol{Z}_{F_2^3F_2^2} & \boldsymbol{Z}_{F_2^3F_2^3} \end{bmatrix}$$

where, the subscript of F indicates fault 1 or 2, and its superscript indicates faulted phase, so $\boldsymbol{Z}_{F_1^1F_1^1}$ is self impedance for phase 1 of fault 1, $\boldsymbol{Z}_{F_1^1F_1^2}$ is transfer impedance between phase 1 and phase 2 of fault 1, $\boldsymbol{Z}_{F_1^1F_2^1}$ is transfer impedance between phase 1 of fault 1 and phase 1 of fault 2, etc.

$\boldsymbol{Z}_{L_1L_2F_1F_2}$ takes the following expanded form:

$$\boldsymbol{Z}_{L_1L_2F_1F_2} = \begin{bmatrix} \boldsymbol{Z}_{L_1^1F_1^1} & \boldsymbol{Z}_{L_1^1F_1^2} & \boldsymbol{Z}_{L_1^1F_1^3} & \boldsymbol{Z}_{L_1^1F_2^1} & \boldsymbol{Z}_{L_1^1F_2^2} & \boldsymbol{Z}_{L_1^1F_2^3} \\ \boldsymbol{Z}_{L_1^2F_1^1} & \boldsymbol{Z}_{L_1^2F_1^2} & \boldsymbol{Z}_{L_1^2F_1^3} & \boldsymbol{Z}_{L_1^2F_2^1} & \boldsymbol{Z}_{L_1^2F_2^2} & \boldsymbol{Z}_{L_1^2F_2^3} \\ \boldsymbol{Z}_{L_1^3F_1^1} & \boldsymbol{Z}_{L_1^3F_1^2} & \boldsymbol{Z}_{L_1^3F_1^3} & \boldsymbol{Z}_{L_1^3F_2^1} & \boldsymbol{Z}_{L_1^3F_2^2} & \boldsymbol{Z}_{L_1^3F_2^3} \\ \boldsymbol{Z}_{L_2^1F_1^1} & \boldsymbol{Z}_{L_2^1F_1^2} & \boldsymbol{Z}_{L_2^1F_1^3} & \boldsymbol{Z}_{L_2^1F_2^1} & \boldsymbol{Z}_{L_2^1F_2^2} & \boldsymbol{Z}_{L_2^1F_2^3} \\ \boldsymbol{Z}_{L_2^2F_1^1} & \boldsymbol{Z}_{L_2^2F_1^2} & \boldsymbol{Z}_{L_2^2F_1^3} & \boldsymbol{Z}_{L_2^2F_2^1} & \boldsymbol{Z}_{L_2^2F_2^2} & \boldsymbol{Z}_{L_2^2F_2^3} \\ \boldsymbol{Z}_{L_2^3F_1^1} & \boldsymbol{Z}_{L_2^3F_1^2} & \boldsymbol{Z}_{L_2^3F_1^3} & \boldsymbol{Z}_{L_2^3F_2^1} & \boldsymbol{Z}_{L_2^3F_2^2} & \boldsymbol{Z}_{L_2^3F_2^3} \end{bmatrix}$$

Since the fault resistances are purely resistive, the reactive power consumed by fault resistances at the two fault locations is zero, i.e.,

$$\text{Imag}\left(\begin{bmatrix} \boldsymbol{E}_{F_1}^T \boldsymbol{I}_{F_1}^* \\ \boldsymbol{E}_{F_2}^T \boldsymbol{I}_{F_2}^* \end{bmatrix}\right) = 0 \tag{3.16}$$

where $\text{Imag}(.)$ denotes the imaginary part of its argument and superscript $*$ denotes complex conjugate.

Then, the two unknown fault location variables m_1 and m_2 can be determined by solving the set of two real equations in (3.16).

An alternative approach is described as follows when more voltage measurements are available. Assume that the voltage measurement from another bus L_3 is known. Then, following (3.14), it is obtained that

$$\boldsymbol{I}_{F_1F_2} = \left(\boldsymbol{Z}_{L_1L_3F_1F_2}^T \boldsymbol{Z}_{L_1L_3F_1F_2}\right)^{-1} \boldsymbol{Z}_{L_1L_3F_1F_2}^T \left(\boldsymbol{Z}_{L_1L_3K}\boldsymbol{I}_K - \boldsymbol{E}_{L_1L_3}\right) \tag{3.17}$$

Combining (3.14) and (3.17) yields

$$\begin{aligned} &\left(\boldsymbol{Z}_{L_1L_2F_1F_2}^T \boldsymbol{Z}_{L_1L_2F_1F_2}\right)^{-1} \boldsymbol{Z}_{L_1L_2F_1F_2}^T \left(\boldsymbol{Z}_{L_1L_2K}\boldsymbol{I}_K - \boldsymbol{E}_{L_1L_2}\right) \\ &\quad = \left(\boldsymbol{Z}_{L_1L_3F_1F_2}^T \boldsymbol{Z}_{L_1L_3F_1F_2}\right)^{-1} \boldsymbol{Z}_{L_1L_3F_1F_2}^T \left(\boldsymbol{Z}_{L_1L_3K}\boldsymbol{I}_K - \boldsymbol{E}_{L_1L_3}\right) \end{aligned} \tag{3.18}$$

Equation (3.18) contains two unknown variables m_1 and m_2. Solving (3.18) will yield the desired fault locations.

3.3 Proposed Type II Fault Location Algorithm

In practice, the short circuit current contribution from DG may not be monitored. In addition, DG power outputs may be intermittent and can no longer be treated as constants in fault location method development. In this subsection, a fault location method without using current measurements is proposed to deal with the aforementioned challenges.

Consider the simultaneous fault illustrated in Figure 3.1 again. Voltage measurements from specified locations are utilized to locate the unknown fault location m_1 and m_2. Note that for the Type II algorithm, the bus impedance matrix constructed does include source impedances. The voltage at any bus L during the fault can be expressed as

$$\boldsymbol{E}_L = \boldsymbol{E}_L^0 - [\boldsymbol{Z}_{LF_1} \quad \boldsymbol{Z}_{LF_2}][\boldsymbol{I}_{F_1} \quad \boldsymbol{I}_{F_2}]^T \tag{3.19}$$

where,

$\boldsymbol{E}_L$: the voltage at bus L during the fault;

$\boldsymbol{E}_L^0$: the voltage at bus L preceding the fault;

$\boldsymbol{Z}_{LF_1}$, $\boldsymbol{Z}_{LF_2}$: the transfer impedance between bus L and fault bus F_1, bus L and fault bus F_2, respectively;

$\boldsymbol{I}_{F_1}$, $\boldsymbol{I}_{F_2}$: the fault currents at the point F_1 and F_2.

Based on the measurements from two buses L_1 and L_2, The following two equations are obtained:

$$\boldsymbol{E}_{L_1} = \boldsymbol{E}_{L_1}^0 - [\boldsymbol{Z}_{L_1F_1} \quad \boldsymbol{Z}_{L_1F_2}][\boldsymbol{I}_{F_1} \quad \boldsymbol{I}_{F_2}]^T \tag{3.20}$$

$$\boldsymbol{E}_{L_2} = \boldsymbol{E}_{L_2}^0 - [\boldsymbol{Z}_{L_2F_1} \quad \boldsymbol{Z}_{L_2F_2}][\boldsymbol{I}_{F_1} \quad \boldsymbol{I}_{F_2}]^T \tag{3.21}$$

or in a compact format,

$$\begin{bmatrix} \boldsymbol{E}_{L_1} \\ \boldsymbol{E}_{L_2} \end{bmatrix} = \begin{bmatrix} \boldsymbol{E}_{L_1}^0 \\ \boldsymbol{E}_{L_2}^0 \end{bmatrix} - \begin{bmatrix} \boldsymbol{Z}_{L_1F_1} & \boldsymbol{Z}_{L_1F_2} \\ \boldsymbol{Z}_{L_2F_1} & \boldsymbol{Z}_{L_2F_2} \end{bmatrix} \begin{bmatrix} \boldsymbol{I}_{F_1} \\ \boldsymbol{I}_{F_2} \end{bmatrix} \tag{3.22}$$

where,

$\boldsymbol{E}_{L_1}$, $\boldsymbol{E}_{L_2}$: the voltage during the fault at bus L_1, L_2, respectively;

$\boldsymbol{E}_{L_1}^0$, $\boldsymbol{E}_{L_2}^0$: the voltage preceding the fault at bus L_1, L_2, respectively;

$\boldsymbol{Z}_{L_1F_1}$, $\boldsymbol{Z}_{L_1F_2}$: transfer impedance matrix between bus L_1 and F_1, bus L_1 and F_2, respectively;

$\boldsymbol{Z}_{L_2F_1}$, $\boldsymbol{Z}_{L_2F_2}$: transfer impedance matrix between bus L_2 and F_1 , bus L_2 and F_2 , respectively.

Equation (3.22) can be written in a more compact form as

$$\boldsymbol{E}_{L_1L_2} = \boldsymbol{E}^0_{L_1L_2} - \boldsymbol{Z}_{L_1L_2F_1F_2}\boldsymbol{I}_{F_1F_2} \tag{3.23}$$

The superimposed quantity, or the voltage change due to a fault, is

$$\Delta\boldsymbol{E}_{L_1L_2} = -\boldsymbol{Z}_{L_1L_2F_1F_2}\boldsymbol{I}_{F_1F_2} \tag{3.24}$$

From (3.24), the fault current vector is obtained as

$$\boldsymbol{I}_{F_1F_2} = -\left(\boldsymbol{Z}^T_{L_1L_2F_1F_2}\boldsymbol{Z}_{L_1L_2F_1F_2}\right)^{-1}\left(\boldsymbol{Z}^T_{L_1L_2F_1F_2}\Delta\boldsymbol{E}_{L_1L_2}\right) \tag{3.25}$$

Based on (3.23), the voltage during the fault at fault buses are given by

$$\boldsymbol{E}_{F_1F_2} = \boldsymbol{E}^0_{F_1F_2} - \boldsymbol{Z}_{F_1F_2F_1F_2}\boldsymbol{I}_{F_1F_2} \tag{3.26}$$

Prefault voltages $\boldsymbol{E}^0_{F_1F_2}$ at the fault bus F_1 and F_2 can be expressed in terms of fault location and the prefault voltages at bus P_1 and Q_1, bus P_2 and Q_2 [43].

Since the fault resistances are purely resistive, the reactive power consumed by fault resistances at the two fault locations is zero, i.e.,

$$Imag\left(\begin{bmatrix}\boldsymbol{E}^T_{F_1}\boldsymbol{I}^*_{F_1}\\ \boldsymbol{E}^T_{F_2}\boldsymbol{I}^*_{F_2}\end{bmatrix}\right) = 0 \tag{3.27}$$

Solving (3.27) will yield the two unknown variables m_1 and m_2.

An alternative approach is described as follows when more measurements are available. Assume that measurements from another bus L_3 is known. The following equation is obtained in a similar way to (3.25),

$$\boldsymbol{I}_{F_1F_2} = -\left(\boldsymbol{Z}^T_{L_1L_3F_1F_2}\boldsymbol{Z}_{L_1L_3F_1F_2}\right)^{-1}\left(\boldsymbol{Z}^T_{L_1L_3F_1F_2}\Delta\boldsymbol{E}_{L_1L_3}\right) \tag{3.28}$$

Equating (3.25) and (3.28), it is obtained that

$$\left(\boldsymbol{Z}_{L_1L_2F_1F_2}^{T}\boldsymbol{Z}_{L_1L_2F_1F_2}\right)^{-1}\left(\boldsymbol{Z}_{L_1L_2F_1F_2}^{T}\Delta\boldsymbol{E}_{L_1L_2}\right) = \left(\boldsymbol{Z}_{L_1L_3F_1F_2}^{T}\boldsymbol{Z}_{L_1L_3F_1F_2}\right)^{-1}\left(\boldsymbol{Z}_{L_1L_3F_1F_2}^{T}\Delta\boldsymbol{E}_{L_1L_3}\right) \quad (3.29)$$

Equation (3.29) contains two unknown variables m_1 and m_2. Separating the equation into two real equations, from which the fault location can be obtained using the Newton-Raphson method.

3.4 Proposed Type III Fault Location Algorithm

This section presents the proposed Type III fault location algorithm. The algorithm has three variants depending on the availability of source currents:

- Variant 1 does not require any information of the source currents.
- Variant 2 utilizes the fault current measurements at the substation.
- Variant 3 utilizes the fault current measurements at the substation and the magnitude of fault currents at all DGs. The rationale is that even if we do not monitor the currents at DGs, the current magnitude at DGs may be largely decided by the current limiter of the DGs, and therefore the magnitude may be known.

In addition, the algorithm needs fault voltage measurements at selected buses. The choice of the buses is related to system configuration and parameters and can be determined through a fault location observability analysis and meter placement method [15]. Note that the used voltage measurements are fundamental frequency phasors, and currents used are phasors for Variant 2 and magnitude for Variant 3.

The algorithm is explained as follows. The unknown source currents $\boldsymbol{I}_K$ and fault current $\boldsymbol{I}_F$ can be obtained based on voltage measurements. Then the obtained currents can be substituted to (3.3) to find the fault voltage $\boldsymbol{E}_F$. We can then solve (3.4) and (3.5) to find the fault location. For this algorithm, voltage measurements at $n+2$ buses are

needed to determine the fault location of a simultaneous fault for a distribution network with n sources. We need two more voltages since $\boldsymbol{I}_{F_1}$ and $\boldsymbol{I}_{F_2}$ are unknown.

Let us assume that the fault voltage measurements at buses L_1 and L_2 are available. Substituting $\boldsymbol{E}_{L_1}$ and $\boldsymbol{E}_{L_2}$ to (3.9) gives

$$\boldsymbol{E}_{L_1} = \boldsymbol{Z}_{L_1K}\boldsymbol{I}_K - \boldsymbol{Z}_{L_1F_1}\boldsymbol{I}_{F_1} - \boldsymbol{Z}_{L_1F_2}\boldsymbol{I}_{F_2} \tag{3.30}$$

$$\boldsymbol{E}_{L_2} = \boldsymbol{Z}_{L_2K}\boldsymbol{I}_K - \boldsymbol{Z}_{L_2F_1}\boldsymbol{I}_{F_1} - \boldsymbol{Z}_{L_2F_2}\boldsymbol{I}_{F_2} \tag{3.31}$$

We can write (3.30) and (3.31) in the matrix form as

$$\begin{bmatrix}\boldsymbol{E}_{L_1}\\ \boldsymbol{E}_{L_2}\end{bmatrix} = \begin{bmatrix}\boldsymbol{Z}_{L_1K} & \boldsymbol{Z}_{L_1F_1} & \boldsymbol{Z}_{L_1F_2}\\ \boldsymbol{Z}_{L_2K} & \boldsymbol{Z}_{L_2F_1} & \boldsymbol{Z}_{L_2F_2}\end{bmatrix}\begin{bmatrix}\boldsymbol{I}_K\\ -\boldsymbol{I}_{F_1}\\ -\boldsymbol{I}_{F_2}\end{bmatrix} \tag{3.32}$$

Let us define $\boldsymbol{I}$ in terms of the current vector in (3.32). That is,

$$\boldsymbol{I} = \begin{bmatrix}\boldsymbol{I}_K\\ -\boldsymbol{I}_{F_1}\\ -\boldsymbol{I}_{F_2}\end{bmatrix} \tag{3.33}$$

Considering a distribution network that has a total of n sources including substation and DGs, then $\boldsymbol{I}$ can be written in the expanded form as

$$\boldsymbol{I} = \begin{bmatrix}\boldsymbol{I}_S\\ \boldsymbol{I}_{DG_1}\\ \boldsymbol{I}_{DG_2}\\ \vdots\\ \boldsymbol{I}_{DG_{n-1}}\\ -\boldsymbol{I}_{F_1}\\ -\boldsymbol{I}_{F_2}\end{bmatrix} \tag{3.34}$$

If fault voltage measurements at buses L_3, L_4, …, L_{n+2} are also available, then equations can be formed for buses L_3 to L_{n+2} in a similar way to (3.30) and (3.31). The matrix format of those equations for buses L_1 to L_{n+2} is

$$\begin{bmatrix} \boldsymbol{E}_{L_1} \\ \boldsymbol{E}_{L_2} \\ \boldsymbol{E}_{L_3} \\ \vdots \\ \boldsymbol{E}_{L_n} \\ \boldsymbol{E}_{n+1} \\ \boldsymbol{E}_{n+2} \end{bmatrix} = \begin{bmatrix} \boldsymbol{Z}_{L_1K} & \boldsymbol{Z}_{L_1F_1} & \boldsymbol{Z}_{L_1F_2} \\ \boldsymbol{Z}_{L_2K} & \boldsymbol{Z}_{L_2F_1} & \boldsymbol{Z}_{L_2F_2} \\ \boldsymbol{Z}_{L_3K} & \boldsymbol{Z}_{L_3F_1} & \boldsymbol{Z}_{L_3F_2} \\ \vdots & \vdots & \vdots \\ \boldsymbol{Z}_{L_nK} & \boldsymbol{Z}_{L_nF_1} & \boldsymbol{Z}_{L_nF_2} \\ \boldsymbol{Z}_{L_{n+1}K} & \boldsymbol{Z}_{L_{n+1}F_1} & \boldsymbol{Z}_{L_{n+1}F_2} \\ \boldsymbol{Z}_{L_{n+2}K} & \boldsymbol{Z}_{L_{n+2}F_1} & \boldsymbol{Z}_{L_{n+2}F_2} \end{bmatrix} \begin{bmatrix} \boldsymbol{I}_S \\ \boldsymbol{I}_{DG_1} \\ \boldsymbol{I}_{DG_2} \\ \vdots \\ \boldsymbol{I}_{DG_{n-1}} \\ -\boldsymbol{I}_{F_1} \\ -\boldsymbol{I}_{F_2} \end{bmatrix} \tag{3.35}$$

This is the fundamental equation for deriving the source currents and fault current based on voltage measurements. For Variant 1, inverting the impedance matrix of (3.35) will yield the current vector $\boldsymbol{I}$. However, it becomes more complicated for Variant 2 and 3. The approaches to the determination of the current vector $\boldsymbol{I}$ for Variant 1, 2, and 3 are presented in subsection 3.4.1, 3.4.2, and 3.4.3, respectively. Subsection 3.4.4 gives a summary.

3.4.1 Variant 1

We may write (3.35) in a more concise form as

$$\boldsymbol{E}_{L_1L_2\dots L_{n+2}} = \boldsymbol{Z}_{L_1L_2\dots L_{n+2}KF_1F_2}\boldsymbol{I} \tag{3.36}$$

In which $\boldsymbol{E}_{L_1L_2\dots L_{n+2}}$ is the fault voltage vector of (11), and $\boldsymbol{Z}_{L_1L_2\dots L_{n+2}KF_1F_2}$ is the impedance matrix of (3.35). Again, Pseudo inverse technique is used to invert $\boldsymbol{Z}_{L_1L_2\dots L_{n+2}KF_1F_2}$ because it may be a non-square matrix. Inverting $\boldsymbol{Z}_{L_1L_2\dots L_{n+2}KF_1F_2}$ yields the current vector $\boldsymbol{I}$, which is

$$\boldsymbol{I} = \left(\boldsymbol{Z}^T_{L_1L_2\dots L_{n+2}KF_1F_2}\boldsymbol{Z}_{L_1L_2\dots L_{n+2}KF_1F_2}\right)^{-1}\boldsymbol{Z}^T_{L_1L_2\dots L_{n+2}KF_1F_2}\boldsymbol{E}_{L_1L_2\dots L_{n+2}} \tag{3.37}$$

3.4.2 Variant 2

Expanding the term K of $\boldsymbol{Z}_{L_1L_2\dots L_{n+2}KF_1F_2}$ according to $K = [substation, DG_1, DG_2, \dots DG_{n-1}]$, and from (3.35) and (3.36) we have

$$\begin{bmatrix} \boldsymbol{E}_{L_1} \\ \boldsymbol{E}_{L_2} \\ \boldsymbol{E}_{L_3} \\ \vdots \\ \boldsymbol{E}_{L_n} \\ \boldsymbol{E}_{n+1} \\ \boldsymbol{E}_{n+2} \end{bmatrix} =$$

$$\begin{bmatrix} \boldsymbol{Z}_{L_1S} & \boldsymbol{Z}_{L_1DG_1} & \boldsymbol{Z}_{L_1DG_2} & \cdots & \boldsymbol{Z}_{L_1DG_{n-1}} & \boldsymbol{Z}_{L_1F_1} & \boldsymbol{Z}_{L_1F_2} \\ \boldsymbol{Z}_{L_2S} & \boldsymbol{Z}_{L_2DG_1} & \boldsymbol{Z}_{L_2DG_2} & \cdots & \boldsymbol{Z}_{L_2DG_{n-1}} & \boldsymbol{Z}_{L_2F_1} & \boldsymbol{Z}_{L_2F_2} \\ \boldsymbol{Z}_{L_3S} & \boldsymbol{Z}_{L_3DG_1} & \boldsymbol{Z}_{L_3DG_2} & \cdots & \boldsymbol{Z}_{L_3DG_{n-1}} & \boldsymbol{Z}_{L_3F_1} & \boldsymbol{Z}_{L_3F_2} \\ \vdots & \vdots & \vdots & \ddots & \vdots & \vdots & \vdots \\ \boldsymbol{Z}_{L_nS} & \boldsymbol{Z}_{L_nDG_1} & \boldsymbol{Z}_{L_nDG_2} & \cdots & \boldsymbol{Z}_{L_nDG_{n-1}} & \boldsymbol{Z}_{L_nF_1} & \boldsymbol{Z}_{L_nF_2} \\ \boldsymbol{Z}_{L_{n+1}S} & \boldsymbol{Z}_{L_{n+1}DG_1} & \boldsymbol{Z}_{L_{n+1}DG_2} & \cdots & \boldsymbol{Z}_{L_{n+1}DG_{n-1}} & \boldsymbol{Z}_{L_{n+1}F_1} & \boldsymbol{Z}_{L_{n+1}F_2} \\ \boldsymbol{Z}_{L_{n+2}S} & \boldsymbol{Z}_{L_{n+2}DG_1} & \boldsymbol{Z}_{L_{n+2}DG_2} & \cdots & \boldsymbol{Z}_{L_{n+2}DG_{n-1}} & \boldsymbol{Z}_{L_{n+2}F_1} & \boldsymbol{Z}_{L_{n+2}F_2} \end{bmatrix} \cdot \begin{bmatrix} \boldsymbol{I}_S \\ \boldsymbol{I}_{DG_1} \\ \boldsymbol{I}_{DG_2} \\ \vdots \\ \boldsymbol{I}_{DG_{n-1}} \\ -\boldsymbol{I}_{F_1} \\ -\boldsymbol{I}_{F_2} \end{bmatrix} \quad (3.38)$$

Since substation current $\boldsymbol{I}_S$ is assumed to be available for Variant 2, we may separate out $\boldsymbol{I}_S$ from the current vector $\boldsymbol{I}$, and (3.38) becomes

$$\begin{bmatrix} \boldsymbol{E}_{L_1} \\ \boldsymbol{E}_{L_2} \\ \boldsymbol{E}_{L_3} \\ \vdots \\ \boldsymbol{E}_{L_n} \\ \boldsymbol{E}_{n+1} \\ \boldsymbol{E}_{n+2} \end{bmatrix} = \begin{bmatrix} \boldsymbol{Z}_{L_1S} \\ \boldsymbol{Z}_{L_2S} \\ \boldsymbol{Z}_{L_3S} \\ \vdots \\ \boldsymbol{Z}_{L_nS} \\ \boldsymbol{Z}_{L_{n+1}S} \\ \boldsymbol{Z}_{L_{n+2}S} \end{bmatrix} \boldsymbol{I}_S +$$

$$\begin{bmatrix} \boldsymbol{Z}_{L_1DG_1} & \boldsymbol{Z}_{L_1DG_2} & \cdots & \boldsymbol{Z}_{L_1DG_{n-1}} & \boldsymbol{Z}_{L_1F_1} & \boldsymbol{Z}_{L_1F_2} \\ \boldsymbol{Z}_{L_2DG_1} & \boldsymbol{Z}_{L_2DG_2} & \cdots & \boldsymbol{Z}_{L_2DG_{n-1}} & \boldsymbol{Z}_{L_2F_1} & \boldsymbol{Z}_{L_2F_2} \\ \boldsymbol{Z}_{L_3DG_1} & \boldsymbol{Z}_{L_3DG_2} & \cdots & \boldsymbol{Z}_{L_3DG_{n-1}} & \boldsymbol{Z}_{L_3F_1} & \boldsymbol{Z}_{L_3F_2} \\ \vdots & \vdots & \ddots & \vdots & \vdots & \vdots \\ \boldsymbol{Z}_{L_nDG_1} & \boldsymbol{Z}_{L_nDG_2} & \cdots & \boldsymbol{Z}_{L_nDG_{n-1}} & \boldsymbol{Z}_{L_nF_1} & \boldsymbol{Z}_{L_nF_2} \\ \boldsymbol{Z}_{L_{n+1}DG_1} & \boldsymbol{Z}_{L_{n+1}DG_2} & \cdots & \boldsymbol{Z}_{L_{n+1}DG_{n-1}} & \boldsymbol{Z}_{L_{n+1}F_1} & \boldsymbol{Z}_{L_{n+1}F_2} \\ \boldsymbol{Z}_{L_{n+2}DG_1} & \boldsymbol{Z}_{L_{n+2}DG_2} & \cdots & \boldsymbol{Z}_{L_{n+2}DG_{n-1}} & \boldsymbol{Z}_{L_{n+2}F_1} & \boldsymbol{Z}_{L_{n+2}F_2} \end{bmatrix} \begin{bmatrix} \boldsymbol{I}_{DG_1} \\ \boldsymbol{I}_{DG_2} \\ \vdots \\ \boldsymbol{I}_{DG_{n-1}} \\ -\boldsymbol{I}_{F_1} \\ -\boldsymbol{I}_{F_2} \end{bmatrix} \quad (3.39)$$

Let us define $\boldsymbol{I}_{\bar{S}}$ for the current vector in (3.39),

$$\boldsymbol{I}_{\bar{S}} = \begin{bmatrix} \boldsymbol{I}_{DG_1} \\ \boldsymbol{I}_{DG_2} \\ \vdots \\ \boldsymbol{I}_{DG_{n-1}} \\ -\boldsymbol{I}_{F_1} \\ -\boldsymbol{I}_{F_2} \end{bmatrix} \tag{3.40}$$

We may then write (3.39) in a more concise form as

$$\boldsymbol{E}_{L_1L_2\ldots L_{n+2}} = \boldsymbol{Z}_{L_1L_2\ldots L_{n+2}S}\boldsymbol{I}_S + \boldsymbol{Z}_{L_1L_2\ldots L_{n+2}DGF_1F_2}\boldsymbol{I}_{\bar{S}} \tag{3.41}$$

Inverting $\boldsymbol{Z}_{L_1L_2\ldots L_{n+2}DGF_1F_2}$ yields the unknown vector $\boldsymbol{I}_{\bar{S}}$, which is

$$\boldsymbol{I}_{\bar{S}} = \left(\boldsymbol{Z}^T_{L_1L_2\ldots L_{n+2}DGF_1F_2}\boldsymbol{Z}_{L_1L_2\ldots L_{n+2}DGF_1F_2}\right)^{-1} \cdot$$

$$\left[\boldsymbol{Z}^T_{L_1L_2\ldots L_{n+2}DGF_1F_2}\left(\boldsymbol{E}_{L_1L_2\ldots L_{n+2}} - \boldsymbol{Z}_{L_1L_2\ldots L_{n+2}S}\boldsymbol{I}_S\right)\right] \tag{3.42}$$

After $\boldsymbol{I}_{\bar{S}}$ is extracted, we can concatenate it with $\boldsymbol{I}_S$ to obtain $\boldsymbol{I}$,

$$\boldsymbol{I} = \begin{bmatrix} \boldsymbol{I}_S \\ \boldsymbol{I}_{\bar{S}} \end{bmatrix} \tag{3.43}$$

3.4.3 Variant 3

Variant 3 assumes that the current magnitudes at DGs are available. If we write $\boldsymbol{I}_{\bar{S}}$ in the form of phasor magnitude and angle, it becomes

$$\boldsymbol{I}_{\bar{S}} = \begin{bmatrix} |\boldsymbol{I}_{DG_1}|\angle\theta_{DG_1} \\ |\boldsymbol{I}_{DG_2}|\angle\theta_{DG_2} \\ \vdots \\ |\boldsymbol{I}_{DG_{n-1}}|\angle\theta_{DG_{n-1}} \\ -\boldsymbol{I}_{F_1} \\ -\boldsymbol{I}_{F_2} \end{bmatrix} \tag{3.44}$$

where, $|.|$ returns the magnitude of its argument, and $\angle\theta$ is the phasor angle.

Substituting (3.44) to (3.39) and (3.40), (3.39) becomes

$$\begin{bmatrix} \boldsymbol{E}_{L_1} \\ \boldsymbol{E}_{L_2} \\ \boldsymbol{E}_{L_3} \\ \vdots \\ \boldsymbol{E}_{L_n} \\ \boldsymbol{E}_{n+1} \\ \boldsymbol{E}_{n+2} \end{bmatrix} = \begin{bmatrix} \boldsymbol{Z}_{L_1 S} \\ \boldsymbol{Z}_{L_2 S} \\ \boldsymbol{Z}_{L_3 S} \\ \vdots \\ \boldsymbol{Z}_{L_n S} \\ \boldsymbol{Z}_{L_{n+1} S} \\ \boldsymbol{Z}_{L_{n+2} S} \end{bmatrix} \boldsymbol{I}_S +$$

$$\begin{bmatrix} \boldsymbol{Z}_{L_1 DG_1} & \boldsymbol{Z}_{L_1 DG_2} & \cdots & \boldsymbol{Z}_{L_1 DG_{n-1}} & \boldsymbol{Z}_{L_1 F_1} & \boldsymbol{Z}_{L_1 F_2} \\ \boldsymbol{Z}_{L_2 DG_1} & \boldsymbol{Z}_{L_2 DG_2} & \cdots & \boldsymbol{Z}_{L_2 DG_{n-1}} & \boldsymbol{Z}_{L_2 F_1} & \boldsymbol{Z}_{L_2 F_2} \\ \boldsymbol{Z}_{L_3 DG_1} & \boldsymbol{Z}_{L_3 DG_2} & \cdots & \boldsymbol{Z}_{L_3 DG_{n-1}} & \boldsymbol{Z}_{L_3 F_1} & \boldsymbol{Z}_{L_3 F_2} \\ \vdots & \vdots & \ddots & \vdots & \vdots & \vdots \\ \boldsymbol{Z}_{L_n DG_1} & \boldsymbol{Z}_{L_n DG_2} & \cdots & \boldsymbol{Z}_{L_n DG_{n-1}} & \boldsymbol{Z}_{L_n F_1} & \boldsymbol{Z}_{L_n F_2} \\ \boldsymbol{Z}_{L_{n+1} DG_1} & \boldsymbol{Z}_{L_{n+1} DG_2} & \cdots & \boldsymbol{Z}_{L_{n+1} DG_{n-1}} & \boldsymbol{Z}_{L_{n+1} F_1} & \boldsymbol{Z}_{L_{n+1} F_2} \\ \boldsymbol{Z}_{L_{n+2} DG_1} & \boldsymbol{Z}_{L_{n+2} DG_2} & \cdots & \boldsymbol{Z}_{L_{n+2} DG_{n-1}} & \boldsymbol{Z}_{L_{n+2} F_1} & \boldsymbol{Z}_{L_{n+2} F_2} \end{bmatrix}.$$

$$\begin{bmatrix} |\boldsymbol{I}_{DG_1}| \angle \theta_{DG_1} \\ |\boldsymbol{I}_{DG_2}| \angle \theta_{DG_2} \\ \vdots \\ |\boldsymbol{I}_{DG_{n-1}}| \angle \theta_{DG_{n-1}} \\ -\boldsymbol{I}_{F_1} \\ -\boldsymbol{I}_{F_2} \end{bmatrix} \tag{3.45}$$

Row-by-column multiplication for current magnitude at DGs in (3.45) yields

$$\begin{bmatrix} \boldsymbol{E}_{L_1} \\ \boldsymbol{E}_{L_2} \\ \boldsymbol{E}_{L_3} \\ \vdots \\ \boldsymbol{E}_{L_n} \\ \boldsymbol{E}_{n+1} \\ \boldsymbol{E}_{n+2} \end{bmatrix} = \begin{bmatrix} \boldsymbol{Z}_{L_1 S} \\ \boldsymbol{Z}_{L_2 S} \\ \boldsymbol{Z}_{L_3 S} \\ \vdots \\ \boldsymbol{Z}_{L_n S} \\ \boldsymbol{Z}_{L_{n+1} S} \\ \boldsymbol{Z}_{L_{n+2} S} \end{bmatrix} \boldsymbol{I}_S +$$

$$\begin{bmatrix} \boldsymbol{Z}_{L_1 DG_1}|\boldsymbol{I}_{DG_1}| & \boldsymbol{Z}_{L_1 DG_2}|\boldsymbol{I}_{DG_2}| & \cdots & \boldsymbol{Z}_{L_1 DG_{n-1}}|\boldsymbol{I}_{DG_{n-1}}| & \boldsymbol{Z}_{L_1 F_1} & \boldsymbol{Z}_{L_1 F_2} \\ \boldsymbol{Z}_{L_2 DG_1}|\boldsymbol{I}_{DG_1}| & \boldsymbol{Z}_{L_2 DG_2}|\boldsymbol{I}_{DG_2}| & \cdots & \boldsymbol{Z}_{L_2 DG_{n-1}}|\boldsymbol{I}_{DG_{n-1}}| & \boldsymbol{Z}_{L_2 F_1} & \boldsymbol{Z}_{L_2 F_2} \\ \boldsymbol{Z}_{L_3 DG_1}|\boldsymbol{I}_{DG_1}| & \boldsymbol{Z}_{L_3 DG_2}|\boldsymbol{I}_{DG_2}| & \cdots & \boldsymbol{Z}_{L_3 DG_{n-1}}|\boldsymbol{I}_{DG_{n-1}}| & \boldsymbol{Z}_{L_3 F_1} & \boldsymbol{Z}_{L_3 F_2} \\ \vdots & \vdots & \ddots & \vdots & \vdots & \vdots \\ \boldsymbol{Z}_{L_n DG_1}|\boldsymbol{I}_{DG_1}| & \boldsymbol{Z}_{L_n DG_2}|\boldsymbol{I}_{DG_2}| & \cdots & \boldsymbol{Z}_{L_n DG_{n-1}}|\boldsymbol{I}_{DG_{n-1}}| & \boldsymbol{Z}_{L_n F_1} & \boldsymbol{Z}_{L_n F_2} \\ \boldsymbol{Z}_{L_{n+1} DG_1}|\boldsymbol{I}_{DG_1}| & \boldsymbol{Z}_{L_{n+1} DG_2}|\boldsymbol{I}_{DG_2}| & \cdots & \boldsymbol{Z}_{L_{n+1} DG_{n-1}}|\boldsymbol{I}_{DG_{n-1}}| & \boldsymbol{Z}_{L_{n+1} F_1} & \boldsymbol{Z}_{L_{n+1} F_2} \\ \boldsymbol{Z}_{L_{n+2} DG_1}|\boldsymbol{I}_{DG_1}| & \boldsymbol{Z}_{L_{n+2} DG_2}|\boldsymbol{I}_{DG_2}| & \cdots & \boldsymbol{Z}_{L_{n+2} DG_{n-1}}|\boldsymbol{I}_{DG_{n-1}}| & \boldsymbol{Z}_{L_{n+2} F_1} & \boldsymbol{Z}_{L_{n+2} F_2} \end{bmatrix}.$$

$$\begin{bmatrix} \angle\theta_{DG_1} \\ \angle\theta_{DG_2} \\ \vdots \\ \angle\theta_{DG_{n-1}} \\ -\boldsymbol{I}_{F_1} \\ -\boldsymbol{I}_{F_2} \end{bmatrix} \tag{3.46}$$

Let us define $\boldsymbol{I}_{DG_\theta F_1 F_2}$ for the vector to be determined in (3.46), that is,

$$\boldsymbol{I}_{DG_\theta F_1 F_2} = \begin{bmatrix} \angle\theta_{DG_1} \\ \angle\theta_{DG_2} \\ \vdots \\ \angle\theta_{DG_{n-1}} \\ -\boldsymbol{I}_{F_1} \\ -\boldsymbol{I}_{F_2} \end{bmatrix} \tag{3.47}$$

Compactly, (3.46) can be rewritten as

$$\boldsymbol{E}_{L_1 L_2 \dots L_{n+2}} = \boldsymbol{Z}_{L_1 L_2 \dots L_{n+2} S} \boldsymbol{I}_S + \boldsymbol{Z}_{L_1 L_2 \dots L_{n+2} DGF_1 F_{2_M}} \boldsymbol{I}_{DG_\theta F_1 F_2} \tag{3.48}$$

where $\boldsymbol{Z}_{L_1 L_2 \dots L_{n+1} DGF_1 F_{2_M}}$ is modified matrix from $\boldsymbol{Z}_{L_1 L_2 \dots L_{n+1} DGF_1 F_2}$. Then $\boldsymbol{I}_{DG_\theta F_1 F_2}$ is obtained as

$$\boldsymbol{I}_{DG_\theta F_1 F_2} = \left(\boldsymbol{Z}^T_{L_1 L_2 \dots L_{n+2} DGF_1 F_{2_M}} \boldsymbol{Z}_{L_1 L_2 \dots L_{n+2} DGF_1 F_{2_M}}\right)^{-1} \cdot$$
$$\left[\boldsymbol{Z}^T_{L_1 L_2 \dots L_{n+2} DGF_1 F_{2_M}} \left(\boldsymbol{E}_{L_1 L_2 \dots L_{n+2}} - \boldsymbol{Z}_{L_1 L_2 \dots L_{n+2} S} \boldsymbol{I}_S\right)\right] \tag{3.49}$$

In the implementation, we will concatenate $\boldsymbol{I}_{DG_\theta F_1 F_2}$ with the known current magnitude at DGs and $\boldsymbol{I}_S$ using (3.43) and (3.44) to form the vector $\boldsymbol{I}$, which will be used for estimating fault location.

3.4.4 Summary

So far, the current vector $\boldsymbol{I}$ for different variants of the fault location algorithm has been derived. If the source currents are available, they will be directly used for fault location. If the source currents are not provided, they will be extracted based on the calculated

current vector $\boldsymbol{I}$. For each variant, the fault location will be estimated based on (3.15) and (3.16). It is noted that the values of source currents and the fault currents can be calculated once the fault location is solved.

3.5 Evaluations Studies

This subsection evaluates the performance of the proposed fault location algorithms. The 21 bus distribution system with DGs shown in Figure 3.2 is used for the evaluation studies. Simulated data are obtained by a short circuit program developed in Matlab that is capable of dealing with simultaneous faults that occur on any section of the system. The system is also modeled in Matlab SimPowerSystems [42]. Simulation studies are performed to obtain required voltage and current measurements by posing faults with various fault conditions with different fault types, impedances, and locations. The short circuit program is corroborated by the Matlab SimPowerSystems simulation results. The voltage obtained by the short circuit program at bus 1 is added a 0.2% error, and then the proposed algorithms are applied to obtain the fault location.

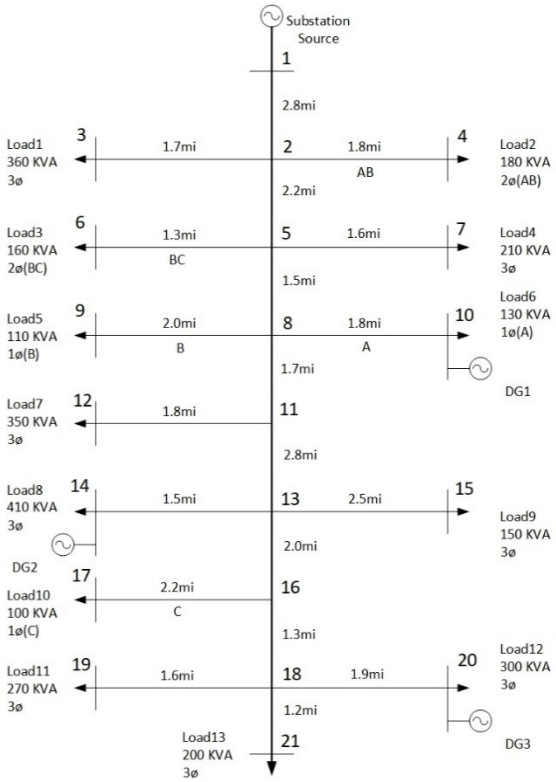

Figure 3.2 A 21 bus distribution system with DGs used for fault location analysis

The Type I algorithm is also tested on the modified IEEE 34 node test system shown in Figure 3.3.

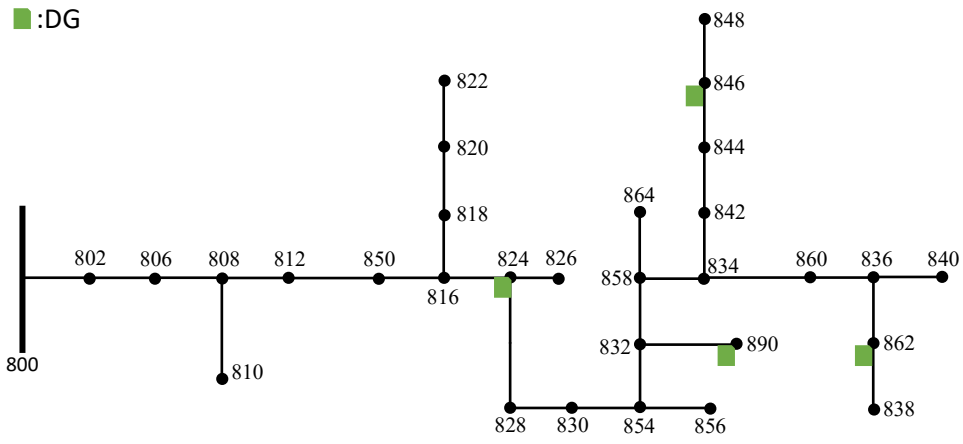

Figure 3.3 Modified IEEE 34 node test system with DGs used for fault location analysis

In the evaluation study, the initial start point for fault location is chosen as 0.5 per unit for all cases. The percentage estimation error is calculated as

$$\%\text{Error} = \frac{|\text{Actual location} - \text{Estimated location}| \times \text{Faulty feeder length}}{\text{The total length of the main feeder}} \times 100 (3.50)$$

The Type I, Type II, and Type III fault location algorithms for 21 bus shown in Figure 3.2 are demonstrated in Subsection 3.5.1, 3.5.3, and 3.5.4, respectively. The Type I algorithm for the modified IEEE 34 Bus distribution system is demonstrated in Subsection 3.5.2.

3.5.1 Locating Faults Using Type I Algorithm for a 21 Bus Distribution System with DGs

Table 3.1 presents the fault location results obtained by Type I algorithm using voltage measurements from bus 1 and 20 and currents from all sources. It is shown that highly accurate results are achieved by the proposed algorithm. Figure 3.4 and Figure 3.5 present the voltage and current waveforms of a simultaneous fault, where an AG fault occurs on the line 1-2, and an LLLG fault occurs on the line 11-13. Figure 3.4 presents the waveforms at bus 1, and Figure 3.5 presents the waveforms at bus 20.

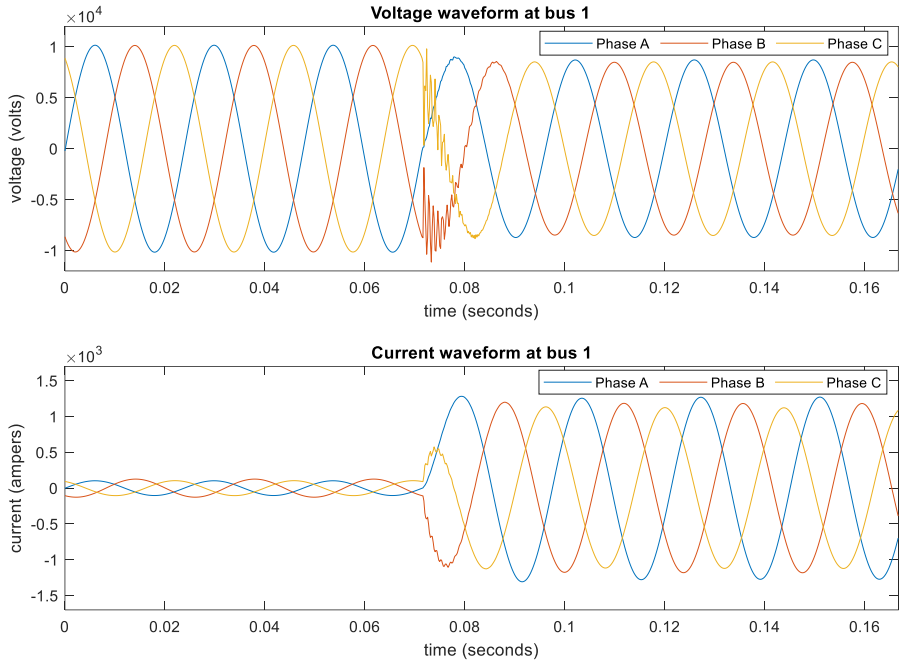

Figure 3.4 Voltage and current waveforms at bus 1 for a simultaneous fault: AG on the line 1-2 and LLLG on the line 11-13

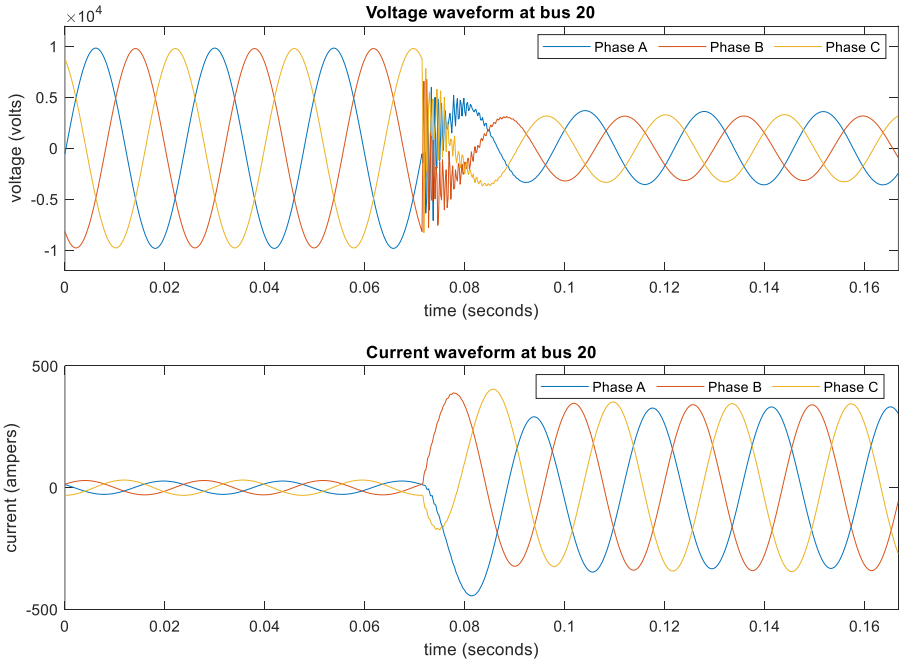

Figure 3.5 Voltage and current waveforms at bus 20 for a simultaneous fault: AG on the line 1-2 and LLLG on the line 11-13

Table 3.1 TYPE I algorithm - fault location results using voltages from bus 1 and 20

Case type	Fault number	Fault section, and fault type	FL (p.u.)	Fault res. (ohm)	FL Esti. Err. (%)
Single fault	Fault 1	(1-2, AG)	0.6	50	0.08
Single fault	Fault 1	(2-5, BC)	0.3	0.5	0.03
Single fault	Fault 1	(5-7, ABCG)	0.8	[1,1,3,5]	0.03
Single fault	Fault 1	(18-20, CG)	0.4	10	0.09
Single fault	Fault 1	(5-8, ABCG)	0.6	[1,1,1,30]	0.08
Multiple faults	Fault 1	(1-2, AG)	0.3	1	0.01
	Fault 2	(16-17, CG)	0.6	10	0.12
Multiple faults	Fault 1	(1-2, BG)	0.7	20	0.62
	Fault 2	(5-8, AB)	0.3	1	0.06
Multiple faults	Fault 1	(2-3, AG)	0.8	10	0.54
	Fault 2	(18-21, ABC)	0.5	[0.5,0.5,0.5]	0.01
Multiple faults	Fault 1	(2-5, CG)	0.6	5	0.00
	Fault 2	(8-10, AG)	0.3	10	0.07
Multiple faults	Fault 1	(1-2, AG)	0.6	20	0.40
	Fault 2	(11-13, ABCG)	0.8	[1,1,1,10]	0.02

It is noted that to locate single faults, voltages from one bus will suffice. For example, using the voltage from bus 1, the fault location results for the first five cases

listed in Table 3.1 can be obtained, and the estimation errors are 0.14%, 0.02%, 0.05%, 0.01%, and 0.07%, respectively.

Table 3.2 presents the fault location results obtained by Type I algorithm using voltage measurements from bus 1, 8, and 20 and currents from all sources, for cases involving three simultaneous faults. Again, accurate results are obtained.

Table 3.2 TYPE I algorithm - fault location results using voltages from bus 1, 8, and 20

Case type	Fault number	Fault section, and fault type	FL (p.u.)	Fault res. (ohm)	FL Esti. err. (%)
Multiple faults	Fault 1	(1-2, AG)	0.4	10	0.61
	Fault 2	(5-6, BG)	0.6	5	0.37
	Fault 3	(8-11, AG)	0.5	5	0.07
Multiple faults	Fault 1	(1-2, BC)	0.8	1	0.01
	Fault 2	(8-11, AG)	0.2	5	0.11
	Fault 3	(13-16, ABC)	0.7	[1,1,1]	0.03
Multiple faults	Fault 1	(2-5, ABCG)	0.6	[0.5,0.5,0.5 ,20]	0.02
	Fault 2	(5-8, BCG)	0.6	[1,1,20]	0.05
	Fault 3	(18-20,CG)	0.5	10	0.01
Multiple faults	Fault 1	(5-7, AB)	0.3	1	0.02
	Fault 2	(8-9, BG)	0.2	5	0.07
	Fault 3	(11-13, ABG)	0.9	[1,1,20]	0.16
Multiple faults	Fault 1	(1-2, AC)	0.2	0.5	0.01
	Fault 2	(5-6, BG)	0.7	5	0.20
	Fault 3	(13-15,BG)	0.5	10	0.23

Table 3.3 presents the fault location results obtained by Type I algorithm using voltage measurements from bus 1, 14, and 20 and currents from all sources, for cases involving three simultaneous faults. It is evinced that the proposed methods have yielded quite accurate results.

Table 3.3 TYPE I algorithm - fault location results using voltages from bus 1, 14, and 20

Case type	Fault number	Fault section, and fault type	FL (p.u.)	Fault res. (ohm)	FL Esti. err. (%)
Multiple faults	Fault 1	(1-2, AG)	0.4	10	0.70
	Fault 2	(8-11, BC)	0.6	0.5	0.10
	Fault 3	(18-19,AG)	0.5	5	0.00
Multiple faults	Fault 1	(1-2, BC)	0.8	1	0.00
	Fault 2	(8-9, BG)	0.2	5	0.07
	Fault 3	(18-19, ABC)	0.7	[1,1,1]	0.02
Multiple faults	Fault 1	(2-5, AG)	0.6	10	0.03
	Fault 2	(8-9, BG)	0.6	15	0.29
	Fault 3	(16-18, AC)	0.5	1	0.32
Multiple faults	Fault 1	(5-7, AB)	0.3	1	0.02
	Fault 2	(8-9, BG)	0.2	5	0.23
	Fault 3	(18-19, ABG)	0.9	[1,1,20]	0.25
Multiple faults	Fault 1	(1-2, AC)	0.2	0.5	0.01
	Fault 2	(11-13, ABG)	0.7	[1,1,20]	0.12
	Fault 3	(18-19,ABCG)	0.5	[0.5,0.5,0.5 ,20]	0.00

From fault location results shown in Table 3.1, Table 3.2, and Table 3.3, it is evidenced that the proposed Type I fault location algorithm is able to pinpoint the fault location for simultaneous faults as well as a single fault accurately.

Table 3.4 provides fault location results for single faults and simultaneous faults using the alternative approach of Type I fault location algorithm. The voltage measurements at bus 1, 14, and 20 are used to obtain the results. It is evidenced the alternative approach can also pinpoint fault locations precisely. Therefore, the alternative approach can serve as a backup for Type I algorithm if redundant voltage measurements are available.

Table 3.4 TYPE I algorithm alternative approach using voltages from bus 1, 14, and 20

Case type	Fault number	Fault section, and fault type	FL (p.u.)	Fault res. (ohm)	FL Esti. err. (%)
Single fault	Fault 1	(1-2, BG)	0.7	50	0.05
Single fault	Fault 1	(2-5, ACG)	0.4	[1,1,5]	0.02
Single fault	Fault 1	(8-11, ABCG)	0.9	[1,2,3,10]	0.06
Single fault	Fault 1	(1-2, ABC)	0.4	[1, 1, 1]	0.01
Single fault	Fault 1	(5-8, AC)	0.6	1	0.05
Multiple faults	Fault 1	(1-2, AG)	0.4	1	0.02
	Fault 2	(18-20, CG)	0.7	10	0.07
Multiple faults	Fault 1	(1-2, BG)	0.7	20	0.18
	Fault 2	(13-14, AB)	0.3	1	0.00
Multiple faults	Fault 1	(5-8, BC)	0.4	0.5	0.02
	Fault 2	(18-20, ABC)	0.6	[0.5,0.50.5]	0.05
Multiple faults	Fault 1	(13-14, CG)	0.6	5	0.12
	Fault 2	(18-20, AG)	0.3	10	0.51
Multiple faults	Fault 1	(1-2, AG)	0.6	20	0.01
	Fault 2	(11-13,ABCG)	0.8	[1, 1,1, 10]	0.01

3.5.2 Locating Faults Using Type I Algorithm for the Modified IEEE 34 node test system with DGs

Results of fault location for single fault scenarios are shown in Table 3.5 and Table 3.6. Table 3.5 illustrates a single fault occurs on the main feeder. Table 3.6 illustrates a single fault occurs on the lateral feeder. In those two tables, the first column lists the faulted line section. The second to fourth columns list the fault types, actual fault locations in per unit, and fault resistance in ohms, respectively. The last two columns summarize the estimation results. Note that the voltage measurement at the substation bus 800 is utilized to obtain the results.

It is observed that quite accurate results are achieved for different fault types, locations, and resistances. This example demonstrates that the fault location algorithm is able to precisely locate the single fault in an unbalanced distribution system with DGs.

Table 3.5 Fault location results for a single fault on the main feeder using the Type I algorithm

Faulted section	Fault type	Actual Fault Location (p.u.)	Fault Resistance (ohm)	Estimated Fault Location (p.u.)	Fault Location Estimation Error (%)
806-808	AG	0.8	25	0.7999	0.0012
	BC	0.1	3	0.1000	0.0001
	ACG	0.6	[1, 1, 25]	0.6000	0.0000
	LLL	0.5	[5, 5, 5]	0.5001	0.0021
	LLLG	0.5	[1, 1, 1, 20]	0.5000	0.0001
828-830	CG	0.6	30	0.5996	0.0041
	AB	0.9	5	0.8999	0.0006
	BCG	0.8	[1, 1, 11]	0.8002	0.0024
	LLL	0.2	[3, 3, 3]	0.2007	0.0073
	LLLG	0.3	[1, 1, 1, 50]	0.3000	0.0005

Table 3.6 Fault location results for a single fault on the lateral feeder using the Type I algorithm

Faulted section	Fault type	Actual Fault Location (p.u.)	Fault Resistance (ohm)	Estimated Fault Location (p.u.)	Fault Location Estimation Error (%)
846-848	BG	0.7	30	0.6860	0.0039
	AB	0.6	5	0.5959	0.0011
	ABG	0.6	[1, 1, 18]	0.5995	0.0001
	LLL	0.3	[2, 2, 2]	0.3159	0.0045
	LLLG	0.8	[1, 1, 1, 20]	0.8076	0.0021
832-890	AG	0.3	35	0.2994	0.0032
	BC	0.1	2	0.1004	0.0022
	ABG	0.9	[1, 1, 30]	0.9000	0.0001
	LLL	0.6	[1, 1, 1]	0.6003	0.0015
	LLLG	0.4	[1, 1, 1, 20]	0.4003	0.0017
808-810	BG	0.7	25	0.6997	0.0010
816-818	AG	0.9	50	0.8982	0.0017
854-856	BG	0.2	20	0.1999	0.0010
862-838	BG	0.6	35	0.5984	0.0040

Table 3.7 presents the results of fault location for simultaneous faults with various faulted sections, fault types, actual locations, and resistances. The voltage measurements at substation bus 800 and another selected bus 836 are used to obtain the results.

From the last two columns of Table 3.7, it is clear that quite accurate results are obtained through the proposed algorithm. It is evidenced that the algorithm is capable of locating the faults for simultaneous faults in distribution systems with high penetration of DGs.

Table 3.7 Fault location results for simultaneous faults using the Type I algorithm

No.	Faulted section	Fault type	Actual Fault Location (p.u.)	Fault Resistance (ohm)	Estimated Fault Location (p.u.)	Fault Location Estimation Error (%)
1st	806-808	LLL	0.5	[5, 5 ,5]	0.4986	0.0232
	862-838	BG	0.6	35	0.6259	0.0665
2nd	808-810	BG	0.7	25	0.6999	0.0003
	832-890	BC	0.1	2	0.0997	0.0015
3rd	806-808	AG	0.8	25	0.7951	0.0842
	828-830	LLLG	0.3	[1, 2, 3, 50]	0.2984	0.0175

The fault location results using the alternative approach are provided in Table 3.8. The voltage measurements at bus 800, 816, and 836 are used to pinpoint the fault location.

From Table 3.8, it is observed that quite accurate results are obtained. It is evidenced that the alternative approach of Type I algorithm is capable of locating the faults in the distribution system integrated with significant DG.

Table 3.8 Fault location results using the Type I algorithm alternative approach

No.	Faulted section	Fault type	Actual Fault Location (p.u.)	Fault Resistance (ohm)	Estimated Fault Location (p.u.)	Fault Location Estimation Error (%)
1st	806-808	AG	0.8	25	0.8007	0.0127
	828-830	LLLG	0.3	[1, 2, 3,50]	0.3002	0.0023
2nd	808-812	AG	0.3	1	0.3000	0.0004
	854-832	BG	0.7	1	0.7001	0.0017

3.5.3 Locating Faults Using Type II Algorithm for a 21 Bus Distribution Systems with DGs

Table 3.9 presents the fault location results obtained by Type II algorithm using voltage measurements from bus 1 and 20. Note that no currents are used for Type II algorithm. Similarly, accurate results are acquired.

Table 3.9 TYPE II algorithm - fault location results using voltages from bus 1 and 20

Case type	Fault number	Fault section, and fault type	FL (p.u.)	Fault res. (ohm)	FL Esti. err. (%)
Single fault	Fault 1	(1-2, AG)	0.4	50	0.06
Single fault	Fault 1	(8-11, AC)	0.3	1	0.26
Single fault	Fault 1	(5-8, BCG)	0.7	[1,1,50]	0.10
Single fault	Fault 1	(8-9, BG)	0.3	30	0.04
Single fault	Fault 1	(13-14, ABCG)	0.6	[1,1,1,30]	0.01
Multiple faults	Fault 1	(1-2, AG)	0.6	1	0.02
	Fault 2	(13-15, BG)	0.5	10	0.12
Multiple faults	Fault 1	(1-2, BG)	0.6	5	0.04
	Fault 2	(5-8, AB)	0.7	0.5	0.02
Multiple faults	Fault 1	(2-3, BC)	0.4	0.5	0.12
	Fault 2	(5-8, ABC)	0.6	[0.5,0.5,0.5]	0.03
Multiple faults	Fault 1	(2-5, CG)	0.6	20	0.25
	Fault 2	(11-12, AG)	0.7	30	0.52
Multiple faults	Fault 1	(8-11, AG)	0.5	50	0.44
	Fault 2	(16-18, ABCG)	0.8	[1,1,1,10]	0.05

It is noted that to pinpoint single faults, voltages from one bus will suffice. For example, using the voltage from bus 1, the fault location results for the first five cases listed in Table 3.9 can be obtained, and the estimation errors are 0.01%, 0.08%, 0.11%, 0.05%, and 0.11%, respectively.

Table 3.10 presents the fault location results obtained by Type II algorithm using voltage measurements from bus 1, 8, and 20 and currents from all sources, for cases involving three simultaneous faults. Very accurate results are achieved.

Table 3.10 TYPE II algorithm - fault location results using voltages from bus 1, 8, and 20

Case type	Fault number	Fault section, and fault type	FL (p.u.)	Fault res. (ohm)	FL Esti. err. (%)
Multiple faults	Fault 1	(1-2, AG)	0.4	30	0.60
	Fault 2	(8-11, BG)	0.6	10	0.44
	Fault 3	(18-19,CG)	0.5	50	0.42
Multiple faults	Fault 1	(1-2, AB)	0.8	0.5	0.02
	Fault 2	(2-5, CG)	0.2	50	0.22
	Fault 3	(8-11, ABC)	0.6	[1,1,1]	0.00
Multiple faults	Fault 1	(1-2, BG)	0.7	10	0.08
	Fault 2	(5-8, BCG)	0.6	[1,1,20]	0.03
	Fault 3	(8-11, CG)	0.3	20	0.02
Multiple faults	Fault 1	(2-5, AB)	0.3	0.5	0.03
	Fault 2	(5-8, AG)	0.3	10	0.35
	Fault 3	(11-13, BCG)	0.8	[1,1,20]	0.01
Multiple faults	Fault 1	(1-2, AC)	0.3	0.5	0.01
	Fault 2	(8-11, AG)	0.6	10	0.61
	Fault 3	(13-15, BG)	0.6	30	0.14

Table 3.11 presents the fault location results obtained by Type II algorithm using voltage measurements from bus 1, 14, and 20 and currents from all sources, for cases involving three simultaneous faults. Again accurate results are obtained.

Table 3.11 TYPE II algorithm - fault location results using voltages from 1, 14, and 20

Case type	Fault number	Fault section, and fault type	FL (p.u.)	Fault res. (ohm)	FL Esti. err. (%)
Multiple faults	Fault 1	(1-2, AG)	0.4	10	0.24
	Fault 2	(5-8, BG)	0.6	5	0.31
	Fault 3	(16-18, CG)	0.5	30	0.00
Multiple faults	Fault 1	(1-2, AB)	0.8	0.5	0.02
	Fault 2	(2-5, CG)	0.2	50	0.60
	Fault 3	(18-20, ABC)	0.6	[1,1,1]	0.00
Multiple faults	Fault 1	(2-3, AG)	0.7	10	0.18
	Fault 2	(8-10, AG)	0.6	30	0.55
	Fault 3	(13-16, CG)	0.3	20	0.00
Multiple faults	Fault 1	(5-7, AB)	0.3	0.5	0.07
	Fault 2	(8-11, BG)	0.3	10	0.31
	Fault 3	(18-19, BCG)	0.8	[1,1,20]	0.00
Multiple faults	Fault 1	(1-2, AC)	0.3	0.5	0.00
	Fault 2	(8-11, AG)	0.6	10	0.69
	Fault 3	(13-16, BG)	0.6	30	0.07

From fault location results shown in Table 3.9, Table 3.10, and Table 3.11, it is evidenced that the proposed Type II fault location algorithm is able to pinpoint the fault location for simultaneous faults as well as a single fault accurately.

Table 3.12 provides fault location results for single faults and simultaneous faults using the alternative approach of Type II fault location algorithm. The voltage measurements at bus 1, 14, and 20 are used to obtain the results. It is evidenced the alternative approach is able to pinpoint fault locations as well. Therefore, the alternative approach can serve as a backup for Type II algorithm if redundant voltage measurements are available.

Table 3.12 TYPE II algorithm alternative approach using voltages from bus 1, 14, and 20

Case type	Fault number	Fault section, and fault type	FL (p.u.)	Fault res. (ohm)	FL Esti. err. (%)
Single fault	Fault 1	(1-2, BG)	0.7	50	0.01
Single fault	Fault 1	(2-5, ACG)	0.4	[1,1,5]	0.03
Single fault	Fault 1	(8-11, ABCG)	0.9	[1,2,3,10]	0.05
Single fault	Fault 1	(1-2, ABC)	0.4	[1, 1, 1]	0.02
Single fault	Fault 1	(5-8, AC)	0.6	1	0.05
Multiple faults	Fault 1	(1-2, AG)	0.4	1	0.01
	Fault 2	(18-20, CG)	0.7	10	0.01
Multiple faults	Fault 1	(1-2, BG)	0.7	20	0.02
	Fault 2	(13-14, AB)	0.3	1	0.00
Multiple faults	Fault 1	(5-8, BC)	0.4	0.5	0.06
	Fault 2	(18-20, ABC)	0.6	[0.5,0.5,0.5]	0.02
Multiple faults	Fault 1	(13-14, CG)	0.6	5	0.06
	Fault 2	(18-20, AG)	0.3	10	0.15
Multiple faults	Fault 1	(1-2, AG)	0.6	20	0.01
	Fault 2	(11-13, ABCG)	0.8	[1,1,1,10]	0.00

3.5.4 Locating Faults Using Type III algorithm for a 21 Bus Distribution Systems with DGs

The voltages obtained by short circuit program are added a random error between 0 to 0.02 percent to emulate the measurement errors. Then the proposed Type III algorithm is used to locate the faults.

Table 3.13 presents the fault location results obtained by Type III algorithm using voltage measurements from bus 1, 7, 10, 14, and 20. Note that 5 voltage measurements are used to locate the single fault location for a network with 4 sources. It is observed that quite accurate results are acquired.

Table 3.13 TYPE III algorithm fault location results using voltage measurements at buses 1, 7, 10, 14, and 20

Faulted section	Fault type	Actual Fault Location (p.u.)	Fault Resistance (ohm)	Fault Location Estimation Error (%)		
				Variant 1	Variant 2	Variant 3
1-2	CG	0.6	5	2.3919	0.0197	0.0014
2-3	AC	0.8	1	0.0373	0.0075	0.0293
2-5	BG	0.5	1	0.3413	0.0382	0.0464
5-7	AB	0.7	1	0.7534	0.0701	0.0515
5-8	ABCG	0.3	[1,1,1,5]	0.0009	0.0209	0.0949
11-13	ABC	0.4	[1,2,3]	0.0321	0.0483	2.3224
11-13	ACG	0.1	[1,1,5]	0.0447	0.0258	1.7797
13-14	AB	0.2	1	0.4802	0.3843	1.4241
13-16	AG	0.5	5	0.3019	0.3684	0.6028
18-20	CG	0.6	5	0.3816	2.7686	0.1152

Table 3.14 presents the fault location results obtained by Type III algorithm using voltage measurements from bus 1, 3, 7, 10, 14, and 20. Note that 6 voltage measurements are used to locate the simultaneous fault locations for a network with 4 sources. It is observed that quite accurate results are acquired.

Table 3.14 TYPE III algorithm fault location results using voltage measurements at buses 1, 3, 7, 10, 14, and 20

No.	Faulted section	Fault type	Actual Fault Location (p.u.)	Fault Resistance (ohm)	Fault Location Estimation Error (%)		
					Variant 1	Variant 2	Variant 3
1st	1-2	BC	0.3	1	0.5485	0.0257	0.0023
	18-20	AG	0.4	1	0.0977	1.1759	3.2432
2nd	2-3	AB	0.7	1	0.1471	0.0043	2.0869
	13-16	BG	0.5	5	1.0037	1.0659	3.4934
3rd	2-5	ABCG	0.1	[1,1,1,1]	0.0170	0.0241	0.0225
	13-14	CG	0.9	3	0.0671	3.0788	0.8916
4th	5-7	AG	0.6	5	2.0993	2.2803	1.4083
	11-13	AC	0.7	1	2.2524	2.9786	0.6949
5th	2-3	AG	0.4	5	0.7065	0.6526	0.0880
	18-20	BC	0.7	1	2.9515	1.4645	0.2226

From fault location results shown in Table 3.13 and Table 3.14, it is evidenced that the proposed Type III fault location algorithm is able to pinpoint the fault location for simultaneous faults as well as a single fault accurately.

3.6 Summary

This chapter proposes three types of algorithms for locating simultaneous faults in distribution systems with DGs, which is also applicable to single faults. Type I algorithm requires currents from all sources and voltages from selected locations but does not need source impedance. Type II algorithm needs only voltages from selected locations, does not need currents from any location, and needs source impedance. Type III algorithm needs voltage measurements captured at selected buses and/or source current measurements. The comparison is tabulated in Table 3.15.

Table 3.15 A comparison between the proposed fault location algorithms

Proposed Fault location Algorithms	Type I	Type II	Type III		
			Variant 1	Variant 2	Variant 3
Need source impedance? (Yes/No)	No	Yes	No	No	No
Need source currents? (Yes/No)	Yes (substation and DG current phasors)	No	No	Yes (substation current phasor)	Yes (substation current phasor and DG current magnitude)
Need voltages at selected locations? (Yes/No)	Yes (phasor)	Yes (phasor)	Yes (phasor)	Yes (phasor)	Yes (phasor)
Need prefault measurements? (Yes/No)	No	Yes (voltage phasor)	No	No	No

All algorithms are capable of handling unbalances and any type of faults and still work for situations where only limited measurements are available. All algorithms produce highly accurate fault location estimates based on simulation studies. With increasing deployment of DGs, the proposed algorithms will speed up the maintenance process when faults occur on the system and thus improve system reliability.

Chapter 4 Optimal Fault Location Methods for Distribution Systems with DGs

As seen in Chapter 3, the proposed fault location algorithms perform well for simultaneous faults based on accurate measurements. In practice, the measurements may have errors due to various reasons, for example, current transformer saturation. A measurement with large error is called bad data. If bad data is used for fault location algorithm, the estimated fault location results will no longer be accurate. Therefore, a method that can identify bad data is strongly desired.

In this chapter, an optimal fault location estimator is developed to detect and identify bad data. The bad data will be removed once it is identified. As a result, only accurate measurements are used for optimal estimation, and the accuracy of fault location is enhanced.

4.1 Optimal Fault Location Estimate Using the Type I Fault Location Algorithm

In this subsection, optimal fault location estimator based on the Type I fault location algorithm is illustrated. Assuming four voltage measurements $\boldsymbol{E}_{L_1}$, $\boldsymbol{E}_{L_2}$, $\boldsymbol{E}_{L_3}$, and $\boldsymbol{E}_{L_4}$ are available for fault location purpose. From (3.14) to (3.16), we have

$$\boldsymbol{I}_{F_1F_2}^1 = \left(\boldsymbol{Z}_{L_1L_2F_1F_2}^T \boldsymbol{Z}_{L_1L_2F_1F_2}\right)^{-1} \boldsymbol{Z}_{L_1L_2F_1F_2}^T \left(\boldsymbol{Z}_{L_1L_2K}\boldsymbol{I}_K - \boldsymbol{E}_{L_1L_2}\right) \tag{4.1}$$

$$\boldsymbol{E}_{F_1F_2}^1 = \boldsymbol{Z}_{F_1F_2K}\boldsymbol{I}_K - \boldsymbol{Z}_{F_1F_2F_1F_2}\boldsymbol{I}_{F_1F_2}^1 \tag{4.2}$$

$$\text{Imag}\left(\begin{bmatrix} \left(\boldsymbol{E}_{F_1}^1\right)^T \left(\boldsymbol{I}_{F_1}^1\right)^* \\ \left(\boldsymbol{E}_{F_2}^1\right)^T \left(\boldsymbol{I}_{F_2}^1\right)^* \end{bmatrix}\right) = 0 \tag{4.3}$$

where the superscript 1 denotes the first combination using $\boldsymbol{E}_{L_1}$ and $\boldsymbol{E}_{L_2}$. Similarly, equations for the second combination using $\boldsymbol{E}_{L_1}$, $\boldsymbol{E}_{L_3}$ and the third combination using $\boldsymbol{E}_{L_1}$, $\boldsymbol{E}_{L_4}$ are given by

$$\boldsymbol{I}^2_{F_1F_2} = \left(\boldsymbol{Z}^T_{L_1L_3F_1F_2}\boldsymbol{Z}_{L_1L_3F_1F_2}\right)^{-1}\boldsymbol{Z}^T_{L_1L_3F_1F_2}\left(\boldsymbol{Z}_{L_1L_3K}\boldsymbol{I}_K - \boldsymbol{E}_{L_1L_3}\right) \tag{4.4}$$

$$\boldsymbol{E}^2_{F_1F_2} = \boldsymbol{Z}_{F_1F_2K}\boldsymbol{I}_K - \boldsymbol{Z}_{F_1F_2F_1F_2}\boldsymbol{I}^2_{F_1F_2} \tag{4.5}$$

$$\text{Imag}\left(\begin{bmatrix}\left(\boldsymbol{E}^2_{F_1}\right)^T\left(\boldsymbol{I}^2_{F_1}\right)^* \\ \left(\boldsymbol{E}^2_{F_2}\right)^T\left(\boldsymbol{I}^2_{F_2}\right)^*\end{bmatrix}\right) = 0 \tag{4.6}$$

and

$$\boldsymbol{I}^3_{F_1F_2} = \left(\boldsymbol{Z}^T_{L_1L_4F_1F_2}\boldsymbol{Z}_{L_1L_4F_1F_2}\right)^{-1}\boldsymbol{Z}^T_{L_1L_4F_1F_2}\left(\boldsymbol{Z}_{L_1L_4K}\boldsymbol{I}_K - \boldsymbol{E}_{L_1L_4}\right) \tag{4.7}$$

$$\boldsymbol{E}^3_{F_1F_2} = \boldsymbol{Z}_{F_1F_2K}\boldsymbol{I}_K - \boldsymbol{Z}_{F_1F_2F_1F_2}\boldsymbol{I}^3_{F_1F_2} \tag{4.8}$$

$$\text{Imag}\left(\begin{bmatrix}\left(\boldsymbol{E}^3_{F_1}\right)^T\left(\boldsymbol{I}^3_{F_1}\right)^* \\ \left(\boldsymbol{E}^3_{F_2}\right)^T\left(\boldsymbol{I}^3_{F_2}\right)^*\end{bmatrix}\right) = 0 \tag{4.9}$$

The measurements vector is given by

$$M = [E_{L_{1a}}, E_{L_{1b}}, E_{L_{1c}}, E_{L_{2a}}, E_{L_{2b}}, E_{L_{2c}}, \ldots$$
$$E_{L_{3a}}, E_{L_{3b}}, E_{L_{3c}}, E_{L_{4a}}, E_{L_{4b}}, E_{L_{4c}}] \tag{4.10}$$

The unknown variable vector is defined as

$$X = [x_1, x_2, \ldots, x_{24}, x_{25}, x_{26}]^T \tag{4.11}$$

where,

T denotes the transpose of a vector;

x_1, x_3, …, x_{23} are the magnitude of $E_{L_{1a}}$, $E_{L_{1b}}$, … $E_{L_{4c}}$, respectively;

x_2, x_4, …, x_{24} are the radians of $E_{L_{1a}}$, $E_{L_{1b}}$, … $E_{L_{4c}}$, respectively;

x_{25} and x_{26} denote fault locations for a simultaneous fault.

There is a total of six equations can be separated from (4.3), (4.6), and (4.9). Let us denote those equations using $f_1, f_2, \ldots, f_6$. Then, the function vector $F(X)$ is defined as

$$F_i(X) = f_i, \qquad i = 1, 2, \ldots, 6 \tag{4.12}$$

$$F_{6+2i-1}(X) = x_{2i-1}, \quad i = 1, 2, \ldots, 12 \tag{4.13}$$

$$F_{6+2i}(X) = x_{2i}, \qquad i = 1, 2, \ldots, 12 \tag{4.14}$$

The measurement vector S is given by

$$S_i = 0, \qquad i = 1, 2, \ldots, 6 \tag{4.15}$$

$$S_{6+2i-1} = x_{2i-1}, \qquad i = 1, 2, \ldots, 12 \tag{4.16}$$

$$S_{6+2i} = x_{2i}, \qquad i = 1, 2, \ldots, 12 \tag{4.17}$$

The function vector $F(X)$ and measurement vector S is related by

$$F(X) = S - \mu \tag{4.18}$$

The mean μ is used to obtain covariance matrix R,

$$R = E(\mu\mu^T) = diag(\sigma_1^2, \sigma_2^2, \ldots, \sigma_N^2) \tag{4.19}$$

where $E(.)$ denotes the expected value of its argument, and $diag(.)$ denotes a diagonal matrix with its arguments as diagonal elements. σ_i^2 denotes the error variance of measurement i. A smaller σ_i^2 indicates measurement S_i is more accurate. N denotes the total number of measurements S.

The optimal estimate of X is obtained by minimizing the cost function as

$$J = [S - F(X)]^T R^{-1} [S - F(X)] \tag{4.20}$$

We can use the iterative method to solve (4.20). At the kth iteration, the unknown variable vector can be updated using the following equations as

$$\Delta X = (H^T R^{-1} H)^{-1} \{H^T R^{-1} [S - F(X_k)]\} \tag{4.21}$$

where

$$H = \frac{\partial F(X_k)}{\partial X} \tag{4.22}$$

and

$$X_{k+1} = X_K + \Delta X \tag{4.23}$$

The iterative process will stop when ΔX is smaller than the selected tolerance. Then the optimal estimation of X is obtained. Note that the last two elements in X are the fault locations desired for a simulations fault.

To detect whether bad data exist in the system, the Chi-square test is used [45]. First, the expected value of the cost function is given by [45]

$$K = num(S) - num(X) \tag{4.24}$$

where $num(.)$ denotes the number of its arguments. K is also called the degree of freedom.

Then, the chi-square value $\chi^2_{K,\alpha}$ is adopted to detect the bad data. $\chi^2_{K,\alpha}$ denotes a value with degree of freedom K and probability $(1-\alpha)$ confidence. The value can be obtained using Matlab built-in function *chi2inv* as $\chi^2_{K,\alpha} = chi2inv(1-\alpha, K)$. For example, chi-square value $\chi^2_{2,0.01}$ is given by $chi2inv(0.99,2)$, and the value is 9.2103.

The calculated value of the cost function is given by [45]

$$\hat{J} = \sum_{1}^{N} \frac{\left(S_i - \overline{F}_i(X)\right)^2}{\sigma_i^2} \tag{4.25}$$

where $\overline{F}_i(X)$ is the estimated measurement value obtained from (4.12) – (4.14) and (4.23). If $\hat{J} > \chi^2_{K,\alpha}$, we suspect that bad data exist in the system with probability $(1-\alpha)$ confidence. Otherwise, the system is free of bad data.

If bad data exists, then the measurement corresponding with the largest standardized error will be identified as bad data. The standardized error is obtained as

$$SE_i = \frac{S_i - \overline{F}_i(X)}{\sqrt{\Omega_{ii}}} \tag{4.26}$$

where Ω_{ii} is the diagonal elements of Ω, which is given by

$$\Omega = R - H(H^T R^{-1} H)^{-1} H^T \tag{4.27}$$

4.2 Evaluation Studies

In this subsection, the proposed optimal fault location estimation method is validated by simulation studies. The method is applied to the distribution system with high penetration of DGs shown in Figure 3.3. Various fault types, fault locations, and measurement error magnitudes are simulated to obtain phasor measurement values for evaluation studies.

In the studies, the initial values for unknown variables vector are selected as follows. The initial values of voltage magnitude and radians are chosen as measurement values to speed up the converge. The initial values of the fault location are selected as 0.5 per unit.

Three different cases will be demonstrated in subsection 4.2.1 to 4.2.3.

4.2.1 Case 1 – A Simultaneous Fault: AG and LLLG

Let us consider a simultaneous fault involving two faults. The first fault is an AG fault that occurs on the line between bus 806 and 808, with actual fault location being 0.8 per unit and fault resistance being 25 ohms. The second fault is an LLLG fault on the line between bus 828 and bus 830, with the actual fault location of 0.3 per unit and fault resistance of 50 ohms. Voltage measurements at buses 800, 816, 836, and 844 are used to study state estimation of fault location.

To demonstrate the effectiveness of the proposed bad data detection and identification, the voltage measurements at bus 836 is multiplied by 2.0 to emulate a bad data. We will then examine whether our method can detect and identify this bad data.

Table 4.1 summarizes the state estimation results in the presence of bad data. In the table, the first column lists the bus numbers, the second to fourth columns list measured voltage value for each bus, the fifth to seventh columns list optimal estimated voltage value for each bus, and the last two columns list the actual fault location and estimated fault location, respectively.

From Table 4.1, it is observed that the estimated fault location is not accurate. To examine whether bad data exists, the proposed method is applied. The estimated value of the cost function is obtained as $\hat{J} = 27.5847$. The degree of freedom is 4, and $\chi^2_{4,0.01}$ is equal to 13.2767. Since $\hat{J} > \chi^2_{4,0.01}$, it is determined that bad measurement data exists in this system with a 99% confidence level. For this case, the voltage measurement at bus 836 corresponds to the largest normalized error. Therefore, measurement at bus 836 is identified as the bad data.

Table 4.1 Optimal estimate of fault location with bad data using the Type I fault location algorithm for a simultaneous AG and LLLG fault

Bus No.	Measured voltage value (p.u.)			Optimal voltage estimates (p.u.)			Act. FL (p.u.)	Esti. FL (p.u.)
	Phase A	Phase B	Phase C	Phase A	Phase B	Phase C		
800	1.1791 -0.2687i	-0.7536 -1.0024i	-0.4970 +1.1509i	1.1789 -0.2683i	-0.7516 -1.0026i	-0.4966 +1.1502i		
816	0.1293 -0.1428i	-0.2559 -0.2260i	-0.1163 +0.2049i	0.1293 -0.1428i	-0.2558 -0.2258i	-0.1160 +0.2044i	m1 = 0.8	m1 = 0.7971
836	0.1589 -0.0122i	-0.0966 -0.2492i	-0.1783 +0.0888i	0.1525 -0.0119i	-0.0943 -0.2418i	-0.1689 +0.0842i	m2 = 0.3	m2 = 0.2530
844	0.0774 -0.0072i	-0.0493 -0.1234i	-0.0885 +0.0436i	0.0778 -0.0073i	-0.0494 -0.1238i	-0.0886 +0.0436i		

We discard the bad measurements of bus 836 and redo the state estimation. Results are summarized in Table 4.2. From the table, it is seen that the estimated fault location results are quite accurate. The new estimated value of the cost function is $\hat{J} =$ 4.6180e-4. The new degree of freedom is 2. Since $\hat{J} < \chi^2_{2,0.01}$, it indicates that no more bad data exists in the system with a 99% confidence level.

Table 4.2 Optimal estimate of fault location with bad data being removed using the Type I fault location algorithm for a simultaneous AG and LLLG fault

Bus No.	Measured voltage value (p.u.)			Optimal voltage estimates (p.u.)			Act. FL (p.u.)	Esti. FL (p.u.)
	Phase A	Phase B	Phase C	Phase A	Phase B	Phase C		
800	1.1791 -0.2687i	-0.7536 -1.0024i	-0.4970 +1.1509i	1.1791 -0.2687i	-0.7536 - 1.0023i	-0.4970 +1.1509i		
816	0.1293 -0.1428i	-0.2559 -0.2260i	-0.1163 +0.2049i	0.1293 -0.1428i	-0.2559 -0.2260i	-0.1163 +0.2049i	m1 = 0.8 m2 = 0.3	m1 = 0.7892 m2 = 0.2991
844	0.0774 -0.0072i	-0.0493 -0.1234i	-0.0885 +0.0436i	0.0774 -0.0072i	-0.0493 -0.1234i	-0.0885 +0.0436i		

4.2.2 Case 2 – A Simultaneous Fault: AG and BG

Let us consider another simultaneous fault. The first fault is an AG fault on the line between bus 806 and 808, with fault location as 0.3 per unit and fault resistance as 1 ohm. The second fault is a BG fault on the line between bus 828 and 830, with fault location being 0.7 per unit and fault resistance as 1 ohm.

The voltage measurements at buses 800, 816, 836, and 844 are selected to study the optimal estimation of fault location. To study the optimal estimation, the voltage magnitudes of bus 816 is multiplied by 1.5 to emulate a bad data.

Table 4.3 summarizes the state estimation results in the presence of bad data. In the table, the last two columns list the actual fault location and estimated fault location, respectively. From the table, it is observed that the estimated fault location is not accurate.

To examine whether bad data exists, the proposed method is applied. The estimated value of the cost function is obtained as $\hat{J} = 292.9536$. The degree of freedom is 4, and $\chi^2_{4,0.01}$ is equal to 13.2767. Since $\hat{J} > \chi^2_{4,0.01}$, it is determined that bad measurement data exists in this system with a 99% confidence level. For this case, the voltage measurement at bus 816 corresponds to the largest normalized error. Therefore, measurement at bus 816 is identified as the bad data.

Table 4.3 Optimal estimate of fault location with bad data using the Type I fault location algorithm for a simultaneous AG and BG fault

Bus No.	Measured voltage value (p.u.)			Optimal voltage estimates (p.u.)			Act. FL (p.u.)	Esti. FL (p.u.)
	Phase A	Phase B	Phase C	Phase A	Phase B	Phase C		
800	0.6757 -0.3271i	-0.7301 -1.0408i	-0.6727 +1.1781i	0.6695 -0.3415i	-0.7608 -1.0326i	-0.6268 +1.2392i		
816	0.3115 -0.1578i	-0.4188 -0.4139i	-1.1638 +1.5776i	0.3005 -0.1500i	-0.3962 -0.4092i	-1.2591 +1.4507i	m1 = 0.3	m1 = 0.2638
836	0.3202 -0.2486i	0.0048 -0.2669i	-0.7373 +0.8549i	0.3218 -0.2503i	0.0042 -0.2673i	-0.7311 +0.8645i	m2 = 0.7	m2 = 0.0597
844	0.3184 -0.2454i	0.0038 -0.2619i	-0.7367 +0.8589i	0.3200 -0.2472i	0.0032 -0.2623i	-0.7305 +0.8685i		

We then discard the bad data at bus 816 and repeat the state estimation process. The results are summarized in Table 4.4. It is seen the fault location estimate results are quite accurate. The new estimated value of the cost function is $\hat{J} = 2.0477\text{e-}4$, and the new degree of freedom is 2. Since $\hat{J} < \chi^2_{2,0.01}$, there exists no bad data in the system. That is, the bad data at bus 816 is correctly identified and removed.

Table 4.4 Optimal estimate of fault location with bad data being removed using the Type I fault location algorithm for a simultaneous AG and BG fault

Bus No.	Measured voltage value (p.u.)			Optimal voltage estimates (p.u.)			Act. FL (p.u.)	Esti. FL (p.u.)
	Phase A	Phase B	Phase C	Phase A	Phase B	Phase C		
800	0.6757 -0.3271i	-0.7301 -1.0408i	-0.6727 +1.1781i	0.6757 -0.3271i	-0.7301 -1.0408i	-0.6727 +1.1781i		
836	0.3202 -0.2486i	0.0048 -0.2669i	-0.7373 +0.8549i	0.3202 -0.2486i	0.0048 -0.2669i	-0.7373 +0.8549i	m1 = 0.3 m2 = 0.7	m1 = 0.3008 m2 = 0.7389
844	0.3184 -0.2454i	0.0038 -0.2619i	-0.7367 +0.8589i	0.3184 -0.2454i	0.0038 -0.2619i	-0.7367 +0.8589i		

4.2.3 Case 3 – A Simultaneous Fault: AG and LLLG

Assuming there is a simultaneous fault in the system. One fault is an AG fault occurs on the line from bus 808 to 812, the fault location is 0.8 per unit, and the fault resistance is 1 ohm. The other fault is an LLLG fault on the line from bus 854 to 832, the fault location is 0.1 per unit, and fault resistance is [1, 1, 1, 1] ohm.

The voltage measurements at buses 800, 850, 858, and 836 are used for the evaluation study. The voltage magnitude at bus 850 is treated as bad data by multiplying it with a factor of 2.

Table 4.5 summarizes the state estimation results in the presence of bad data. In the table, the last two columns list the actual fault location and estimated fault location, respectively. It is seen that the estimated fault location is not accurate. The proposed method is applied to detect whether a bad exist. The estimated value of the cost function is obtained as $\hat{J} = 347.0965$. The degree of freedom is 4, and $\chi^2_{4,0.01}$ is equal to 13.2767. Since $\hat{J} > \chi^2_{4,0.01}$, it is determined that bad measurement data exists in this system with a

99% confidence level. For this case, the voltage measurement at bus 850 corresponds to the largest normalized error. Thus, measurement at bus 850 is identified as the bad data.

Table 4.5 Optimal estimate of fault location with bad data using the Type I fault location algorithm for a simultaneous AG and LLLG fault

Bus No.	Measured voltage value (p.u.)			Optimal voltage estimates (p.u.)			Act. FL (p.u.)	Esti. FL (p.u.)
	Phase A	Phase B	Phase C	Phase A	Phase B	Phase C		
800	1.1448 -0.2067i	-0.7510 -1.0329i	-0.5234 +1.1714i	1.1264 -0.2678i	-0.8611 -0.9846i	-0.4388 +1.2289i		
850	0.0768 -0.0524i	-0.8037 -0.7016i	-0.4260 +0.7848i	0.0651 -0.0443i	-0.7404 -0.7069i	-0.4438 +0.7477i	m1 = 0.8	m1 = 0.7987
858	0.0481 +0.0251i	-0.0392 -0.0625i	-0.0535 +0.0585i	0.0475 +0.0247i	-0.0386 -0.0616i	-0.0524 +0.0574i	m2 = 0.1	m2 = 0.9774
836	0.0558 +0.0276i	-0.0377 -0.0712i	-0.0595 +0.0606i	0.0552 +0.0273i	-0.0371 -0.0701i	-0.0583 +0.0594i		

Then, bad data at bus 850 is discarded. The proposed method is repeated using measurements at buses 800, 858, and 836. The results are shown in Table 4.6, and the estimated fault location results are accurate. The new estimated value of the cost function is $\hat{J} = 4.6135\text{e-}8$, and the new degree of freedom is 2. Since $\hat{J} < \chi^2_{2,0.01}$, there exists no more bad data in the system. That is, the bad data at bus 850 is correctly identified and removed.

Again, it is evidenced that the proposed optimal fault location estimation method is capable of detecting and identifying the bad data. In a result, the accuracy of the estimated fault location is greatly enhanced.

Table 4.6 Optimal estimate of fault location with bad data being removed using the Type I fault location algorithm for a simultaneous AG and LLLG fault

Bus No.	Measured voltage value (p.u.)			Optimal voltage estimates (p.u.)			Act. FL (p.u.)	Esti. FL (p.u.)
	Phase A	Phase B	Phase C	Phase A	Phase B	Phase C		
800	1.1448 -0.2067i	-0.7510 -1.0329i	-0.5234 +1.1714i	1.1448 -0.2067i	-0.7510 -1.0329i	-0.5234 +1.1714i		
858	0.0481 +0.0251i	-0.0392 -0.0625i	-0.0535 +0.0585i	0.0481 +0.0251i	-0.0392 -0.0625i	-0.0535 +0.0585i	m1 = 0.8 m2 = 0.1	m1 = 0.7943 m2 = 0.0994
836	0.0558 +0.0276i	-0.0377 -0.0712i	-0.0595 +0.0606i	0.0558 +0.0276i	-0.0377 -0.0712i	-0.0595 +0.0606i		

4.3 Optimal Fault Location Estimate Using the Alternative Approach of Type I algorithm

In this subsection, the optimal estimate of fault location using the alternative approach of Type I algorithm is illustrated. Assuming there are four voltage measurements $\boldsymbol{E}_{L_1}$, $\boldsymbol{E}_{L_2}$, $\boldsymbol{E}_{L_3}$, and $\boldsymbol{E}_{L_4}$ are available for state estimation. From (3.18), the following two equations are obtained as

$$\begin{aligned}&\left(\boldsymbol{Z}_{L_1L_2F_1F_2}^{T}\boldsymbol{Z}_{L_1L_2F_1F_2}\right)^{-1}\boldsymbol{Z}_{L_1L_2F_1F_2}^{T}\left(\boldsymbol{Z}_{L_1L_2K}\boldsymbol{I}_K-\boldsymbol{E}_{L_1L_2}\right)\\&\quad=\left(\boldsymbol{Z}_{L_1L_3F_1F_2}^{T}\boldsymbol{Z}_{L_1L_3F_1F_2}\right)^{-1}\boldsymbol{Z}_{L_1L_3F_1F_2}^{T}\left(\boldsymbol{Z}_{L_1L_3K}\boldsymbol{I}_K-\boldsymbol{E}_{L_1L_3}\right)\end{aligned}\tag{4.28}$$

And

$$\begin{aligned}&\left(\boldsymbol{Z}_{L_1L_2F_1F_2}^{T}\boldsymbol{Z}_{L_1L_2F_1F_2}\right)^{-1}\boldsymbol{Z}_{L_1L_2F_1F_2}^{T}\left(\boldsymbol{Z}_{L_1L_2K}\boldsymbol{I}_K-\boldsymbol{E}_{L_1L_2}\right)\\&\quad=\left(\boldsymbol{Z}_{L_1L_4F_1F_2}^{T}\boldsymbol{Z}_{L_1L_4F_1F_2}\right)^{-1}\boldsymbol{Z}_{L_1L_4F_1F_2}^{T}\left(\boldsymbol{Z}_{L_1L_4K}\boldsymbol{I}_K-\boldsymbol{E}_{L_1L_4}\right)\end{aligned}\tag{4.29}$$

The measurement vector is

$$\begin{aligned}M=[&E_{L_{1a}},E_{L_{1b}},E_{L_{1c}},E_{L_{2a}},E_{L_{2b}},E_{L_{2c}},\\&E_{L_{3a}},E_{L_{3b}},E_{L_{3c}},E_{L_{4a}},E_{L_{4b}},E_{L_{4c}}]\end{aligned}\tag{4.30}$$

The unknown variables vector is defined as

$$X=[x_1,x_2,\dots,x_{24},x_{25},x_{26}]^T\tag{4.31}$$

where,

T denotes the transpose of a vector;

$x_1, x_3, \ldots, x_{23}$ are the magnitude of $E_{L_{1a}}, E_{L_{1b}}, \ldots E_{L_{4c}}$, respectively;

$x_2, x_4, \ldots, x_{24}$ are the radians of $E_{L_{1a}}, E_{L_{1b}}, \ldots E_{L_{4c}}$, respectively;

x_{25} and x_{26} denote fault locations for a simultaneous fault.

There are a total of 6 equations can be separated from (4.28). The first three equations (h_1, h_2, h_3) are related to the first fault for phase A, B, and C, respectively. The last three equations (h_4, h_5, h_6) are related to the second fault for phase A, B, and C, respectively. We can further separate those six equations into twelve real equations as

$$\mathrm{RE}(h_i) = 0, i = 1, 2, \ldots, 6 \tag{4.32}$$

$$\mathrm{IM}(h_i) = 0, \ i = 1, 2, \ldots, 6 \tag{4.33}$$

where $\mathrm{RE}(.)$ returns the real part of its argument, and $\mathrm{IM}(.)$ returns the imaginary part of its argument. Similarly, there is another total of 12 real equations can be separated from (4.29). If we let

$$f_{2i-1}(X) = \mathrm{RE}(h_i), \qquad i = 1, 2, \ldots, 12 \tag{4.34}$$

$$f_{2i}(X) = \mathrm{IM}(h_i), \qquad i = 1, 2, \ldots, 12 \tag{4.35}$$

Then, the function vector will be defined as

$$F_i(X) = f_i(X), \qquad i = 1, 2, \ldots, 24 \tag{4.36}$$

$$F_{24+2i-1} = x_{2i-1}, \qquad i = 1, 2, \ldots, 12 \tag{4.37}$$

$$F_{24+2i} = x_{2i}, \qquad i = 1, 2, \ldots, 12 \tag{4.38}$$

The measurement vector S is defined as

$$S_i(X) = 0, \qquad i = 1, 2, \ldots, 24 \tag{4.39}$$

$$S_{24+2i-1} = x_{2i-1}, \qquad i = 1, 2, \ldots, 12 \tag{4.40}$$

$$S_{24+2i} = x_{2i}, \qquad i = 1, 2, \dots, 12 \tag{4.41}$$

The measurement vector S and the function vector $F(X)$ are related by (4.18). The mean μ is characterized by (4.19). The optimal estimator is obtained by following (4.20) – (4.23). Then, the chi-square test is performed to detect and identify the bad data by (4.24) – (4.27).

4.4 Evaluation Studies

In this subsection, the proposed optimal estimation of fault location method using the alternative approach of Type I algorithm is verified by case studies. Again, the method is applied to the distribution system in the presence of DGs shown in Figure 3.3. Different fault types, fault locations, and bad data are simulated to get the phasor values for case studies.

The initial values of voltage magnitude and radians are selected as the same to the measurement values to increase the converge speed. The initial values of fault locations are chosen as 0.5 per unit. Three cases with different fault scenarios are demonstrated in subsection 4.4.1 to 4.4.2.

4.4.1 Case 1 – A Simultaneous Fault: CG and BG

Assuming there is a simultaneous fault in the system. One fault is a CG fault on the line from bus 806 to 808, with fault location as 0.2 per unit and fault resistance is 1 ohm. The other fault is a BG fault on the line from bus 854 to 832, with fault location being 0.9 per unit and fault resistance as 1 ohm.

Voltage measurements at buses 800, 816, 836, and 844 are used for optimal fault location estimate. The voltage at bus 844 is multiplied by 1.35 to emulate a bad data. The results are summarized in Table 4.7.

In Table 4.7, the first column lists the bus numbers, the second to fourth columns list measured voltage value for each bus, the fifth to seventh columns list optimal estimated voltage value for each bus, and the last two columns list the actual fault location and estimated fault location, respectively.

From Table 4.7, it is observed that the estimated fault location is not accurate. To examine whether bad data exists, the proposed method is applied. The estimated value of the cost function is obtained as $\hat{J} = 47.8541$. The degree of freedom is 22, and $\chi^2_{22,0.01}$ is equal to 40.2894. Since $\hat{J} > \chi^2_{22,0.01}$, it is determined that bad measurement data exists in this system with a 99% confidence level. For this case, the voltage measurement at bus 844 corresponds to the largest normalized error. Therefore, measurement at bus 844 is identified as the bad data.

Table 4.7 Optimal estimate of fault location with bad data using the alternative approach of Type I fault location algorithm for a simultaneous CG and BG fault

Bus No.	Measured voltage value (p.u.)			Optimal voltage estimates (p.u.)			Act. FL (p.u.)	Esti. FL (p.u.)
	Phase A	Phase B	Phase C	Phase A	Phase B	Phase C		
800	1.3778 -0.0266i	-0.7343 -1.0763i	-0.0254 +0.6454i	1.3700 -0.0319i	-0.7321 -1.0737i	-0.0229 +0.6456i		
816	1.1345 +0.0947i	-0.3872 -0.4912i	-0.2830 +0.2510i	1.1503 +0.0997i	-0.3914 -0.4964i	-0.2908 +0.2565i	m1 = 0.2	m1 = 0.2149
836	0.8916 +0.2456i	-0.0676 -0.0421i	-0.5920 +0.3297i	0.8926 +0.2457i	-0.0674 -0.0420i	-0.5930 +0.3304i	m2 = 0.9	m2 = 0.9981
844	1.2084 +0.3323i	-0.0867 -0.0528i	-0.7923 +0.4481i	1.1992 +0.3315i	-0.0841 -0.0512i	-0.7855 +0.4461i		

After bad data at bus 844 is removed, we redo the optimal estimation. Results are summarized in Table 4.8. It is evidenced the fault location results become accurate after the bad data is removed. The new estimated value of the cost function is $\hat{J} = 0.0013$. The new degree of freedom is $K = 10$, and $\chi^2_{10,0.01} = 23.2093$. Since $\hat{J} < \chi^2_{10,0.01}$, it indicates no bad data exist in the system any more.

Table 4.8 Optimal estimate of fault location with bad data being removed using the alternative approach of Type I fault location algorithm for a simultaneous CG and BG fault

Bus No.	Measured voltage value (p.u.)			Optimal voltage estimates (p.u.)			Act. FL (p.u.)	Esti. FL (p.u.)
	Phase A	Phase B	Phase C	Phase A	Phase B	Phase C		
800	1.3778 -0.0266i	-0.7343 -1.0763i	-0.0254 +0.6454i	1.3778 -0.0267i	-0.7343 -1.0763i	-0.0254 +0.6454i		
816	1.1345 +0.0947i	-0.3872 -0.4912i	-0.2830 +0.2510i	1.1344 +0.0948i	-0.3872 -0.4912i	-0.2830 +0.2510i	m1 = 0.2 m2 = 0.9	m1 = 0.2000 m2 = 0.9014
836	0.8916 +0.2456i	-0.0676 -0.0421i	-0.5920 +0.3297i	0.8916 +0.2455i	-0.0675 -0.0421i	-0.5920 +0.3297i		

4.4.2 Case 2 – A Simultaneous Fault: AG and BG

Let us consider a simultaneous fault. The first fault is an AG fault imposed on the line between bus 806 and 808, with fault location as 0.3 per unit and fault resistance is 1 ohm. The second fault is a BG fault imposed on the line from bus 828 to 830, with fault location being 0.7 per unit, and fault resistance as 1 ohm.

Voltage measurements at buses 800, 816, 836, and 844 are used for optimal fault location estimate. The voltage at bus 836 is multiplied by 1.3 to emulate a bad data.

Table 4.9 summarizes the state estimation results. In the table, the last two columns list the actual fault location and estimated fault location, respectively. From the table, it is observed that the estimated fault location is not accurate. To examine whether

bad data exists, the proposed method is applied. The estimated value of the cost function is obtained as $\hat{J} = 85.2873$. The degree of freedom is 22, and $\chi^2_{22,0.01}$ is equal to 40.2894. Since $\hat{J} > \chi^2_{4,0.01}$, it is determined that bad measurement data exists in this system with a 99% confidence level. For this case, the voltage measurement at bus 836 corresponds to the largest normalized error. Therefore, measurement at bus 836 is identified as the bad data.

Table 4.9 Optimal estimate of fault location with bad data using the alternative approach of Type I fault location algorithm for a simultaneous AG and BG fault

Bus No.	Measured voltage value (p.u.)			Optimal voltage estimates (p.u.)			Act. FL (p.u.)	Esti. FL (p.u.)
	Phase A	Phase B	Phase C	Phase A	Phase B	Phase C		
800	0.6757 -0.3271i	-0.7301 -1.0408i	-0.6727 +1.1781i	0.6736 -0.3261i	-0.7325 -1.0364i	-0.6659 +1.1745i		
816	0.2077 -0.1052i	-0.2792 -0.2760i	-0.7758 +1.0518i	0.2144 -0.1086i	-0.2833 -0.2823i	-0.7927 +1.0681i	m1 = 0.3	m1 = 0.3766
836	0.4163 -0.3231i	0.0062 -0.3469i	-0.9585 +1.1113i	0.4094 -0.3178i	0.0059 -0.3388i	-0.9464 +1.0954i	m2 = 0.7	m2 = 0.7911
844	0.3184 -0.2454i	0.0038 -0.2619i	-0.7367 +0.8589i	0.3210 -0.2474i	0.0038 -0.2609i	-0.7387 +0.8608i		

After the bad data at bus 836 is removed, the new estimation results are summarized in Table 4.10. It is seen the fault location estimate results are quite accurate. The new estimated value of the cost function is $\hat{J} = 3.2500\text{e-}5$, and the new degree of freedom is 10. Since $\hat{J} < \chi^2_{10,0.01}$, there exists no bad data in the system. That is, the bad data at bus 836 is correctly identified and removed.

Table 4.10 Optimal estimate of fault location with bad data being removed using the alternative approach of Type I fault location algorithm for a simultaneous AG and BG fault

Bus No.	Measured voltage value (p.u.)			Optimal voltage estimates (p.u.)			Act. FL (p.u.)	Esti. FL (p.u.)
	Phase A	Phase B	Phase C	Phase A	Phase B	Phase C		
800	0.6757 -0.3271i	-0.7301 -1.0408i	-0.6727 +1.1781i	0.6757 -0.3271i	-0.7301 -1.0408i	-0.6727 +1.1781i		
816	0.2077 -0.1052i	-0.2792 -0.2760i	-0.7758 +1.0518i	0.2077 -0.1052i	-0.2792 -0.2760i	-0.7758 +1.0518i	m1 = 0.3 m2 = 0.7	m1 = 0.3000 m2 = 0.6996
844	0.3184 -0.2454i	0.0038 -0.2619i	-0.7367 +0.8589i	0.3184 -0.2454i	0.0038 -0.2619i	-0.7367 +0.8589i		

4.4.3 Case 3 – A Simultaneous Fault: AG and BG

Considering a simultaneous fault in the system. One fault is an AG fault imposed on the line from bus 808 to 812, with fault location as 0.3 per unit and fault resistance as 1 ohm. The other fault is a BG fault imposed on the line between bus 854 and 832, with fault location being 0.7 per unit and fault resistance is 1 ohm.

Voltage measurements at buses 800, 816, 836, and 844 are used for optimal fault location estimate. The voltage at bus 844 is multiplied by 1.5 to emulate a bad data. The optimal estimation results are summarized in Table 4.11.

In Table 4.11, the last two columns list the actual fault location and estimated fault location, respectively. It is seen that the estimated fault location is not accurate. The proposed method is applied to detect whether a bad exist. The estimated value of the cost function is obtained as $\hat{J} = 133.0911$. The degree of freedom is 22, and $\chi^2_{22,0.01}$ is equal to 40.2894. Since $\hat{J} > \chi^2_{22,0.01}$, it is determined that bad measurement data exists in this system with a 99% confidence level. For this case, the voltage measurement at bus 844

corresponds to the largest normalized error. Thus, measurement at bus 844 is identified as the bad data.

Table 4.11 Optimal estimate of fault location with bad data using the alternative approach of Type I fault location algorithm for a simultaneous AG and BG fault

Bus No.	Measured voltage value (p.u.)			Optimal voltage estimates (p.u.)			Act. FL (p.u.)	Esti. FL (p.u.)
	Phase A	Phase B	Phase C	Phase A	Phase B	Phase C		
800	0.6757 -0.3271i	-0.7301 -1.0408i	-0.6727 +1.1781i	0.6736 -0.3261i	-0.7325 -1.0364i	-0.6659 +1.1745i		
816	0.2077 -0.1052i	-0.2792 -0.2760i	-0.7758 +1.0518i	0.2144 -0.1086i	-0.2833 -0.2823i	-0.7927 +1.0681i	m1 = 0.3	m1 = 0.3766
836	0.4163 -0.3231i	0.0062 -0.3469i	-0.9585 +1.1113i	0.4094 -0.3178i	0.0059 -0.3388i	-0.9464 +1.0954i	m2 = 0.7	m2 = 0.7911
844	0.3184 -0.2454i	0.0038 -0.2619i	-0.7367 +0.8589i	0.3210 -0.2474i	0.0038 -0.2609i	-0.7387 +0.8608i		

Then, bad data at bus 844 is discarded. The proposed method is repeated using measurements at buses 800, 816, and 836. The results are shown in Table 4.12, and the estimated fault location results are accurate. The new estimated value of the cost function is $\hat{J} = 2.2790\text{e-}4$, and the new degree of freedom is 10. Since $\hat{J} < \chi^2_{10,0.01}$, there exists no more bad data in the system. That is, the bad data at bus 844 is correctly identified and removed.

Again, it is evidenced that the proposed optimal fault location estimation method is capable of detecting and identifying the bad data. In a result, the accuracy of the estimated fault location is greatly enhanced.

Table 4.12 Optimal estimate of fault location with bad data being removed using the alternative approach of Type I fault location algorithm for a simultaneous AG and BG fault

Bus No.	Measured voltage value (p.u.)			Optimal voltage estimates (p.u.)			Act. FL (p.u.)	Esti. FL (p.u.)
	Phase A	Phase B	Phase C	Phase A	Phase B	Phase C		
800	1.0883 -0.2291i	-0.7262 -1.0693i	-0.6602 +1.1780i	1.0883 -0.2291i	-0.7263 -1.0692i	-0.6602 +1.1780i		
816	0.1795 -0.0969i	-0.4751 -0.5294i	-0.8322 +0.9029i	0.1795 -0.0969i	-0.4751 -0.5294i	-0.8322 +0.9028i	m1 = 0.3 m2 = 0.7	m1 = 0.3001 m2 = 0.6999
836	0.2864 -0.1729i	-0.0072 -0.1376i	-0.8083 +0.7462i	0.2864 -0.1729i	-0.0072 -0.1376i	-0.8083 +0.7462i		

4.5 Optimal Fault Location Estimate Using the Type II Fault Location Algorithm

In this subsection, optimal fault location estimator based on the type II fault location algorithm is illustrated. It is assumed that the bad data is captured during the fault. Assuming four voltage measurements $\boldsymbol{E}_{L_1}$, $\boldsymbol{E}_{L_2}$, $\boldsymbol{E}_{L_3}$, and $\boldsymbol{E}_{L_4}$ are available for fault location purpose. From (3.25) to (3.27), we have

$$\boldsymbol{I}^1_{F_1F_2} = -\left(\boldsymbol{Z}^T_{L_1L_2F_1F_2}\boldsymbol{Z}_{L_1L_2F_1F_2}\right)^{-1}\left(\boldsymbol{Z}^T_{L_1L_2F_1F_2}\Delta\boldsymbol{E}_{L_1L_2}\right) \tag{4.42}$$

$$\boldsymbol{E}^1_{F_1F_2} = \boldsymbol{E}^0_{F_1F_2} - \boldsymbol{Z}_{F_1F_2F_1F_2}\boldsymbol{I}^1_{F_1F_2} \tag{4.43}$$

$$\text{Imag}\left(\begin{bmatrix}\left(\boldsymbol{E}^1_{F_1}\right)^T\left(\boldsymbol{I}^1_{F_1}\right)^* \\ \left(\boldsymbol{E}^1_{F_2}\right)^T\left(\boldsymbol{I}^1_{F_2}\right)^*\end{bmatrix}\right) = 0 \tag{4.44}$$

where the superscript 1 denotes the first combination using $\boldsymbol{E}_{L_1}$ and $\boldsymbol{E}_{L_2}$. Similarly, equations for the second combination using $\boldsymbol{E}_{L_1}$, $\boldsymbol{E}_{L_3}$ and the third combination using $\boldsymbol{E}_{L_1}$, $\boldsymbol{E}_{L_4}$ are given by

$$\boldsymbol{I}^2_{F_1F_2} = -\left(\boldsymbol{Z}^T_{L_1L_3F_1F_2}\boldsymbol{Z}_{L_1L_3F_1F_2}\right)^{-1}\left(\boldsymbol{Z}^T_{L_1L_3F_1F_2}\Delta\boldsymbol{E}_{L_1L_3}\right) \tag{4.45}$$

$$\boldsymbol{E}^{2}_{F_1F_2} = \boldsymbol{E}^{0}_{F_1F_2} - \boldsymbol{Z}_{F_1F_2F_1F_2}\boldsymbol{I}^{2}_{F_1F_2} \tag{4.46}$$

$$\text{Imag}\left(\begin{bmatrix}\left(\boldsymbol{E}^{2}_{F_1}\right)^{T}\left(\boldsymbol{I}^{2}_{F_1}\right)^{*}\\ \left(\boldsymbol{E}^{2}_{F_2}\right)^{T}\left(\boldsymbol{I}^{2}_{F_2}\right)^{*}\end{bmatrix}\right) = 0 \tag{4.47}$$

and

$$\boldsymbol{I}^{3}_{F_1F_2} = -\left(\boldsymbol{Z}^{T}_{L_1L_4F_1F_2}\boldsymbol{Z}_{L_1L_4F_1F_2}\right)^{-1}\left(\boldsymbol{Z}^{T}_{L_1L_2F_1F_2}\Delta\boldsymbol{E}_{L_1L_2}\right) \tag{4.48}$$

$$\boldsymbol{E}^{3}_{F_1F_2} = \boldsymbol{E}^{0}_{F_1F_2} - \boldsymbol{Z}_{F_1F_2F_1F_2}\boldsymbol{I}^{3}_{F_1F_2} \tag{4.49}$$

$$\text{Imag}\left(\begin{bmatrix}\left(\boldsymbol{E}^{3}_{F_1}\right)^{T}\left(\boldsymbol{I}^{3}_{F_1}\right)^{*}\\ \left(\boldsymbol{E}^{3}_{F_2}\right)^{T}\left(\boldsymbol{I}^{3}_{F_2}\right)^{*}\end{bmatrix}\right) = 0 \tag{4.50}$$

Then we follow the steps introduced in subsection 4.1 to detect and identify the bad data.

4.6 Evaluation Studies

In this subsection, the proposed optimal fault location estimation method is validated by simulation studies. The phasor measurements obtained from Matlab is multiplied by 1.002 to emulate field data. It is assumed the bad data is captured during the fault. The method is applied to the 21 bus distribution system with DG shown in Figure 3.2. Various fault types, fault locations, and measurement error magnitudes are simulated to obtain phasor measurement values for evaluation studies.

In the studies, the initial values for unknown variables vector are selected as follows. The initial values of voltage magnitude and radians are chosen as measurement values to speed up the converge. The initial values of the fault location are selected as 0.5 per unit.

Three different cases will be demonstrated in subsection 4.6.1 to 4.6.3.

4.6.1 Case 1 – A Simultaneous Fault: AG and CG

Let us consider a simultaneous fault involving two faults. The first fault is an AG fault that occurs on the line between bus 1 and 2, with actual fault location being 0.6 per unit and fault resistance being 1 ohm. The second fault is a CG fault on the line between bus 13 and bus 15, with actual fault location of 0.5 per unit and fault resistance of 1 ohm. Voltage measurements at buses 1, 7, 15, and 20 are used to study state estimation of fault location.

To demonstrate the effectiveness of the proposed bad data detection and identification, the voltage measurements at bus 20 is multiplied by 1.1 to emulate a bad data. We will then examine whether our method can detect and identify this bad data.

Table 4.13 summarizes the state estimation results in the presence of bad data. In the table, the first column lists the bus numbers, the second to fourth columns list measured voltage value for each bus, the fifth to seventh columns list optimal estimated voltage value for each bus, and the last two columns list the actual fault location and estimated fault location, respectively.

From Table 4.13, it is observed that the estimated fault location is not accurate. To examine whether bad data exists, the proposed method is applied. The estimated value of the cost function is obtained as $\hat{J} = 32.2682$. The degree of freedom is 4, and $\chi^2_{4,0.01}$ is equal to 13.2767. Since $\hat{J} > \chi^2_{4,0.01}$, it is determined that bad measurement data exists in this system with a 99% confidence level. For this case, the voltage measurement at bus 20 corresponds to the largest normalized error. Therefore, measurement at bus 20 is identified as the bad data.

Table 4.13 Optimal estimate of fault location with bad data using the Type II fault location algorithm for a simultaneous AG and CG fault

Bus No.	Measured voltage value (p.u.)			Optimal voltage estimates (p.u.)			Act. FL (p.u.)	Esti. FL (p.u.)
	Phase A	Phase B	Phase C	Phase A	Phase B	Phase C		
1	0.6778 -0.3024i	-0.5081 -0.8066i	-0.3342 +0.8805i	0.6793 -0.3045i	-0.5140 -0.8068i	-0.3334 +0.8793i		
7	0.4890 -0.3077i	-0.5492 -0.7832i	-0.2176 +0.6922i	0.4925 -0.3107i	-0.5554 -0.7849i	-0.2151 +0.6941i	m1 = 0.6	m1 = 0.6055
15	0.6948 -0.4501i	-0.4720 -0.9415i	0.0491 +0.1757i	0.6956 -0.4514i	-0.4758 -0.9413i	0.0501 +0.1792i	m2 = 0.5	m2 = 0.1991
20	0.8661 -0.3532i	-0.4984 -0.8778i	0.0335 +0.5851i	0.8540 -0.3419i	-0.4792 -0.8693i	0.0279 +0.5740i		

We discard the bad measurements of bus 20 and redo the state estimation. Results are summarized in Table 4.14. From the table, it is seen that the estimated fault location results are quite accurate. The new estimated value of the cost function is $\hat{J} = 1.1506\text{e-}4$. The new degree of freedom is 2. Since $\hat{J} < \chi^2_{2,0.01}$, it indicates that no more bad data exists in the system with a 99% confidence level. So, the obtained estimates are acceptable.

Table 4.14 Optimal estimate of fault location with bad data being removed using the Type II fault location algorithm for a simultaneous AG and CG fault

Bus No.	Measured voltage value (p.u.)			Optimal voltage estimates (p.u.)			Act. FL (p.u.)	Esti. FL (p.u.)
	Phase A	Phase B	Phase C	Phase A	Phase B	Phase C		
1	0.6778 -0.3024i	-0.5081 -0.8066i	-0.3342 +0.8805i	0.6778 -0.3024i	-0.5081 -0.8066i	-0.3342 +0.8805i		
7	0.4890 -0.3077i	-0.5492 -0.7832i	-0.2176 +0.6922i	0.4890 -0.3077i	-0.5491 -0.7832i	-0.2177 +0.6922i	m1 = 0.6 m2 = 0.5	m1 = 0.6007 m2 = 0.4986
15	0.6948 -0.4501i	-0.4720 -0.9415i	0.0491 +0.1757i	0.6948 -0.4501i	-0.4720 -0.9415i	0.0491 +0.1757i		

4.6.2 Case 2 – A Simultaneous Fault: CG and LLLG

Let us consider another simultaneous fault. The first fault is a CG fault on the line between bus 2 and 5, with fault location as 0.6 per unit and fault resistance as 1 ohm. The second fault is an LLLG fault on the line between bus 11 and 12, with fault location being 0.7 per unit and fault resistance as [1, 1, 1, 5] ohm.

The voltage measurements at buses 1, 8, 14, and 18 are selected to study the optimal estimation of fault location. To study the optimal estimation, the voltage magnitudes of bus 18 is multiplied by 1.15 to emulate a bad data.

Table 4.15 summarizes the state estimation results in the presence of bad data. In the table, the last two columns list the actual fault location and estimated fault location, respectively. From the table, it is observed that the estimated fault location is not accurate. To examine whether bad data exists, the proposed method is applied. The estimated value of the cost function is obtained as $\hat{J} = 31.6507$. The degree of freedom is 4, and $\chi^2_{4,0.01}$ is equal to 13.2767. Since $\hat{J} > \chi^2_{4,0.01}$, it is determined that bad measurement data exists in this system with a 99% confidence level. For this case, the voltage measurement at bus 18 corresponds to the largest normalized error. Therefore, measurement at bus 18 is identified as the bad data.

Table 4.15 Optimal estimate of fault location with bad data using the Type II fault location algorithm for a simultaneous CG and LLLG fault

Bus No.	Measured voltage value (p.u.)			Optimal voltage estimates (p.u.)			Act. FL (p.u.)	Esti. FL (p.u.)
	Phase A	Phase B	Phase C	Phase A	Phase B	Phase C		
1	0.8798 -0.1420i	-0.5741 -0.6338i	-0.1666 +0.7383i	0.8865 -0.1470i	-0.5789 -0.6360i	-0.1615 +0.7407i		
8	0.5243 -0.2891i	-0.3507 -0.3841i	0.0994 +0.1757i	0.5295 -0.2951i	-0.3561 -0.3854i	0.1018 +0.1797i	m1 = 0.6	m1 = 0.4320
14	0.5464 -0.2813i	-0.3972 -0.2901i	0.1105 +0.3838i	0.5499 -0.2852i	-0.4017 -0.2917i	0.1116 +0.3859i	m2 = 0.7	m2 = 0.6393
18	0.6309 -0.3177i	-0.4511 -0.3431i	0.1118 +0.4404i	0.6191 -0.3036i	-0.4353 -0.3381i	0.1080 +0.4328i		

We then discard the bad data at bus 18 and repeat the state estimation process. The results are summarized in Table 4.16. It is seen the fault location estimate results are quite accurate. The new estimated value of the cost function is $\hat{J} = 4.0560\text{e-}4$, and the new degree of freedom is 2. Since $\hat{J} < \chi^2_{2,0.01}$, there exists no bad data in the system. That is, the bad data at bus 18 is correctly identified and removed.

Table 4.16 Optimal estimate of fault location with bad data being removed using the Type II fault location algorithm for a simultaneous CG and LLLG fault

Bus No.	Measured voltage value (p.u.)			Optimal voltage estimates (p.u.)			Act. FL (p.u.)	Esti. FL (p.u.)
	Phase A	Phase B	Phase C	Phase A	Phase B	Phase C		
1	0.8798 -0.1420i	-0.5741 -0.6338i	-0.1666 +0.7383i	0.8797 -0.1420i	-0.5741 -0.6338i	-0.1666 +0.7383i		
8	0.5243 -0.2891i	-0.3507 -0.3841i	0.0994 +0.1757i	0.5243 -0.2890i	-0.3507 -0.3842i	0.0994 +0.1757i	m1 = 0.6 m2 = 0.7	m1 = 0.6133 m2 = 0.6964
14	0.5464 -0.2813i	-0.3972 -0.2901i	0.1105 +0.3838i	0.5464 -0.2813i	-0.3972 -0.2901i	0.1105 +0.3838i		

4.6.3 Case 3 – A Simultaneous Fault: AG and BCG

Assuming there is a simultaneous fault in the system. One fault is an AG fault occurs on the line from bus 5 to 8, the fault location is 0.5 per unit, and the fault resistance is 1 ohm. The other fault is a BCG fault on the line from bus 16 to 18, the fault location is 0.8 per unit, and fault resistance is [1, 1, 1] ohm.

The voltage measurements at buses 1, 11, 14, and 21 are used for the evaluation study. The voltage magnitude at bus 21 is treated as bad data by multiplying it with a factor of 1.2.

Table 4.17 summarizes the state estimation results in the presence of bad data. In the table, the last two columns list the actual fault location and estimated fault location, respectively. It is seen that the estimated fault location is not accurate. The proposed method is applied to detect whether a bad exist. The estimated value of the cost function is obtained as $\hat{J} = 15.9931$. The degree of freedom is 4, and $\chi^2_{4,0.01}$ is equal to 13.2767. Since $\hat{J} > \chi^2_{4,0.01}$, it is determined that bad measurement data exists in this system with a 99% confidence level. For this case, the voltage measurement at bus 21 corresponds to the largest normalized error. Thus, measurement at bus 21 is identified as the bad data.

Table 4.17 Optimal estimate of fault location with bad data using the Type II fault location algorithm for a simultaneous CG and LLLG fault

Bus No.	Measured voltage value (p.u.)			Optimal voltage estimates (p.u.)			Act. FL (p.u.)	Esti. FL (p.u.)
	Phase A	Phase B	Phase C	Phase A	Phase B	Phase C		
1	0.8431 -0.2106i	-0.5808 -0.6974i	-0.3505 +0.8230i	0.8505 -0.2213i	-0.5782 -0.6974i	-0.3488 +0.8199i		
11	0.3673 -0.2336i	-0.5528 -0.2504i	-0.2373 +0.5767i	0.3690 -0.2351i	-0.5557 -0.2504i	-0.2365 +0.5787i	m1 = 0.5	m1 = 0.3794
14	0.5432 -0.2921i	-0.4980 -0.1850i	-0.1248 +0.4738i	0.5445 -0.2934i	-0.5006 -0.1852i	-0.1246 +0.4756i	m2 = 0.8	m2 = 0.9822
21	0.7196 -0.3508i	-0.3796 -0.0041i	-0.0212 +0.2938i	0.7144 -0.3443i	-0.3709 -0.0053i	-0.0217 +0.2916i		

Then, bad data at bus 21 is discarded. The proposed method is repeated using measurements at buses 1, 11, and 14. The results are shown in Table 4.18, and the estimated fault location results are accurate. The new estimated value of the cost function is $\hat{J} = 4.6873\text{e-}4$, and the new degree of freedom is 2. Since $\hat{J} < \chi^2_{2,0.01}$, there exists no more bad data in the system. That is, the bad data at bus 21 is correctly identified and removed.

Again, it is evidenced that the proposed optimal fault location estimation method is capable of detecting and identifying the bad data. In a result, the accuracy of the estimated fault location is greatly enhanced.

Table 4.18 Optimal estimate of fault location with bad data being removed using the Type II fault location algorithm for a simultaneous CG and LLLG fault

Bus No.	Measured voltage value (p.u.)			Optimal voltage estimates (p.u.)			Act. FL (p.u.)	Esti. FL (p.u.)
	Phase A	Phase B	Phase C	Phase A	Phase B	Phase C		
1	0.8431 -0.2106i	-0.5808 -0.6974i	-0.3505 +0.8230i	0.8432 -0.2107i	-0.5809 -0.6974i	-0.3505 +0.8231i		
11	0.3673 -0.2336i	-0.5528 -0.2504i	-0.2373 +0.5767i	0.3673 -0.2336i	-0.5528 -0.2504i	-0.2373 +0.5767i	m1 = 0.5 m2 = 0.8	m1 = 0.4960 m2 = 0.7951
14	0.5432 -0.2921i	-0.4980 -0.1850i	-0.1248 +0.4738i	0.5432 -0.2921i	-0.4980 -0.1850i	-0.1248 +0.4737i		

4.7 Optimal Fault Location Estimate Using the Alternative Approach of Type II algorithm

In this subsection, the optimal estimate of fault location using the alternative approach of Type II algorithm is illustrated. It is assumed the bad data is captured during the fault. Assuming there are four voltage measurements $\boldsymbol{E}_{L_1}$, $\boldsymbol{E}_{L_2}$, $\boldsymbol{E}_{L_3}$, and $\boldsymbol{E}_{L_4}$ are available for state estimation. From (3.29), the following two equations are obtained as

$$\left(\boldsymbol{Z}_{L_1L_2F_1F_2}^{T}\boldsymbol{Z}_{L_1L_2F_1F_2}\right)^{-1}\left(\boldsymbol{Z}_{L_1L_2F_1F_2}^{T}\Delta\boldsymbol{E}_{L_1L_2}\right) = \left(\boldsymbol{Z}_{L_1L_3F_1F_2}^{T}\boldsymbol{Z}_{L_1L_3F_1F_2}\right)^{-1}\left(\boldsymbol{Z}_{L_1L_3F_1F_2}^{T}\Delta\boldsymbol{E}_{L_1L_3}\right) \quad (4.51)$$

and

$$\left(\boldsymbol{Z}_{L_1L_2F_1F_2}^{T}\boldsymbol{Z}_{L_1L_2F_1F_2}\right)^{-1}\left(\boldsymbol{Z}_{L_1L_2F_1F_2}^{T}\Delta\boldsymbol{E}_{L_1L_2}\right) = \left(\boldsymbol{Z}_{L_1L_4F_1F_2}^{T}\boldsymbol{Z}_{L_1L_4F_1F_2}\right)^{-1}\left(\boldsymbol{Z}_{L_1L_4F_1F_2}^{T}\Delta\boldsymbol{E}_{L_1L_4}\right) \quad (4.52)$$

There is a total of 6 equations can be separated from (4.51). The first three equations (h_1, h_2, h_3) are related to the first fault for phase A, B, and C, respectively. The last three equations (h_4, h_5, h_6) are related to the second fault for phase A, B, and C, respectively. We can further separate those six equations into twelve real equations as

$$\mathrm{RE}(h_i) = 0, \qquad i = 1, 2, \dots, 6 \quad (4.53)$$

$$\mathrm{IM}(h_i) = 0, \qquad i = 1, 2, \dots, 6 \quad (4.54)$$

where $\mathrm{RE}(.)$ returns the real part of its argument, and $\mathrm{IM}(.)$ returns the imaginary part of its argument. Similarly, there is another total of 12 real equations can be separated from (4.52). If we let

$$f_{2i-1}(X) = \mathrm{RE}(h_i), \qquad i = 1, 2, \dots, 12 \quad (4.55)$$

$$f_{2i}(X) = \mathrm{IM}(h_i), \qquad i = 1, 2, \dots, 12 \quad (4.56)$$

Then, the function vector will be defined as

$$F_i(X) = f_i(X), \qquad i = 1, 2, \dots, 24 \quad (4.57)$$

$$F_{24+2i-1} = x_{2i-1}, \qquad i = 1, 2, \dots, 12 \quad (4.58)$$

$$F_{24+2i} = x_{2i}, \qquad i = 1, 2, \dots, 12 \quad (4.59)$$

The measurement vector S is defined as

$$S_i(X) = 0, \qquad i = 1, 2, \dots, 24 \quad (4.60)$$

$$S_{24+2i-1} = x_{2i-1}, \qquad i = 1, 2, \dots, 12 \quad (4.61)$$

$$S_{24+2i} = x_{2i}, \qquad i = 1, 2, \dots, 12 \tag{4.62}$$

The measurement vector S and the function vector $F(X)$ are related by (4.18). The mean μ is characterized by (4.19). The optimal estimator is obtained by following (4.20) – (4.23). Then, the chi-square test is performed to detect and identify the bad data by (4.24) – (4.27).

4.8 Evaluation Studies

In this subsection, the proposed optimal estimation of fault location method using the alternative approach of Type II algorithm is verified by case studies. Again, the method is applied to the 21 bus distribution system shown in Figure 3.2. The phasor measurements obtained from Matlab is multiplied by 1.002 to emulate field data. Different fault types, fault locations, and bad data are simulated to get the phasor values for case studies.

The initial values of voltage magnitude and radians are selected as the same to the measurement values to increase the converge speed. The initial values of fault locations are chosen as 0.5 per unit. Three cases with different fault scenarios are demonstrated in subsection 4.8.1 to 4.8.3.

4.8.1 Case 1 – A Simultaneous Fault: CG and CG

Assuming there is a simultaneous fault in the system. One fault is a CG fault on the line from bus 1 to 2, with fault location as 0.6 per unit and fault resistance is 1 ohm. The other fault is a CG fault on the line from bus 13 to 15, with fault location being 0.5 per unit and fault resistance as 1 ohm.

Voltage measurements at buses 1, 7, 15, and 20 are used for optimal fault location estimate. The voltage at bus 20 is multiplied by 1.2 to emulate a bad data. The results are summarized in Table 4.19.

In Table 4.19, the first column lists the bus numbers, the second to fourth columns list measured voltage value for each bus, the fifth to seventh columns list optimal estimated voltage value for each bus, and the last two columns list the actual fault location and estimated fault location, respectively.

From Table 4.19, it is observed that the estimated fault location is not accurate. To examine whether bad data exists, the proposed method is applied. The estimated value of the cost function is obtained as $\hat{J} = 91.9758$. The degree of freedom is 22, and $\chi^2_{22,0.01}$ is equal to 40.2894. Since $\hat{J} > \chi^2_{22,0.01}$, it is determined that bad measurement data exists in this system with a 99% confidence level. For this case, the voltage measurement at bus 20 corresponds to the largest normalized error. Therefore, measurement at bus 20 is identified as the bad data.

Table 4.19 Optimal estimate of fault location with bad data using the alternative approach of Type II fault location algorithm for a simultaneous CG and CG fault

Bus No.	Measured voltage value (p.u.)			Optimal voltage estimates (p.u.)			Act. FL (p.u.)	Esti. FL (p.u.)
	Phase A	Phase B	Phase C	Phase A	Phase B	Phase C		
1	0.6778 -0.3024i	-0.5081 -0.8066i	-0.3342 +0.8805i	0.6731 -0.2995i	-0.5023 -0.7970i	-0.3292 +0.8693i		
7	0.4890 -0.3077i	-0.5492 -0.7832i	-0.2176 +0.6922i	0.4975 -0.3128i	-0.5611 -0.7956i	-0.2198 +0.7075i	m1 = 0.6	m1 = 0.6269
15	0.6948 -0.4501i	-0.4720 -0.9415i	0.0491 +0.1757i	0.7028 -0.4539i	-0.4821 -0.9477i	0.0504 +0.1804i	m2 = 0.5	m2 = 0.7978
20	0.9448 -0.3853i	-0.5437 -0.9576i	0.0365 +0.6383i	0.9255 -0.3809i	-0.5278 -0.9384i	0.0348 +0.6248i		

After bad data at bus 20 is removed, we redo the optimal estimation. Results are summarized in Table 4.20. It is evidenced the fault location results become accurate after the bad data is removed. The new estimated value of the cost function is $\hat{J} = 0.0011$. The new degree of freedom is $K = 10$, and $\chi^2_{10,0.01} = 23.2093$. Since $\hat{J} < \chi^2_{10,0.01}$, it indicates no bad data exist in the system any more.

Table 4.20 Optimal estimate of fault location with bad data being removed using the alternative approach of Type II fault location algorithm for a simultaneous CG and CG fault

Bus No.	Measured voltage value (p.u.)			Optimal voltage estimates (p.u.)			Act. FL (p.u.)	Esti. FL (p.u.)
	Phase A	Phase B	Phase C	Phase A	Phase B	Phase C		
1	0.6778 -0.3024i	-0.5081 -0.8066i	-0.3342 +0.8805i	0.6778 -0.3025i	-0.5080 -0.8066i	-0.3342 +0.8806i		
7	0.4890 -0.3077i	-0.5492 -0.7832i	-0.2176 +0.6922i	0.4890 -0.3076i	-0.5492 -0.7832i	-0.2177 +0.6922i	m1 = 0.6 m2 = 0.5	m1 = 0.6021 m2 = 0.4969
15	0.6948 -0.4501i	-0.4720 -0.9415i	0.0491 +0.1757i	0.6948 -0.4501i	-0.4720 -0.9415i	0.0491 +0.1757i		

4.8.2 Case 2 – A Simultaneous Fault: CG and LLLG

Let us consider a simultaneous fault. The first fault is a CG fault imposed on the line between bus 2 and 5, with fault location as 0.3 per unit and fault resistance is 1 ohm. The second fault is and LLLG fault imposed on the line from bus 11 to 12, with fault location being 0.8 per unit, and fault resistance as [1, 1, 1, 5] ohm.

Voltage measurements at buses 1, 7, 12, and 20 are used for optimal fault location estimate. The voltage at bus 7 is multiplied by 1.15 to emulate a bad data.

Table 4.21 summarizes the state estimation results. In the table, the last two columns list the actual fault location and estimated fault location, respectively. From the table, it is observed that the estimated fault location is not accurate. To examine whether

bad data exists, the proposed method is applied. The estimated value of the cost function is obtained as $\hat{J} = 63.3406$. The degree of freedom is 22, and $\chi^2_{22,0.01}$ is equal to 40.2894. Since $\hat{J} > \chi^2_{22,0.01}$, it is determined that bad measurement data exists in this system with a 99% confidence level. For this case, the voltage measurement at bus 7 corresponds to the largest normalized error. Therefore, measurement at bus 7 is identified as the bad data.

Table 4.21 Optimal estimate of fault location with bad data using the alternative approach of Type II fault location algorithm for a simultaneous CG and LLLG fault

Bus No.	Measured voltage value (p.u.)			Optimal voltage estimates (p.u.)			Act. FL (p.u.)	Esti. FL (p.u.)
	Phase A	Phase B	Phase C	Phase A	Phase B	Phase C		
1	0.8807 -0.1373i	-0.5763 -0.6370i	-0.1404 +0.7281i	0.9228 -0.1319i	-0.5927 -0.6687i	-0.1458 +0.7511i		
7	0.6944 -0.3199i	-0.4742 -0.5510i	0.0929 +0.2434i	0.6672 -0.3119i	-0.4521 -0.5297i	0.0872 +0.2275i	m1 = 0.3	m1 = 0.3404
12	0.2353 -0.2305i	-0.1592 -0.1468i	0.1415 +0.0488i	0.2353 -0.2306i	-0.1592 -0.1468i	0.1415 +0.0488i	m2 = 0.8	m2 = 0.8309
20	0.5911 -0.2703i	-0.4372 -0.3083i	0.0930 +0.4614i	0.6020 -0.2726i	-0.4457 -0.3155i	0.0939 +0.4678i		

After the bad data at bus 7 is removed, the new estimation results are summarized in Table 4.22. It is seen the fault location estimate results are quite accurate. The new estimated value of the cost function is $\hat{J} = 1.7789\text{e-}4$, and the new degree of freedom is 10. Since $\hat{J} < \chi^2_{10,0.01}$, there exists no bad data in the system. That is, the bad data at bus 7 is correctly identified and removed.

Table 4.22 Optimal estimate of fault location with bad data being removed using the alternative approach of Type II fault location algorithm for a simultaneous CG and LLLG fault

Bus No.	Measured voltage value (p.u.)			Optimal voltage estimates (p.u.)			Act. FL (p.u.)	Esti. FL (p.u.)
	Phase A	Phase B	Phase C	Phase A	Phase B	Phase C		
1	0.8807 -0.1373i	-0.5763 -0.6370i	-0.1404 +0.7281i	0.8807 -0.1373i	-0.5763 -0.6370i	-0.1404 +0.7281i		
12	0.2353 -0.2305i	-0.1592 -0.1468i	0.1415 +0.0488i	0.2353 -0.2305i	-0.1592 -0.1468i	0.1416 +0.0489i	m1 = 0.3 m2 = 0.8	m1 = 0.3042 m2 = 0.7988
20	0.5911 -0.2703i	-0.4372 -0.3083i	0.0930 +0.4614i	0.5911 -0.2703i	-0.4372 -0.3083i	0.0930 +0.4614i		

4.8.3 Case 3 – A Simultaneous Fault: AG and BG

Considering a simultaneous fault in the system. One fault is an AG fault imposed on the line from bus 1 to 2, with fault location as 0.4 per unit and fault resistance as 1 ohm. The other fault is a BG fault imposed on the line between bus 13 and 14, with fault location being 0.7 per unit and fault resistance is 1 ohm.

Voltage measurements at buses 1, 7, 14, and 20 are used for optimal fault location estimate. The voltage at bus 20 is multiplied by 1.2 to emulate a bad data. The optimal estimation results are summarized in Table 4.23.

Table 4.23 summarizes the state estimation results in the presence of bad data. In the table, the last two columns list the actual fault location and estimated fault location, respectively. It is seen that the estimated fault location is not accurate. The proposed method is applied to detect whether a bad exist. The estimated value of the cost function is obtained as $\hat{J} = 95.0947$. The degree of freedom is 22, and $\chi^2_{22,0.01}$ is equal to 40.2894. Since $\hat{J} > \chi^2_{22,0.01}$, it is determined that bad measurement data exists in this system with a 99% confidence level. For this case, the voltage measurement at bus 20

corresponds to the largest normalized error. Thus, measurement at bus 20 is identified as the bad data.

Table 4.23 Optimal estimate of fault location with bad data using the alternative approach of Type II fault location algorithm for a simultaneous AG and BG fault

Bus No.	Measured voltage value (p.u.)			Optimal voltage estimates (p.u.)			Act. FL (p.u.)	Esti. FL (p.u.)
	Phase A	Phase B	Phase C	Phase A	Phase B	Phase C		
1	0.6292 -0.3753i	-0.5237 -0.7061i	-0.4398 +0.8716i	0.6239 -0.3713i	-0.5152 -0.7005i	-0.4316 +0.8606i		
7	0.5417 -0.2875i	-0.4466 -0.4144i	-0.4218 +0.9345i	0.5529 -0.2939i	-0.4565 -0.4209i	-0.4277 +0.9544i	m1 = 0.4	m1 = 0.4261
14	0.7956 -0.2064i	-0.2217 -0.0466i	-0.3446 +0.9920i	0.8061 -0.2111i	-0.2263 -0.0477i	-0.3470 +1.0030i	m2 = 0.7	m2 = 0.8555
20	0.9117 -0.3140i	-0.4820 -0.2523i	-0.4835 +1.1134i	0.8921 -0.3063i	-0.4712 -0.2464i	-0.4738 +1.0902i		

Then, bad data at bus 20 is discarded. The proposed method is repeated using measurements at buses 1, 7, and 14. The results are shown in Table 4.24, and the estimated fault location results are accurate. The new estimated value of the cost function is $\hat{J} = 0.0016$, and the new degree of freedom is 10. Since $\hat{J} < \chi^2_{10,0.01}$, there exists no more bad data in the system. That is, the bad data at bus 20 is correctly identified and removed.

Again, it is evidenced that the proposed optimal fault location estimation method is capable of detecting and identifying the bad data. In a result, the accuracy of the estimated fault location is greatly enhanced.

Table 4.24 Optimal estimate of fault location with bad data being removed using the alternative approach of Type II fault location algorithm for a simultaneous AG and BG fault

Bus No.	Measured voltage value (p.u.)			Optimal voltage estimates (p.u.)			Act. FL (p.u.)	Esti. FL (p.u.)
	Phase A	Phase B	Phase C	Phase A	Phase B	Phase C		
1	0.6292 -0.3753i	-0.5237 -0.7061i	-0.4398 +0.8716i	0.6292 -0.3755i	-0.5237 -0.7060i	-0.4397 +0.8716i		
7	0.5417 -0.2875i	-0.4466 -0.4144i	-0.4218 +0.9345i	0.5417 -0.2873i	-0.4467 -0.4145i	-0.4218 +0.9345i	m1 = 0.4 m2 = 0.7	m1 = 0.4017 m2 = 0.6980
14	0.7956 -0.2064i	-0.2217 -0.0466i	-0.3446 +0.9920i	0.7956 -0.2064i	-0.2217 -0.0466i	-0.3446 +0.9920i		

4.9 Summary

Optimal fault location estimation methods are proposed in this chapter. The methods are based on phasor values. They aim to detect and identify bad data to minimize the impacts of measurement errors. The methods are applied to distribution systems integrated with DGs. Case studies show that the proposed methods are capable of detecting and identifying the bad data. The fault location results are enhanced after bad data is removed. It is expected that the presented optimal estimator is also applicable to transmission systems.

Chapter 5 Fault Location Algorithms for Simultaneous Faults in Transmission Systems

The electric power is delivered from generation sources to distribution systems and end-use customers through the transmission systems. Faults occurring on any section of the transmission system will disturb or even interrupt the power delivery service [38]. Thus, it is of great importance to quickly and accurately locate the fault so that the system can be restored in a timely manner.

In this chapter, we propose a fault location algorithm [39] for pinpointing simultaneous faults in transmission systems. The algorithm utilizes synchronized voltage measurements at the fundamental system frequency. Bus impedance matrix technique is used to establish the relationship between measurements and impedances. Evaluation studies show that the proposed algorithm can locate a single fault on the transmission line as well.

The rest of this chapter is as follows. The method for finding driving point and transfer impedance is described in Section 5.1. Proposed fault location algorithm is provided in Section 5.2. Section 5.3 reports evaluation studies, followed by the conclusion.

5.1 Derivation of Driving Point and Transfer Impedances

In this section, we will derive the driving point and transfer impedances during the fault for transmission lines. The impedances between non-fault nodes and faults nodes are derived first in subsection 5.1.1. The impedances between fault nodes are derived in subsection 5.1.2.

Figure 5.1 illustrates the one-line diagram of a three-phase transmission line segment. Symbols p and q represent the buses of the line. Bus p comprises nodes p_1, p_2, and p_3. Bus q comprises nodes q_1, q_2, and q_3. Define the fictitious fault bus to be r, consisting of nodes r_1, r_2, and r_3. The remaining notations in Figure 5.1 are explained as follows:

$\boldsymbol{E}_p$: node voltage vector during the fault for bus p. $\boldsymbol{E}_p = \left[E_{p1}, E_{p2}, E_{p3}\right]^T$, with T denoting vector transpose;

$\boldsymbol{E}_q$: node voltage vector during the fault for bus q. $\boldsymbol{E}_q = \left[E_{q1}, E_{q2}, E_{q3}\right]^T$;

$\boldsymbol{E}_r$: node voltage vector during the fault for bus r. $\boldsymbol{E}_r = [E_{r1}, E_{r2}, E_{r3}]^T$;

$\boldsymbol{z}_{pr}$, $\boldsymbol{z}_{qr}$: the equivalent series impedance matrix of the line segment pr and qr, respectively;

$\boldsymbol{y}_{pr}$, $\boldsymbol{y}_{qr}$: the equivalent shunt admittance matrix of the line segment pr and qr, respectively.

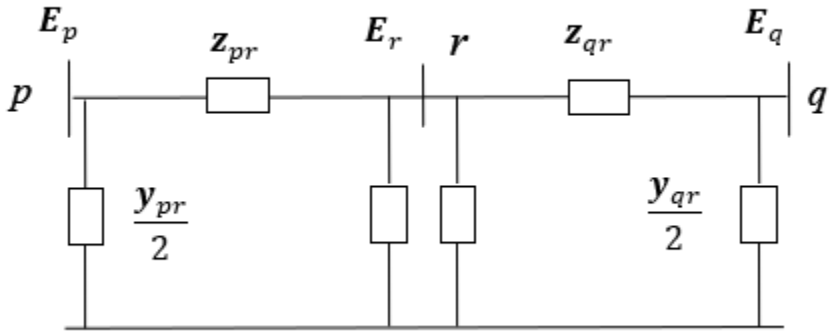

Figure 5.1 Illustration of a transmission system segment

The parameters of the equivalent PI model [46] of line segment pr are as follows:

$$\boldsymbol{z}_{pr} = \boldsymbol{z}\boldsymbol{B}diag\left[\sinh\left(\boldsymbol{\gamma} l_{pr}\right)./\boldsymbol{\gamma}\right]\boldsymbol{B}^{-1} \tag{5.1}$$

$$\boldsymbol{y}_{pr} = 2\boldsymbol{B}diag\left[\tanh\left(\boldsymbol{\gamma} l_{pr}/2\right)./\boldsymbol{\gamma}\right]\boldsymbol{B}^{-1}\boldsymbol{y} \tag{5.2}$$

where,

$diag(.)$: a diagonal matrix with input vector as its diagonal element;

$./$: element-wise division;

$\boldsymbol{z}$: series impedance matrix of the line pq in per unit length;

$\boldsymbol{y}$: shunt admittance matrix of the line pq in per unit length;

$\boldsymbol{B}$: eigenvector of $(\boldsymbol{yz})$;

$\boldsymbol{\gamma}$: vector consisting of $\boldsymbol{\gamma}_j$ that is the square root of the jth eigenvalue of $(\boldsymbol{yz})$.

l_{pr}: length of the line segment pr.

Similarly, the parameters of the equivalent PI model of line segment qr can be derived. It should be noted that (5.1) and (5.2) hold for both transposed and untransposed lines. Moreover, they are applicable to single-circuit lines with $j = 1, 2, 3$ as well as to double-circuit lines with $j = 1, 2, \dots, 6$.

In addition, define the following variables:

m: per unit fault distance from bus p to the fault bus r;

n: the total number of nodes of the transmission system without counting fictitious fault nodes;

$\boldsymbol{Z}_0$: the bus impedance matrix in phase domain of the network preceding the fault, excluding fictitious fault nodes;

$\boldsymbol{Z}_{0,kl}$: the element in the kth row and lth column of $\boldsymbol{Z}_0$;

$\boldsymbol{Z}$: the bus impedance matrix in the phase domain of the network during the fault, including fictitious fault nodes;

$\boldsymbol{Z}_{kl}$: the element in the kth row and lth column of $\boldsymbol{Z}$;

Based on the definition, the size of $\boldsymbol{Z}_0$ is n by n. The size of $\boldsymbol{Z}$ is $(n + 3n_f)$ by $(n + 3n_f)$, where n_f represents the total number of faults in the transmission system.

Matrix $\boldsymbol{Z}_0$ can be readily developed following the established method in [45]. It can be shown that the first n rows and n columns of $\boldsymbol{Z}$ are identical to $\boldsymbol{Z}_0$, and the rest of rows and columns of $\boldsymbol{Z}$ consist of the driving point and transfer impedances related to the fault nodes.

5.1.1 Derivation of the Transfer Impedance Between A Non-Fault Node and Fault Nodes

This subsection describes the method to obtain transfer impedance between a non-fault node and fault nodes [2]. We first remove all the source in the network shown in Figure 5.1 and then inject 1-ampere current into node k [2]. Applying Kirchhoff's Current Law (KCL) at bus r, it is obtained that

$$\frac{(\boldsymbol{y}_{pr} + \boldsymbol{y}_{qr})}{2}\boldsymbol{E}_r + \boldsymbol{z}_{pr}^{-1}(\boldsymbol{E}_r - \boldsymbol{E}_p) + \boldsymbol{z}_{qr}^{-1}(\boldsymbol{E}_r - \boldsymbol{E}_q) = 0 \tag{5.3}$$

From (5.3), $\boldsymbol{E}_r$ can be written as

$$\boldsymbol{E}_r = \left[\frac{(\boldsymbol{y}_{pr} + \boldsymbol{y}_{qr})}{2} + \boldsymbol{z}_{pr}^{-1} + \boldsymbol{z}_{qr}^{-1}\right]^{-1}(\boldsymbol{z}_{pr}^{-1}\boldsymbol{E}_p + \boldsymbol{z}_{qr}^{-1}\boldsymbol{E}_q) \tag{5.4}$$

Based on the definition of transfer impedance, the value of the transfer impedance between a non-fault node k and a fault node is equal to the voltage at the fault node, when 1 Ampere current is injected into node k, with all the sources in the network being removed [2]. Therefore, the values of $\boldsymbol{E}_p$ and $\boldsymbol{E}_q$ are equal to $\boldsymbol{Z}_{kp}$ and $\boldsymbol{Z}_{kq}$, respectively. Hence, the transfer impedance between node k and fault nodes are:

$$\boldsymbol{Z}_{kr} = \left[\frac{\left(\boldsymbol{y}_{pr} + \boldsymbol{y}_{qr}\right)}{2} + \boldsymbol{z}_{pr}^{-1} + \boldsymbol{z}_{qr}^{-1}\right]^{-1} \left(\boldsymbol{z}_{pr}^{-1}\boldsymbol{Z}_{kp} + \boldsymbol{z}_{qr}^{-1}\boldsymbol{Z}_{kq}\right) \tag{5.5}$$

where,

$\boldsymbol{Z}_{kr} = [Z_{kr_1}, Z_{kr_2}, Z_{kr_3}]^T$, with T denotes vector transpose;

$\boldsymbol{Z}_{kp} = [Z_{kp_1}, Z_{kp_2}, Z_{kp_3}]^T$;

$\boldsymbol{Z}_{kq} = [Z_{kq_1}, Z_{kq_2}, Z_{kq_3}]^T$;

Z_{kr_1}, Z_{kr_2}, Z_{kr_3}: the transfer impedance between node k and fault node r_1, r_2, and r_3, respectively;

Z_{kp_1}, Z_{kp_2}, Z_{kp_3}: the transfer impedance between node k and node p_1, p_2, and p_3, respectively;

Z_{kq_1}, Z_{kq_2}, Z_{kq_3}: the transfer impedance between node k and node q_1, q_2, and q_3, respectively.

Note that Z_{kp_1}, Z_{kq_1} and so on are elements of the bus impedance matrix of the prefault network. Furthermore, $\mathbf{y}_{pr}$, $\mathbf{y}_{qr}$, $\mathbf{z}_{pr}$, and $\mathbf{z}_{qr}$ are functions of the fault location m. Therefore, the transfer impedance $\boldsymbol{Z}_{kr}$ is a function of the fault location m as well.

The prefault voltage at fictitious fault nodes can be calculated using the prefault terminal voltages based on (5.4):

$$\boldsymbol{E}_r^0 = \left[\frac{\left(\boldsymbol{y}_{pr} + \boldsymbol{y}_{qr}\right)}{2} + \boldsymbol{z}_{pr}^{-1} + \boldsymbol{z}_{qr}^{-1}\right]^{-1} \left(\boldsymbol{z}_{pr}^{-1}\boldsymbol{E}_p^0 + \boldsymbol{z}_{qr}^{-1}\boldsymbol{E}_q^0\right) \tag{5.6}$$

where,

$\boldsymbol{E}_r^0$: node voltage vector preceding the fault at fictitious bus r. $\boldsymbol{E}_r^0 = [E_{r1}^0, E_{r2}^0, E_{r3}^0]^T$, with T denotes vector transpose;

$\boldsymbol{E}_{p0}$: node voltage vector preceding the fault at bus p. $\boldsymbol{E}_p^0 = \left[E_{p1}^0, E_{p2}^0, E_{p3}^0\right]^T$,

$\boldsymbol{E}_{q0}$: node voltage vector preceding the fault at bus q. $\boldsymbol{E}_q = \left[E_{q1}^0, E_{q2}^0, E_{q3}^0\right]^T$.

5.1.2 Derivation of the Driving Point Impedance At Fault Nodes and Transfer Impedance Between Fault Nodes

The method to obtain the transfer impedance between fault nodes and driving point impedance is presented in this subsection [2]. Remove all the sources in the network shown in Figure 5.1. Then inject 1 Ampere current into node r_i, where $i = 1, 2, 3$ for a single circuit line, and $i = 1, 2, \ldots, 6$ for a double-circuit line. Applying KCL at bus r yields

$$\frac{\left(\boldsymbol{y}_{pr} + \boldsymbol{y}_{qr}\right)}{2}\boldsymbol{E}_r + \boldsymbol{z}_{pr}^{-1}\left(\boldsymbol{E}_r - \boldsymbol{E}_p\right) + \boldsymbol{z}_{qr}^{-1}\left(\boldsymbol{E}_r - \boldsymbol{E}_q\right) = \boldsymbol{u}_i \tag{5.7}$$

where $\boldsymbol{u}_i$ is the ith column of a three by three or six by six identity matrix. From (5.7), $\boldsymbol{E}_r$ can be written as

$$\boldsymbol{E}_r = \left[\frac{\left(\boldsymbol{y}_{pr} + \boldsymbol{y}_{qr}\right)}{2} + \boldsymbol{z}_{pr}^{-1} + \boldsymbol{z}_{qr}^{-1}\right]^{-1}\left(\boldsymbol{z}_{pr}^{-1}\boldsymbol{E}_p + \boldsymbol{z}_{qr}^{-1}\boldsymbol{E}_q + \boldsymbol{u}_i\right) \tag{5.8}$$

Based on the definition, the value of the transfer impedance between a fault node and other fault nodes is equal to the voltage at other fault nodes, and the value of the driving point impedance at a fault node is equal to the voltage at the fault node [2]. Therefore, the values of $\boldsymbol{E}_r$, $\boldsymbol{E}_p$, and $\boldsymbol{E}_q$ are equal to $\boldsymbol{Z}_{rr_i}$, $\boldsymbol{Z}_{pr_i}$, and $\boldsymbol{Z}_{qr_i}$, respectively. Hence, the transfer impedance and driving point impedance at fault nodes are:

$$\boldsymbol{Z}_{rr_i} = \left[\frac{\left(\boldsymbol{y}_{pr} + \boldsymbol{y}_{qr}\right)}{2} + \boldsymbol{z}_{pr}^{-1} + \boldsymbol{z}_{qr}^{-1}\right]^{-1}\left(\boldsymbol{z}_{pr}^{-1}\boldsymbol{Z}_{pr_i} + \boldsymbol{z}_{qr}^{-1}\boldsymbol{Z}_{qr_i} + \boldsymbol{u}_i\right) \tag{5.9}$$

where,

$\boldsymbol{Z}_{rr_i} = [Z_{r_1r_i}, Z_{r_2r_i}, Z_{r_3r_i}]^T$, with T denotes vector transpose;

$\boldsymbol{Z}_{pr_i} = [Z_{p_1r_i}, Z_{p_2r_i}, Z_{p_3r_i}]^T$;

$\boldsymbol{Z}_{qr_i} = [Z_{q_1r_i}, Z_{q_2r_i}, Z_{q_3r_i}]^T$.

$Z_{r_1r_i}$, $Z_{r_2r_i}$, $Z_{r_3r_i}$: the transfer impedance between fault nodes and driving point impedance at fault nodes;

$Z_{p_1r_i}$, $Z_{p_2r_i}$, $Z_{p_3r_i}$: the transfer impedance between nodes of bus p and fault nodes;

$Z_{q_1r_i}$, $Z_{q_2r_i}$, $Z_{q_3r_i}$: the transfer impedance between nodes of bus q and fault nodes.

Setting $i = 1, 2, 3$ for single circuit lines and $i = 1, 2, \dots, 6$ for double-circuit lines will give all relevant driving point and transfer impedances related to fault nodes.

Similarly, as discussed in subsection 5.1.1, it is revealed that these driving point and transfer impedances are functions of fault locations as well.

5.2 Fault Location Algorithm

This subsection presents the proposed fault location algorithm to locate simultaneous faults in transmission systems. Figure 5.2 illustrates a scenario involving two simultaneous faults. Two faults occur at the point F_1 on line segment P_1Q_1 with fault location m_1, and at point F_2 on line segment P_2Q_2 with fault location m_2, respectively.

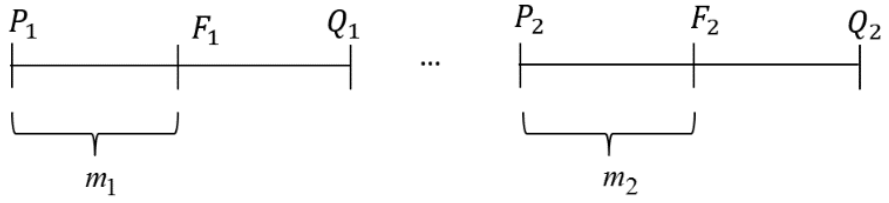

Figure 5.2. An illustration of simultaneous faults for transmission systems

Voltage measurements from specified locations are utilized to locate the unknown fault location m_1 and m_2. The voltage at any bus L during the fault can be expressed as

$$\boldsymbol{E}_L = \boldsymbol{E}_L^0 - [\boldsymbol{Z}_{LF_1} \quad \boldsymbol{Z}_{LF_2}][\boldsymbol{I}_{F_1} \quad \boldsymbol{I}_{F_2}]^T \tag{5.10}$$

where,

$\boldsymbol{E}_L$: the voltage at bus L during the fault;

$\boldsymbol{E}_L^0$: the voltage at bus L preceding the fault;

$\boldsymbol{Z}_{LF_1}$, $\boldsymbol{Z}_{LF_2}$: the transfer impedance between bus L and fault bus F_1, bus L and fault bus F_2, respectively;

$\boldsymbol{I}_{F_1}$, $\boldsymbol{I}_{F_2}$: the fault currents at the point F_1 and F_2.

Based on the measurements from two buses L_1 and L_2, The following two equations are obtained:

$$\boldsymbol{E}_{L_1} = \boldsymbol{E}_{L_1}^0 - [\boldsymbol{Z}_{L_1F_1} \quad \boldsymbol{Z}_{L_1F_2}][\boldsymbol{I}_{F_1} \quad \boldsymbol{I}_{F_2}]^T \tag{5.11}$$

$$\boldsymbol{E}_{L_2} = \boldsymbol{E}_{L_2}^0 - [\boldsymbol{Z}_{L_2F_1} \quad \boldsymbol{Z}_{L_2F_2}][\boldsymbol{I}_{F_1} \quad \boldsymbol{I}_{F_2}]^T \tag{5.12}$$

or in a compact format,

$$\begin{bmatrix}\boldsymbol{E}_{L_1}\\ \boldsymbol{E}_{L_2}\end{bmatrix} = \begin{bmatrix}\boldsymbol{E}_{L_1}^0\\ \boldsymbol{E}_{L_2}^0\end{bmatrix} - \begin{bmatrix}\boldsymbol{Z}_{L_1F_1} & \boldsymbol{Z}_{L_1F_2}\\ \boldsymbol{Z}_{L_2F_1} & \boldsymbol{Z}_{L_2F_2}\end{bmatrix}\begin{bmatrix}\boldsymbol{I}_{F_1}\\ \boldsymbol{I}_{F_2}\end{bmatrix} \tag{5.13}$$

where,

$\boldsymbol{E}_{L_1}$, $\boldsymbol{E}_{L_2}$: the voltage during the fault at bus L_1, L_2, respectively;

$\boldsymbol{E}_{L_1}^0$, $\boldsymbol{E}_{L_2}^0$: the voltage preceding the fault at bus L_1, L_2, respectively;

$\boldsymbol{Z}_{L_1F_1}$, $\boldsymbol{Z}_{L_1F_2}$: transfer impedance matrix between bus L_1 and F_1, bus L_1 and F_2, respectively;

$\boldsymbol{Z}_{L_2F_1}$, $\boldsymbol{Z}_{L_2F_2}$: transfer impedance matrix between bus L_2 and F_1, bus L_2 and F_2, respectively.

Equation (5.13) can be written in a more compact form as

$$\boldsymbol{E}_{L_1L_2} = \boldsymbol{E}_{L_1L_2}^0 - \boldsymbol{Z}_{L_1L_2F_1F_2}\boldsymbol{I}_{F_1F_2} \tag{5.14}$$

The superimposed quantity, or the voltage change due to a fault, is

$$\Delta\boldsymbol{E}_{L_1L_2} = -\boldsymbol{Z}_{L_1L_2F_1F_2}\boldsymbol{I}_{F_1F_2} \tag{5.15}$$

From (5.15), the fault current vector is obtained as

$$\boldsymbol{I}_{F_1F_2} = -\left(\boldsymbol{Z}^T_{L_1L_2F_1F_2}\boldsymbol{Z}_{L_1L_2F_1F_2}\right)^{-1}\left(\boldsymbol{Z}^T_{L_1L_2F_1F_2}\Delta\boldsymbol{E}_{L_1L_2}\right) \tag{5.16}$$

Furthermore, the voltage during the fault at fault buses are given by

$$\begin{bmatrix}\boldsymbol{E}_{F_1}\\ \boldsymbol{E}_{F_2}\end{bmatrix} = \begin{bmatrix}\boldsymbol{E}^0_{F_1}\\ \boldsymbol{E}^0_{F_2}\end{bmatrix} - \begin{bmatrix}\boldsymbol{Z}_{F_1F_1} & \boldsymbol{Z}_{F_1F_2}\\ \boldsymbol{Z}_{F_2F_1} & \boldsymbol{Z}_{F_2F_2}\end{bmatrix}\begin{bmatrix}\boldsymbol{I}_{F_1}\\ \boldsymbol{I}_{F_2}\end{bmatrix} \tag{5.17}$$

where,

$\boldsymbol{E}_{F_1}$, $\boldsymbol{E}_{F_2}$: the voltage during the fault at fault bus F_1, F_2, respectively;

$\boldsymbol{E}^0_{F_1}$, $\boldsymbol{E}^0_{F_2}$: the voltage preceding the fault at fault bus F_1, F_2, respectively;

$\boldsymbol{Z}_{F_1F_1}$, $\boldsymbol{Z}_{F_2F_2}$: driving point impedance matrix at F_1, F_2, respectively;

$\boldsymbol{Z}_{F_1F_2}$, $\boldsymbol{Z}_{F_2F_1}$: the transfer impedance matrix between F_1 and F_2.

Equation (5.17) can be written in a more compact form as

$$\boldsymbol{E}_{F_1F_2} = \boldsymbol{E}^0_{F_1F_2} - \boldsymbol{Z}_{F_1F_2F_1F_2}\boldsymbol{I}_{F_1F_2} \tag{5.18}$$

Based on (5.6), prefault voltages at the fault bus F_1 and F_2 can be expressed in terms of fault locations and the prefault voltages at the bus P_1 and Q_1, bus P_2 and Q_2. For example, $\boldsymbol{E}^0_{F_1}$ is derived as follows:

$$\boldsymbol{E}^0_{F_1} = \left[\frac{\left(\boldsymbol{y}_{P_1F_1} + \boldsymbol{y}_{Q_1F_1}\right)}{2} + \boldsymbol{z}^{-1}_{P_1F_1} + \boldsymbol{z}^{-1}_{Q_1F_1}\right]^{-1} \cdot \left(\boldsymbol{z}^{-1}_{P_1F_1}\boldsymbol{E}^0_{P_1} + \boldsymbol{z}^{-1}_{Q_1F_1}\boldsymbol{E}^0_{Q_1}\right) \tag{5.19}$$

where,

$\boldsymbol{z}_{P_1F_1}$, $\boldsymbol{z}_{Q_1F_1}$: equivalent series impedance matrix of segment P_1F_1 *and* Q_1F_1;

$\boldsymbol{y}_{P_1F_1}$, $\boldsymbol{y}_{Q_1F_1}$: equivalent shunt admittance matrix of segment P_1F_1 *and* Q_1F_1;

$\boldsymbol{E}^0_{P_1}$, $\boldsymbol{E}^0_{Q_1}$: prefault voltages at P_1 and Q_1, which can be obtained by the wide area measurement system.

Since the fault resistances are purely resistive, the reactive power consumed by fault resistances at the two fault locations is zero, i.e.,

$$Imag\left(\begin{bmatrix} \boldsymbol{E}_{F_1}^T \boldsymbol{I}_{F_1}^* \\ \boldsymbol{E}_{F_2}^T \boldsymbol{I}_{F_2}^* \end{bmatrix}\right) = 0 \tag{5.20}$$

Solving (5.20) will yield the two unknown variables m_1 and m_2.

An alternative approach is described as follows when more measurements are available. Assuming that measurements from another two buses L_3 and L_4 are known. The following equation is obtained in a similar way to (5.16),

$$\boldsymbol{I}_{F_1F_2} = -\left(\boldsymbol{Z}_{L_3L_4F_1F_2}^T \boldsymbol{Z}_{L_3L_4F_1F_2}\right)^{-1}\left(\boldsymbol{Z}_{L_3L_4F_1F_2}^T \Delta\boldsymbol{E}_{L_3L_4}\right) \tag{5.21}$$

Equating (5.16) and (5.21), it is obtained that

$$\begin{aligned}&\left(\boldsymbol{Z}_{L_1L_2F_1F_2}^T \boldsymbol{Z}_{L_1L_2F_1F_2}\right)^{-1}\left(\boldsymbol{Z}_{L_1L_2F_1F_2}^T \Delta\boldsymbol{E}_{L_1L_2}\right) \\ &\quad = \left(\boldsymbol{Z}_{L_3L_4F_1F_2}^T \boldsymbol{Z}_{L_3L_4F_1F_2}\right)^{-1}\left(\boldsymbol{Z}_{L_3L_4F_1F_2}^T \Delta\boldsymbol{E}_{L_3L_4}\right)\end{aligned} \tag{5.22}$$

Equation (5.22) contains two unknown variables m_1 and m_2. Separating the equation into two real equations, from which the fault location can be obtained using the Newton-Raphson method.

5.3 Evaluation Studies

This section presents the evaluation results based on simulation studies. The developed fault location algorithm proposed is applied to a 27 bus transmission system shown in Figure 5.3. In the figure, the lengths of transmission lines are shown in parentheses. In particular, the line between bus 9 and bus 10 is a long double-circuit transmission line.

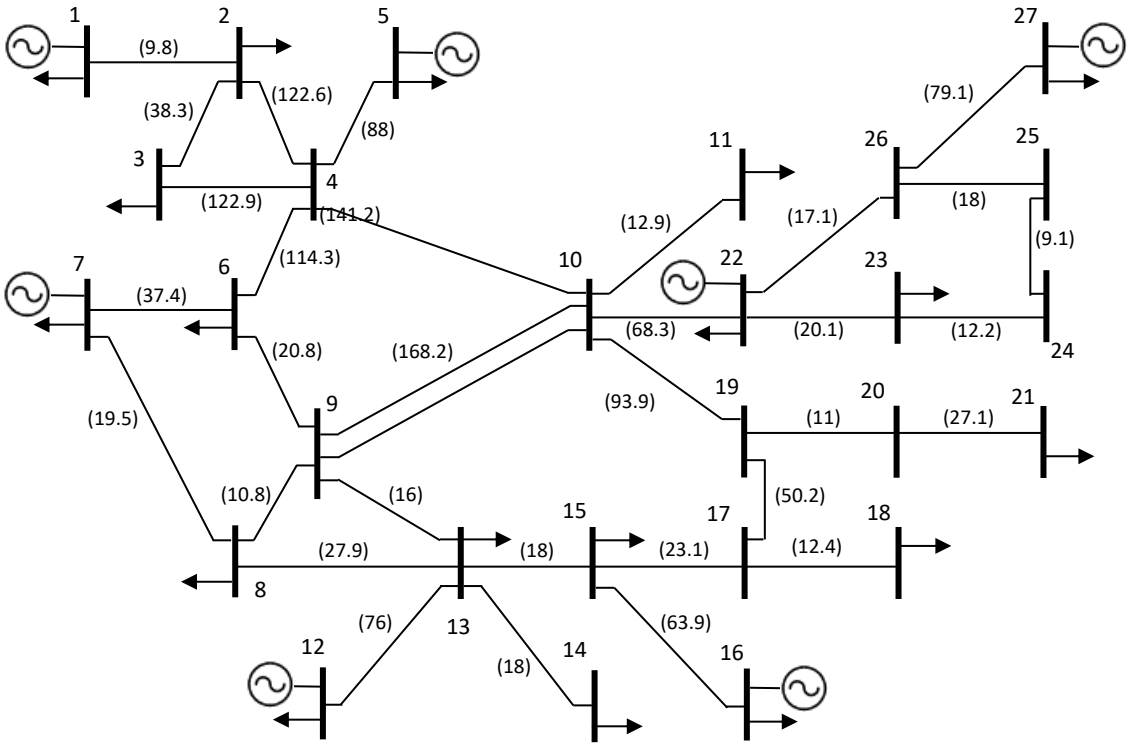

Figure 5.3 The 27 bus transmission system used for fault location analysis

The transmission system is modeled in the Electromagnetic Transients Program (EMTP) [46] to obtain the measurements at each bus for fault scenarios with different fault locations, types, and resistances. The measurements obtained then are utilized to test the developed method and algorithm that are implemented in Matlab.

In the study, the initial fault location is selected as 0.5 per unit for all cases. The fault location estimation accuracy is evaluated based on percentage error as

$$\%\text{Error} = \frac{|\text{Actual Location} - \text{Estimated Location}|}{\text{Total length of faulted line}} \cdot 100 \qquad (5.23)$$

The fault location algorithm will be demonstrated in subsection 5.3.1 and 5.3.2 for single fault and simultaneous faults on transposed lines, respectively. Subsection 5.3.3 and 5.3.4 demonstrate the fault location results for single fault and simultaneous faults on

untransposed lines, respectively. Various cases with different fault locations, types, and fault resistances are simulated. Representative results are shown.

5.3.1 Fault Location for a Single Fault on Transposed Line

Table 5.1 presents the fault location results. The first four columns of Table 5.1 list the faulted line segments, fault types, actual fault locations in per unit, and fault resistances in ohms, respectively. The last column of Table 5.1 lists the fault location estimation accuracy.

Table 5.1 Fault location results for single faults on transposed lines

Faulted lines	Fault types	Actual FL (p.u.)	Fault Res. (Ω)	FL Est. error (%) using data from selected buses	
				1	1&16
4-10	AG	0.8	1	0.01	0.01
4-10	AG	0.8	15	0.01	0.01
6-9	BC	0.3	1	0.43	0.05
4-10	BC	0.5	1	0.00	0.01
4-10	ABC	0.2	1	0.00	0.00
4-10	BCG	0.3	20	0.00	0.01
9-10	BG	0.9	15	0.01	0.36
9-10	BC	0.2	1	0.35	0.00
9-10	ABC	0.7	1	0.01	0.12

From Table 5.1, it is observed that quite accurate results are achieved under various fault conditions. Moreover, it should be noted that one bus measurement is enough to pinpoint the fault location for a single fault.

5.3.2 Fault Location for Simultaneous Faults on Transposed Lines

Table 5.2 presents the fault location results for simultaneous faults. All cases have a fault occurring on the double-circuit line between bus 9 and bus 10. Different fault types and fault resistances are considered. Voltage measurements from buses 1, 8, and 16 are utilized to estimate the fault locations. As an example, Figure 5.4 presents the voltage waveforms at bus 8 and 16 during a simultaneous fault.

The first column of Table 5.2 lists the case numbers. The second to fifth columns list the faulted lines, fault types, actual fault locations in per unit, and fault resistances in ohms, respectively. The last column lists the percentage error of the estimated fault location.

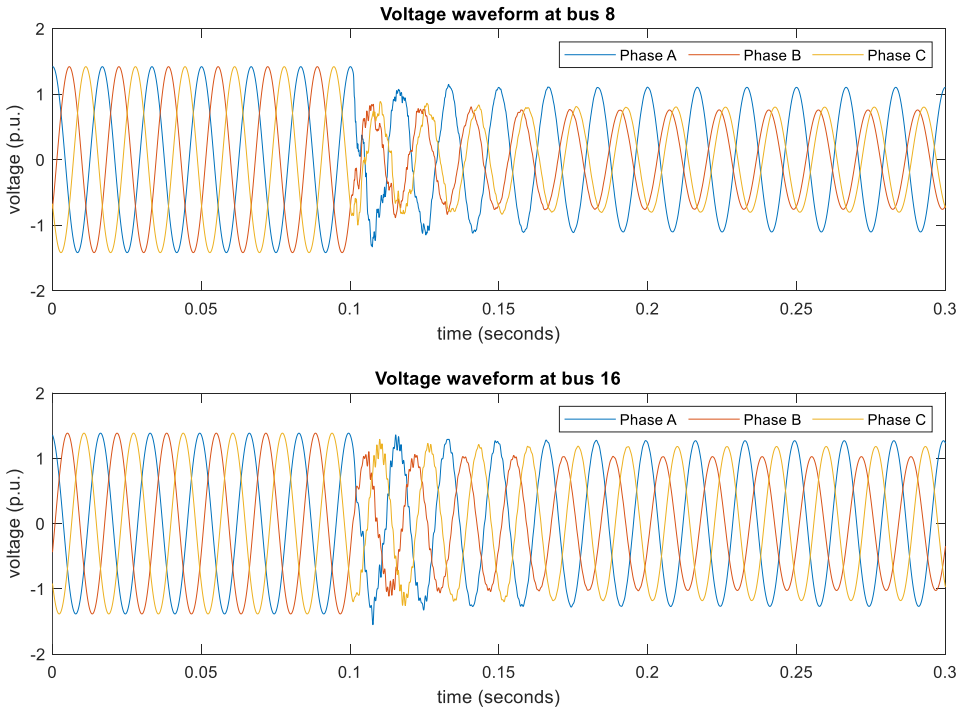

Figure 5.4 Voltage waveforms for a simultaneous fault in a transmission system: AG on the line 4-10 and BC on the line 6-9

Table 5.2 Fault location results for multiple simultaneous faults on transposed lines

No.	Fault lines	Fault types	Actual FL (p.u.)	Fault Res. (Ω)	FL Est. error (%) using data from selected buses	
					1&8	1,8& 16
1st	4-10	AG	0.8	25	0.02	0.02
	6-9	BC	0.3	10	0.49	0.40
2nd	4-10	AG	0.8	50	0.01	0.00
	9-10	BG	0.9	25	0.02	0.01
3rd	6-9	BC	0.3	1	0.05	0.07
	9-10	BG	0.9	15	0.01	0.01

The results demonstrate that quite accurate results are obtained by the proposed method, and the proposed method is able to handle simultaneous faults involving double-circuit line.

5.3.3 Fault Location for a Single Fault on Untransposed Line

To emulate the untransposed line, the line between bus 9 and 10 is made untransposed in this study. Table 5.3 tabulates fault location results for the untransposed double-circuit line between bus 9 and bus 10 under various fault conditions. Measurements at buses 1 and 16 are utilized to carry out the estimated fault locations.

Table 5.3 Fault location results for single faults on the untransposed line

Faulted lines	Fault types	Actual FL (p.u.)	Fault Res. (Ω)	FL Est. error (%) using data from selected buses	
				1	1&16
9-10	AG	0.3	50	0.04	0.01
9-10	AG	0.8	1	0.01	0.25
9-10	BC	0.7	15	0.02	0.08
9-10	BC	0.2	1	0.34	0.01
9-10	BCG	0.4	20	0.04	0.02
9-10	BCG	0.6	1	0.02	0.01
9-10	ABC	0.6	1	0.01	0.02
9-10	ABC	0.7	20	0.01	0.12

From Table 5.3, it is manifested that the estimation is quite accurate even for untransposed transmission lines. It is also noted that one measurement is enough to derive the fault location for single fault cases.

5.3.4 Fault Location for Simultaneous Faults Involving Untransposed Line

In Table 5.4, fault location results for simultaneous faults that involve untransposed lines under diverse fault conditions are presented. Column 1 lists fault case number. Column 2 to 5 list actual fault conditions. The last two columns list the estimated fault location errors. It is important to note that the double circuit line between bus 9 and bus 10 is an untransposed line in this study.

Table 5.4 demonstrates that the proposed fault location algorithm yield accurate results and thus can deal with simultaneous faults involving untransposed lines.

Table 5.4 Fault location results for multiple simultaneous faults involving untransposed line

No	Fault lines	Fault types	Actual FL (p.u.)	Fault Res. (Ω)	FL Est. error (%) using data from selected buses	
					1&8	1,8& 16
1st	4-10	AG	0.8	10	0.01	0.01
	9-10	BC	0.3	1	0.01	0.01
2nd	4-10	AG	0.8	10	0.29	0.08
	9-10	BG	0.5	10	0.19	0.05
3rd	4-10	AG	0.7	1	0.01	0.02
	9-10	BG	0.4	20	0.03	0.04

5.4 Summary

In this chapter, the fault location algorithm for simultaneous faults in the transmission systems is proposed. It utilizes the bus impedance matrix technique to link the driving point and transfer impedances to voltage measurements. The algorithm is validated by simulation studies for a 27 bus transmission system. Simulation results for faults occur on transposed and untransposed transmission lines are presented. The method is applicable to both single and double-circuit lines. From the results, it is evidenced that the proposed

algorithm is able to locate simultaneous faults and single fault occur in transmission systems accurately.

Chapter 6 Conclusions

Accurate fault location speeds up power system restoration, reduces outage times, and enhances power system reliability. This dissertation advances fault location research to pinpoint simultaneous faults for transmission and distribution systems integrated with DGs.

Chapter 2 presents the proposed fault area identification method. A power system can be divided into several protection areas based on the topology of that system. Then, an identification vector is calculated using the connection matrix and line current vector. The identification vector reveals the faulted phase(s) and faulted area(s). Once the faulted area(s) is identified, the fault location algorithms proposed in later chapters can be utilized to pinpoint the fault by examining the line segments in the faulted area(s). In this way, the proposed fault area identification method reduces the number of line sections that need to be examined for fault location purpose. Case studies demonstrate that the proposed fault area identification method is accurate and effective for transmission and distribution systems with DGs.

Chapter 3 presents the proposed fault location algorithms for locating simultaneous faults in the distribution systems with DG. There is a total of three types of fault location algorithms proposed depending on the utilization of voltage and/or current measurements and source impedance. In which, Type I and Type III algorithms do not need the information of source impedances and prefault measurements to locate a fault. Another feature is that no fault types and fault resistance are needed to determine the fault locations. Furthermore, limited voltage measurements are needed to find the fault locations for a simultaneous fault. In addition, the proposed algorithms are applicable to

distribution systems integrated with DGs. Moreover, the effects of shunt capacitance are fully considered to improve fault location accuracy. Extensive evaluation studies have been carried out, and the highly accurate estimation results validate the proposed algorithms.

The voltage and current measurements may have errors, and thus the accuracy of fault location estimation will be impacted. Chapter 4 proposes the optimal fault location method to address this challenge. The method first detects and identifies bad data based on non-linear estimation theory. Then, the bad data is discarded. After that, only accurate measurements will be used to estimate the fault location. As a result, the impacts of measurement errors are minimized. The proposed optimal fault location estimation method is applied to distribution systems with DGs. The results show that the proposed method has the ability to detect and identify bad data. The accuracy of fault location estimation is improved after the bad data is removed.

The proposed fault location algorithm for transmission systems is presented in Chapter 5. It is capable of pinpointing simultaneous faults for transmission systems with double circuit lines. The lines can be either transposed or untransposed. The algorithm establishes the relationship between driving point and transfer impedances with voltage measurements based on bus impedance matrix technique. Evaluation studies are performed on a 27 transmission system with double circuit lines. The results manifest that the proposed fault location algorithm is able to locate simultaneous faults precisely for transmission systems.

References

[1] R. Krishnathevar and E. E. Ngu, "Generalized impedance-based fault location for distribution systems," IEEE Transactions on Power Delivery, vol. 27, no. 1, pp. 449 - 451, Jan. 2012.

[2] Y. Liao, "Electric distribution system fault location considering shunt capacitances," Electric Power Components and Systems, vol. 41, no. 5, pp. 519-536, Feb. 2013.

[3] Energy.gov. (2019). Distribution automation: results from the smart grid investment grant program. [online] Available at: https://www.energy.gov/sites/prod/files/2016/11/f34/Distribution%20Automation%20Summary%20Report_09-29-16.pdf [Accessed 24 Jan. 2019].

[4] LG&E and KU. (2019). LG&E and KU | Distribution Power Line Tree Clearance. [online] Available at: https://lge-ku.com/safety/distribution-powerline-clearance [Accessed 19 Mar. 2019].

[5] M. Kezunovic, "Smart Fault Location for Smart Grids," IEEE Transactions on Smart Grid, vol. 2, no. 1, pp. 11-22, 2011.

[6] T. Takagi, Y. Yamakoshi, M. Yamaura, R. Kondow and T. Matsushima, "Development of a New Type Fault Locator Using the One-Terminal Voltage and Current Data," IEEE Transactions on Power Apparatus and Systems, vol. PAS-101, no. 8, pp. 2892-2898, 1982.

[7] C. E. de Morais Pereira and L. C. Zanetta, "Fault location in transmission lines using one-terminal postfault voltage data," IEEE Transactions on Power Delivery, vol. 19, no. 2, pp. 570-575, 2004.

[8] C. J. Lee, J. B. Park, J. R. Shin and Z. M. Radojevie, “A new two-terminal numerical algorithm for fault location, distance protection, and arcing fault recognition,” IEEE Transactions on Power Systems, vol. 21, no. 3, pp. 1460-1462, 2006.

[9] Y. Liao and S. Elangovan, “Unsynchronized two-terminal transmission-line fault-location without using line parameters,” IEE Proceedings - Generation, Transmission and Distribution, vol. 153, no. 6, pp. 639-643, 2006.

[10] N. Kang, J. Chen and Y. Liao, “A Fault-Location Algorithm for Series-Compensated Double-Circuit Transmission Lines Using the Distributed Parameter Line Model,” IEEE Transactions on Power Delivery, vol. 30, no. 1, pp. 360-367, 2015.

[11] A. S. Dobakhshari and A. M. Ranjbar, “A Novel Method for Fault Location of Transmission Lines by Wide-Area Voltage Measurements Considering Measurement Errors,” in IEEE Transactions on Smart Grid, vol. 6, no. 2, pp. 874-884, 2015.

[12] X. Jiao and Y. Liao, “Accurate Fault Location for Untransposed/Transposed Transmission Lines Using Sparse Wide-Area Measurements,” IEEE Transactions on Power Delivery, vol. 31, no. 4, pp. 1797-1805, 2016.

[13] G. Feng and A. Abur, “Fault Location Using Wide-Area Measurements and Sparse Estimation," IEEE Transactions on Power Systems, vol. 31, no. 4, pp. 2938-2945, 2016.

[14] M. Shahraeini, M. S. Ghazizadeh and M. H. Javidi, “Co-Optimal Placement of Measurement Devices and Their Related Communication Infrastructure in Wide Area Measurement Systems,” IEEE Transactions on Smart Grid, vol. 3, no. 2, pp. 684-691, 2012.

[15] W. Xiu and Y. Liao, “Fault Location Observability Analysis on Power Distribution Systems,” Electric Power Components and Systems, vol. 42, no. 16, pp. 1862-1871, 2014.

[16] S. M. Brahma, Fault location in power distribution system with penetration of distributed generation, IEEE Transactions on Power Delivery, 26 (3) (2011) 1545-1553.

[17] A. H. AI-mohammed, M. A. Abido, An adaptive fault location algorithm for power system networks based on synchrophasor measurements, Electric Power Systems Research 108 (2014) 153-163.

[18] S. F. Alwash, V. K. Ramachandaramurthy, N. Mithulananthan, Fault-location scheme for power distribution system with distributed generation, IEEE Transactions on Power Delivery, 30 (3) (2015) 1187-1195.

[19] J. J. Mora-Flórez, R. A. Herrera-Orozco, A. F. Bedoya-Cadena, Fault location considering load uncertainty and distributed generation in power distribution systems, IET Generation, Transmission & Distribution, 9 (3) (2015) 287-295.

[20] A. M. EI-Zonkoly, Fault diagnosis in distribution network with distributed generation, Electric Power Systems Research, 81 (7) (2011) 1482-1490.

[21] C. Grajales-Espinal, J. Mora-Florez, S. Perez-Londono, Advanced fault location strategy for modern power distribution systems based on phase and sequence components and the minimum fault reactance concept, Electric Power Systems Research, 140 (2016) 933-941.

[22] K. Jia, T. Bi, Z. Ren, D. W. P. Thomas, M. Sumner, High frequency impedance based fault location in distribution system with DGs, IEEE Transactions on Smart Grid, 9 (2) (2018) 807-816.

[23] M. A. Mora, J. V. Milanovic, Generalized formulation of the optimal monitor placement problem for fault location, Electric Power Systems Research, 93 (2012) 120-126.

[24] M. Majidi, M. Etezadi-Amoli, A new fault location technique in smart distribution networks using synchronized/nonsynchronized measurements, IEEE Transactions on Power Delivery, 33 (3) (2018) 1358-1368.

[25] M. Majidi, M. Etezadi-Amoli, and M. Sami Fadali, "A novel method for single and simultaneous fault location in distribution networks," IEEE Transactions on Power Systems, vol. 30, no. 6, pp. 3368 - 3376, November 2015.

[26] F. H. Magnago and A. Abur, "Fault Location Using Wavelets," IEEE Transactions on Power Delivery, vol. 13, no. 4, pp. 1475-1480, 1998.

[27] D. Spoor and J. Zhu, "Improved Single-Ended Traveling-Wave Fault-Location Algorithm Based on Experience with Conventional Substation Transducers," IEEE Transactions on Power Delivery, vol. 21, no. 3, pp. 1714-1720, 2006.

[28] F. V. Lopes, K. M. Silva, F. B. Costa, W. L. A. Neves and D. Fernandes, "Real-Time Traveling-Wave-Based Fault Location Using Two-Terminal Unsynchronized Data," IEEE Transactions on Power Delivery, vol. 30, no. 3, pp. 1067-1076, 2015.

[29] M. Korkali, H. Lev-Ari and A. Abur, "Traveling-Wave-Based Fault-Location Technique for Transmission Grids Via Wide-Area Synchronized Voltage

Measurements," IEEE Transactions on Power Systems, vol. 27, no. 2, pp. 1003-1011, 2012.

[30] D. Thukaram, H. P. Khincha and H. P. Vijaynarasimha, "Artificial neural network and support vector machine approach for locating faults in radial distribution systems," in IEEE Transactions on Power Delivery, vol. 20, no. 2, pp. 710-721, April 2005.

[31] M. A. Al-shaher, M. M. Sabry, A. S. Saleh, "Fault location in multi-ring distribution network using artificial neural network", Electric Power System Research, vol. 64, no. 2, pp. 87-92, 2003.

[32] Z. Galijasevic and A. Abur, "Fault location using voltage measurements," in IEEE Transactions on Power Delivery, vol. 17, no. 2, pp. 441-445, April 2002.

[33] H. Livani and C. Y. Evrenosoglu, "A Machine Learning and Wavelet-Based Fault Location Method for Hybrid Transmission Lines," in *IEEE Transactions on Smart Grid*, vol. 5, no. 1, pp. 51-59, Jan. 2014.

[34] G. Manassero, S. G. Di Santo, L. Souto, Heuristic method for fault location in distribution feeders with the presence of distributed generation, IEEE Transactions on Smart Grid, 8 (6) (2017) 2849-2858.

[35] Y. Jiang, C. Liu, M. Diedesch, E. Lee, A. K. Srivastava, Outage management of distribution systems incorporating information from smart meters, IEEE Transactions on Power Systems, 31 (5) (2016) 4144-4154.

[36] D. S. Gazzana, G. D. Ferreira, A. S. Bretas, A. L. Bettiol, A. Carniato, L. F. N. Passos, A. H. Ferreira, J. E. M. Silva, An integrated technique for fault location and

section identification in distribution systems, Electric Power Systems Research, 115 (2014) 65-73.

[37] Y. Liao, "Identification of faulted feeder section in distribution systems using overcurrent information from switching devices," International Journal of Emerging Electric Power Systems, vol. 15, no. 2, pp. 171-176, April 2014.

[38] W. Fan and Y. Liao, "Transmission line parameter-free fault location results using field data," *Power and Energy Conference at Illinois (PECI)*, Champaign, IL, USA, February 22-23, 2018.

[39] W. Fan and Y. Liao, "Wide area measurements based fault detection and location method for transmission lines," Protection and Control of Modern Power Systems, Mar 2019.

[40] W. Fan and Y. Liao, "Fault identification and location for distribution network with distributed generations," International Journal of Emerging Electric Power Systems, vol. 19, no. 3, 2018.

[41] IEEE PES 34 Node Test System. [Available at] http://sites.ieee.org/pes-testfeeders/resources/.

[42] The MathWorks, Inc, Matlab Help Manual (R2016b), Natick, USA, 2016.

[43] W. Fan and Y. Liao, "Fault location techniques for simultaneous faults in power distribution systems with distributed generations," *International Energy and Sustainability Conference (IESC)*, Farmingdale, NY, USA, October 19-20, 2017.

[44] W. Fan and Y. Liao, "Fault location for distribution systems with distributed generations without using source impedance," *North American Power Symposium*, Wichita, KS, USA, October 12-15, 2019.

[45] J. Grainger, W. Stevenson, Power System Analysis, McGraw-Hill, 1994.

[46] Leuven EMTP Centre, Alternative Transient Program. User Manual and Rule Book, Leuven, Belgium, 1987.

Vita

Wen Fan is a doctoral student in the Electrical and Computer Engineering department at the University of Kentucky. He is interested in power system modeling and simulation, fault analysis and protection, and renewable energy integration. He is a member of IEEE and IEEE PES.